

THESE

Présentée devant



(INSTITUT NATIONAL DES SCIENCES APPLIQUEES DE LYON)

Pour obtenir

LE GRADE DE DOCTEUR

Ecole Doctorale des Sciences de l'Ingénieur de Lyon:

Mécanique, Energétique, Génie civil, Acoustique (MEGA)

Spécialité:

MECANIQUE – GENIE MECANIQUE

Par

Muhammad Aurangzeb KHAN

**NUMERICAL AND EXPERIMENTAL FORMING ANALYSES OF
TEXTILE COMPOSITE REINFORCEMENTS BASED ON
A HYPOELASTIC BEHAVIOUR**

***ANALYSE NUMERIQUE ET EXPERIMENTALE DE LA MISE EN FORME DES
RENFORTS DE COMPOSITE TEXTILES BESEE SUR
UN COMPORTEMENT HYPOELASTIQUE***

Thèse soutenue le 09 octobre 2009 devant la commission d'examen

Jury :

Olivier POLIT	Professeur (Université de Paris 10)	Rapporteur
Laurent GUILLAUMAT	Professeur (Université de Bourgogne)	Rapporteur
Philippe OLIVIER	Professeur (Université de Toulouse 3)	Examineur
Philippe BOISSE	Professeur (INSA de Lyon)	Directeur
Tarek MABROUKI	Maître de Conférence (INSA de Lyon)	Codirecteur



LaMCoS, INSA-Lyon, CNRS UMR5259, F69621.
(Laboratoire de Mécanique des Contacts et des Structures)
20, Av. Albert Einstein, 69621 Villeurbanne Cedex, France.



INSA Direction de la Recherche - Ecoles Doctorales – Quadriennal 2007-2010

SIGLE	ECOLE DOCTORALE	NOM ET COORDONNEES DU RESPONSABLE
CHIMIE	CHIMIE DE LYON http://sakura.cpe.fr/ED206 M. Jean Marc LANCELIN Insa : R. GOURDON	M. Jean Marc LANCELIN Université Claude Bernard Lyon 1 Bât CPE 43 bd du 11 novembre 1918 69622 VILLEURBANNE Cedex Tél : 04.72.43 13 95 Fax : lancelin@hikari.cpe.fr
E.E.A.	ELECTRONIQUE, ELECTROTECHNIQUE, AUTOMATIQUE http://www.insa-lyon.fr/eea M. Alain NICOLAS Insa : C. PLOSSU ede2a@insa-lyon.fr Secrétariat : M. LABOUNE AM. 64.43 – Fax : 64.54	M. Alain NICOLAS Ecole Centrale de Lyon Bâtiment H9 36 avenue Guy de Collongue 69134 ECULLY Tél : 04.72.18 60 97 Fax : 04 78 43 37 17 eea@ec-lyon.fr Secrétariat : M.C. HAVGOUDOUKIAN
E2M2	EVOLUTION, ECOSYSTEME, MICROBIOLOGIE, MODELISATION http://biomserv.univ-lyon1.fr/E2M2 M. Jean-Pierre FLANDROIS Insa : H. CHARLES	M. Jean-Pierre FLANDROIS CNRS UMR 5558 Université Claude Bernard Lyon 1 Bât G. Mendel 43 bd du 11 novembre 1918 69622 VILLEURBANNE Cédex Tél : 04.26 23 59 50 Fax 04 26 23 59 49 06 07 53 89 13 e2m2@biomserv.univ-lyon1.fr
EDISS	INTERDISCIPLINAIRE SCIENCES- SANTÉ Sec : Safia Boudjema M. Didier REVEL Insa : M. LAGARDE	M. Didier REVEL Hôpital Cardiologique de Lyon Bâtiment Central 28 Avenue Doyen Lépine 69500 BRON Tél : 04.72.68 49 09 Fax :04 72 35 49 16 Didier.revel@creatis.uni-lyon1.fr
INFOMATHS	INFORMATIQUE ET MATHEMATIQUES http://infomaths.univ-lyon1.fr M. Alain MILLE Secrétariat : C. DAYEYAN	M. Alain MILLE Université Claude Bernard Lyon 1 LIRIS - INFOMATHS Bâtiment Nautibus 43 bd du 11 novembre 1918 69622 VILLEURBANNE Cedex Tél : 04.72. 44 82 94 Fax 04 72 43 13 10 infomaths@bat710.univ-lyon1.fr - alain.mille@liris.cnrs.fr
Matériaux	MATERIAUX DE LYON M. Jean Marc PELLETIER Secrétariat : C. BERNAVON 83.85	M. Jean Marc PELLETIER INSA de Lyon MATEIS Bâtiment Blaise Pascal 7 avenue Jean Capelle 69621 VILLEURBANNE Cédex Tél : 04.72.43 83 18 Fax 04 72 43 85 28 Jean-marc.Pelletier@insa-lyon.fr
MEGA	MECANIQUE, ENERGETIQUE, GENIE CIVIL, ACOUSTIQUE M. Jean Louis GUYADER Secrétariat : M. LABOUNE PM : 71.70 –Fax : 87.12	M. Jean Louis GUYADER INSA de Lyon Laboratoire de Vibrations et Acoustique Bâtiment Antoine de Saint Exupéry 25 bis avenue Jean Capelle 69621 VILLEURBANNE Cedex Tél :04.72.18.71.70 Fax : 04 72 43 72 37 mega@lva.insa-lyon.fr
ScSo	ScSo* M. OBADIA Lionel Insa : J.Y. TOUSSAINT	M. OBADIA Lionel Université Lyon 2 86 rue Pasteur 69365 LYON Cedex 07 Tél : 04.78.69.72.76 Fax : 04.37.28.04.48 Lionel.Obadia@univ-lyon2.fr

*ScSo : Histoire, Géographie, Aménagement, Urbanisme, Archéologie, Science politique, Sociologie, Anthropologie

Dedicated to;

My beloved Family

ACKNOWLEDGMENTS

First of all, I am extremely grateful to my ALLAH: the most gracious and the most compassionate, Who made me able to do this work.

I would like to express my deepest gratitude to my project directors: Professor Dr. Philippe Boisse and Dr. Tarek Mabrouki, for their support, contribution and interest for this work. Their consistent concern and valuable guidance has helped to complete my PhD thesis. Indeed, both of my PhD supervisors have remained kind throughout and favoured me a lot.

I am very much thankful to my predecessors of the same research group: Dr. Nahiène Hamila, Dr. Pierre Badel and Dr. Emmanuel De Luckyer for their assistance during my research work.

I owe my special thanks to the team managing the composite forming benchmark group for exploiting double dome model in my thesis.

I would like to acknowledge the financial support provided by Higher Education Commission (HEC) of Pakistan in pursuing my higher studies in France. I also pay thanks to my research laboratory, LaMCoS, INSA de Lyon, for their financial and technical support.

I also thank to my research contemporary friends: Mr. Muhammad Zain-ul-Abedin, Muhammad Asad and Syed Mushtaq Shah, for participating in the technical discussions and knowledge-sharing during my time spent for PhD thesis.

Finally, I am always grateful to my loving parents who ever prayed for me and encouraged me in life. Last but not the least; I heartily acknowledge the kind support rendered by my wife during my studies and for our combined stay in France. I would also like to express my love to Somia and Abdullah: Tom and Jerry.

ABSTRACT

Numerical simulations of the composite forming processes are essential in the design phase of composite structures. Fabric Forming simulations have many objectives: these determine the feasibility of forming or conditions of this feasibility and help determine the position of fibres after forming. This is important for the identification of mechanical characteristics of composites in service and to calculate the permeability after dry reinforcement draping for correct analysis of injection moulding process. This particular study has been accomplished with three main stages: the development of a stress computation algorithm for numerical analysis of fibrous materials; the experimental forming analysis of textile fabrics with an in-house development of double dome benchmark forming device; and finite element forming simulations using the benchmark model.

Continuous approach has been used to predict the mechanical characteristics of woven composite fabrics during forming which considers the fibrous materials as a continuum on average at macroscopic scale. An algorithm based on a hypoelastic behaviour has been proposed for composite reinforcement forming simulations. It has been shown that using hypoelastic law with an objective derivative based on warp and weft fibre rotation tensors can successfully trace the correct behaviour of fibrous materials in deformation. The algorithm has been validated through a number of elementary tests with theoretical results. The de-facto standard in-plane shear tests of picture-frame and bias-extension have also been validated numerically. Double dome fabric forming tests have been carried out experimentally. 3D optical strain measurements were performed exploiting digital image correlation system of Vic-3D in order to measure the shear angles of the deformed fabrics. The forming simulations performed with the proposed numerical approach show a good agreement with the experimental results obtained with double dome device.

Keywords: Textile Reinforcement, Composite Processing, Forming Simulation, Hypoelasticity, Continuous Approach, International Forming Benchmark

RESUMÉ

Le travail présenté dans le cadre de cette thèse concerne la mise en forme des renforts tissés avant injection de la résine. L'objectif étant de déterminer des critères de faisabilité et aussi de prédire la position des fibres après formage. Cela permettra de dimensionner convenablement les pièces composites en service. Pour cela, deux approches ont été abordées dans cette contribution. La première, concerne l'élaboration d'un algorithme numérique basée sur une loi hypoélastique traduisant le comportement d'un milieu fibreux lors d'une opération de préformage. Cette formulation a été programmée via une routine utilisateur au sein du code de calcul élément finis ABAQUS/Explicit. En outre, elle a été validée par des essais numériques élémentaires et qui ont été à leur tour comparés à des résultats analytiques. La seconde approche est expérimentale et est considérée comme l'une des apports importants de cette thèse. En effet, elle correspond à la réalisation d'un benchmark international qui a la géométrie d'un double dôme et qui a servi à valider les résultats de la simulation numérique.

Par ailleurs, le modèle numérique a été alimenté par des essais expérimentaux (bias et picture frame tests) traduisant le comportement du milieu fibreux en cisaillement. Parallèlement, des essais de mesures optiques 3D de la déformation du milieu fibreux ont été réalisés en exploitant le logiciel de corrélation d'image Vic-3D. Cela a permis de mesurer les angles de cisaillement des tissus considérés lors du préformage. Les résultats de la simulation numérique montrent une très bonne concordance avec ceux obtenus expérimentalement.

Mots Clés: Renforts Tissés, Mise en forme, Simulations, Hypoélasticité, Approche Continue, Benchmark International

CONTENTS

1	<i>Introduction</i>	1
1.1	Textile Composites	2
1.1.1	Composite Forming Processes	2
1.1.2	Finite Element Simulations	3
1.2	Research Objectives and Contributions	4
1.3	Outlines of the Thesis	6
2	<i>Textile Composites: The Current and Potential Use</i>	9
2.1	Introduction	9
2.2	Textile Reinforcement Geometry	10
2.2.1	Woven Fabrics	10
a)	Plain weave	11
b)	Twill weave	11
c)	Satin weave	12
2.2.2	Non Crimp Fabrics (NCF)	12
2.2.3	3D-Fabrics	14
2.3	Mechanical Properties of Textile Reinforcements	15
2.3.1	Deformation Mechanisms	16
a)	In-plane shear	16
b)	Biaxial tension	17
c)	Transverse compaction	18
d)	Bending	19
e)	In plane shear coupled with tensions	20
f)	Non-sliding between warp and weft	20
2.3.2	Characterization of Mechanical Properties	21
a)	Biaxial tensile device	21
2.4	Composite Forming Processes	25
2.4.1	Resin Transfer Moulding (RTM)	25
2.5	Woven Reinforcement Modelling	27
2.5.1	The Scales of Modelling	28
a)	Micro-scale models	28
b)	Meso-scale models	29

c) Macro-scale models	32
2.5.2 The Modelling Approaches	33
a) Kinematic approaches	33
b) Discrete approaches	34
c) Continuous approaches	36
d) Semi-discrete approach	37
2.6 Mechanical Behaviour Models	38
2.6.1 Approach of Yu	39
2.6.2 Modelling Approach of Ten Thije	40
2.6.3 Non-orthogonal Approach	41
2.6.4 Hypoelastic Approach developed by Hagège	42
Conclusions of Chapter-2	43
3 Numerical Modelling of Woven Composite Reinforcements	45
3.1 Introduction	45
3.2 Explicit Dynamic Scheme of Analysis	46
3.3 Hypoelastic Approach	48
3.3.1 Objectivity of Hypoelastic Laws	49
a) The principle of objectivity	49
b) Objectivity of rate constitutive equations	50
3.4 Hypoelastic Model for Fibrous Materials	52
3.4.1 Stress Computation Algorithm for Fibrous Materials	52
3.4.2 Modelling Methods for Fibrous Media	58
a) Unidirectional fibres with two superimposed elements (1DF2E)	58
b) Bidirectional fibres within single element (2DF1E)	59
3.5 Validating the Algorithm Formulations	60
3.5.1 Elementary Tests	60
3.5.2 Discussion and Analysis: Elementary Tests	62
3.6 Picture Frame Test	63
3.7 Bias Extension Test	68
3.8 Fabric Material Behaviour with VFABRIC	70
3.8.1 Elementary Tests using VFABRIC	71
3.9 Numerical Modelling for Composite Prepreg	72
Conclusions of Chapter-3	75
4 Experimental Forming Analysis of Woven Composites	77
4.1 Introduction	77
4.2 Benchmark Study Fabrics	78
4.2.1 Types of Fabrics	78
4.2.2 Material Characterisation and Specifications	79
4.2.3 Shear Modulus Determination	83
a) PW fabrics	83
b) BTW fabrics	85
4.2.4 Double Dome Benchmark	86
4.3 Composite Forming Experiments	87

4.3.1	Development of Forming Tools.....	87
4.3.2	Double Dome Forming Tests.....	88
4.4	3D Optical Strain Measurement (OSM).....	91
4.4.1	Digital Image Correlations (DIC).....	92
4.4.2	DIC in The Dissertation.....	94
	Conclusions of Chapter-4.....	98
5	<i>Numerical Forming Simulations of Textile Woven Composites.....</i>	99
5.1	Introduction.....	99
5.2	FEM Model of Double Dome.....	100
5.2.1	Model Setup.....	100
5.2.2	Material Characteristics and Process Parameters.....	102
5.3	Numerical Forming Tests.....	103
5.3.1	Balanced Plain Weave (BPW).....	104
5.3.2	Balanced Twill Weave (BTW).....	105
5.4	Comparison between Experimental and Numerical Results.....	106
5.4.1	Material Draw-In.....	106
5.4.2	Shear Angle Measurements.....	106
5.5	Multilayer Simulations.....	114
5.6	Parametric Sensitivity Study.....	115
5.6.1	Shear Rigidity.....	116
5.6.2	Punch Velocity.....	117
5.6.3	Mesh Orientation.....	119
5.6.4	Element Type.....	119
5.6.5	Coefficient of Friction.....	120
5.6.6	Blank Holder Shape.....	122
5.6.7	Binder Force.....	122
5.7	Thermo-forming Case Study.....	125
	Conclusions of Chapter-5.....	128
6	<i>Summary and Conclusions.....</i>	129
	BIBLIOGRAPHY.....	133

Nomenclature

List of symbols

\cdot :	Scalar/dot product
\times :	Vector/Cross product
\otimes :	dyadic/tensorial product
$\cos(\alpha)$:	Cosine of an angle
$\sin(\alpha)$:	Sine of an angle
$\ln(\alpha)$:	Natural logarithm
$\ \alpha\ $:	Eucledian norm of a vector
$d\alpha$:	Total differential
$\partial\alpha$:	Partial differential
ψ :	Enclosed angle between warp and weft directions
γ :	In-plane shear angle
B :	Initial configuration
B^* :	Final configuration
L_{fab} :	Length of the fabric
F_{nom} :	Normalised force
W_{ext} :	External virtual work
$\underline{\eta}$:	Virtual displacement field
W_{int} :	Internal virtual work
W_{acc} :	Virtual work due to acceleration
ϵ_{11} :	Virtual axial strain in the warp direction.
ϵ_{22} :	Virtual axial strain in the weft direction.
T^{11} :	Tension on the unit woven cell in warp direction
T^{22} :	Tension on the unit woven cell in weft direction
L_1 :	Length of unit woven cell in warp directions
L_2 :	Length of unit woven cell in weft directions
χ_{11} :	Virtual curvatures of warp yarns

χ_{22} :	Virtual curvatures of weft yarns
M^{11} :	Bending moments of warp yarns
M^{22} :	Bending moments of weft yarns
$\underline{\underline{C}}$:	Right Cauchy-Green tensor
Ψ :	Free energy function
$\underline{\underline{E}}$:	Constant fourth order material tensor
$\underline{\underline{F}}$:	Deformation gradient
$\underline{\underline{S}}$:	Second Piola Kirchhoff tensor
$\underline{\underline{C}}$:	Eulerian constitutive tensor
$\underline{\underline{D}}$:	Eulerian tensor of strain rate
$\underline{\underline{\sigma}}$:	Cauchy stress tensor
$\underline{\underline{\sigma}}^{\nabla}$:	Objective derivative of Cauchy stress rate
$\underline{\underline{W}}$:	Jaumann rate
$\underline{\underline{\Omega}}$:	Green-Naghdi stress rate
$\underline{\underline{\Delta}}$:	Fibre rotation tensor
$\underline{\underline{f}}_1^0$:	Normalized vector along initial warp (first fibre) direction
$\underline{\underline{f}}_1$:	Normalized vector along current warp (second fibre) direction
$\underline{\underline{f}}_2^0$:	Normalized vector along initial weft direction
$\underline{\underline{f}}_2$:	Normalized vector along current weft direction
$\underline{\underline{f}}^1$:	A contravariant vector orthogonal to $\underline{\underline{f}}_2$
$\underline{\underline{f}}^2$:	A contravariant vector orthogonal to $\underline{\underline{f}}_1$
e_{α}^0 :	Initial Green-Naghdi (GN) frame
e_1 :	First current GN axis
e_2 :	Second current GN axis
α :	1 and/or 2
f_1 :	An orthogonal frame containing first fibre direction
f_2 :	An orthogonal frame containing second fibre direction
e :	Current GN frame

θ_1 :	Angle between first current axis of ‘GN frame and fibre direction’
θ_2 :	Angle between second current axis of ‘GN frame and fibre direction’
$[\mathbf{T}_1]$:	Transformation matrix between e and f_1
$[\mathbf{T}_1]^T$:	Transpose of $[\mathbf{T}_1]$
$[\mathbf{T}_2]$:	Transformation matrix between e and f_2
$[d\boldsymbol{\varepsilon}]$:	Incremental strain tensor
$d\varepsilon_{12}^{f_1}$:	Incremental shear strain calculated in f_1
$d\varepsilon_{12}^{f_2}$:	Incremental shear strain calculated in f_2
$[\mathbf{C}]_{f_1}$:	Constitutive matrix in f_1
$[\mathbf{C}]_{f_2}$:	Constitutive matrix in f_2
$\underline{\underline{\mathbf{U}}}$:	Right stretch tensor
$\underline{\underline{\mathbf{R}}}$:	Orthogonal rotation matrix
δ_{β}^{α} :	Kronecker delta
E_1 :	Young’s modulus in the warp direction
E_2 :	Young’s modulus in the weft direction
G_{12} :	In-plane shear rigidity
λ :	Stretch ratio
L :	Original length
l :	Current length
ε_{nom} :	Nominal strain
A :	Cross-sectional area of the fabric
t_{fabric} :	Thickness of the fabric
F_s :	Shear force
F :	Total force required to deform the fabric
τ :	Shear stress
μ :	Coefficient of friction

List of abbreviations

FE	finite elements
FEA	finite element analysis
FEM	finite element method
RTM	resin transfer moulding
VARTM	vacuum assisted resin transfer moulding
RFI	resin film injection
LCM	liquid composite moulding
NCF	non crimp fabric
DIC	digital image correlation
OSM	optical strain measurement
ROI	region of interest
AOI	area of interest
CCD	charge coupled device
GN	Green and Naghdi
1DF2E	two (set of) superimposed element(s) with unidirectional material data
2DF1E	single (set) of element(s) with bidirectional material data
UC	unit cell
CFRP	carbon fibre reinforced plastics
BPW	balanced plain weave
BTW	balanced twill weave
UTW	unbalanced twill weave
HKUST	Hong Kong University of Science and Technology
KUL	Katholieke Universiteit Leuven
NU	Northwestern University
CAD	computer aided design

1 Introduction

Over the recent few decades, there has been an increased trend to use composite materials as an alternate and better choice to the traditional metallic structures. The demand for high stiffness and strength and low weight materials, such as fibre reinforced plastics, has grown in the transport industry. Especially in the aeronautical industry, the use of fabric reinforced plastics increased significantly. By decreasing the cost with short production cycle times and increasing reproducibility by automation, fabric reinforced plastics are becoming better economical competitors to other construction materials such as aluminium [LEG09]. Typically, thin walled structures are produced with composite materials.

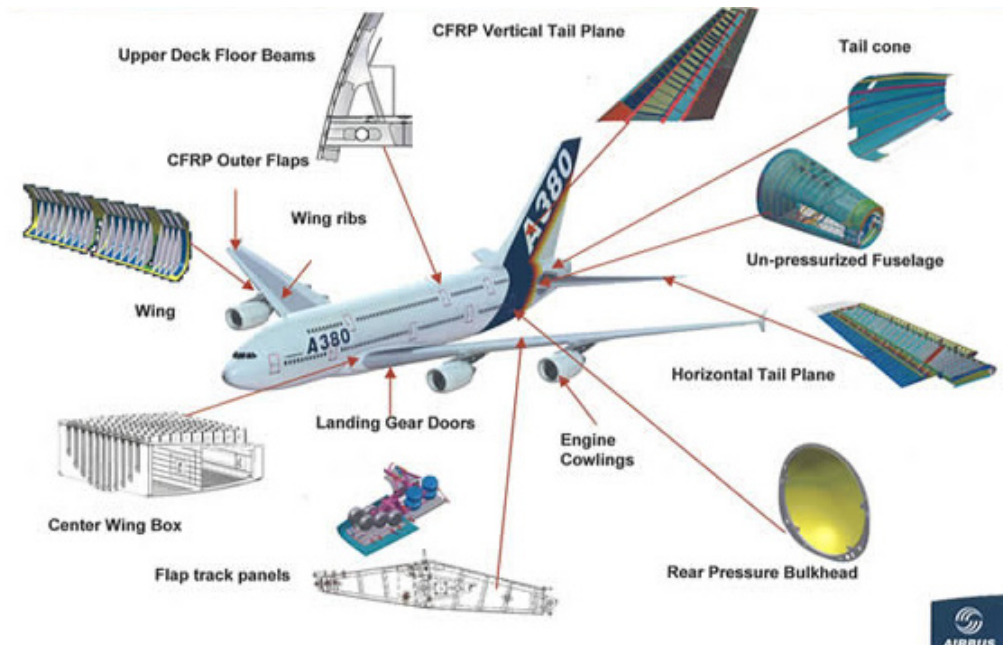


Fig. 1.1 Applications of carbon fibre reinforced plastics (CFRP) and thermoplastics in A380

Product optimisation with respect to both cost and efficiency has compelled the industries, like aeronautics and automotive, to ameliorate their products by introducing composites with a futuristic approach to cope with energy crisis. For example, the central chamber linking the wings of the A380 is of composites, the future A350 will have its full wings and its fuselage of composite while competitor Boeing announces Boeing787 with a composite fuselage.

1.1 Textile Composites

With the advent and exploitation of textile processing technology for fibrous reinforcement materials, there exists great potential of fibre reinforced composites to be employed as load-bearing structural parts. In this context, the research and development of composite parts is a subject of prime interest especially for the domains with high performance applications. Composites with continuous reinforcements are ideally suited for such applications because of their very good formability and possibility of obtaining parts with complex form. Textile composites have textile reinforcement, constituted of continuous fibres that are arranged in a repetitive structure. This internal structure is characterized by its smallest repetitive entity, called the unit cell (UC) or repeat. The continuous fibres give the textile composite a good impact and fatigue resistance [KHO97][KEL06].

1.1.1 Composite Forming Processes

The composite forming process is a critical stage for the manufacture of composite parts with requisite mechanical properties. The research in this thesis deals with a forming process which has more than one stage. The dry forming of textile reinforcements in RTM (Resin Transfer Moulding) process is a stage which largely holds a crucial role in predicting the mechanical properties and is also important in successful realisation of the process. The dry forming stage is indeed not much studied in proportion to its significance. The critical defects such as wrinkles in the shell composite structures can create a serious defect which not only alters the final quality of the part but also deteriorate its mechanical properties leading to fracture of fabric yarns. The final orientation of fibres in a part largely depends on this first phase of dry forming.

The preforming of dry textile reinforcements introduces large local deformations in it when draped to conform to mould. These deformations include large change in fibre orientations, fibre volume fraction and thickness of the fabric. Typically large in-plane shear deformations (the relative rotation of different fibre or yarn families) occur in the reinforcement as the shear resistance is usually much lower than other deformation modes. Local deformations, especially in-plane shear, and the fibre volume fraction, affect the subsequent processing (e.g. the permeability during resin injection [HEA01] [SON06]). Therefore, the success of this phase involves optimization of many process parameters which otherwise may create adverse effects. Among the notable parameters of preforming, the application of blankholder largely controls the elimination of wrinkles (out of plane buckling due to compressive stresses). The design and development of new and quality products require therefore optimization of experimental and numerical process conditions.

1.1.2 Finite Element Simulations

Numerical simulation has already been an established and extensively-used tool in product design and optimization of process conditions. This creates a link between the quality of the final product and process parameters while taking into account the material characteristics. In the present context, the draping simulations are used for producing shell structures (curved panels, ribs, stiffeners...) of textile composites. The study of dry fabric forming is carried out by knowing their specific behaviour and deformation modes. During deformation the reinforcement is subjected to tensile, shear, compression and bending loads. The privileged mode of deformation, which permits to obtain non-developable forms, is the in-plane shear. This example of the mode of deformations illustrates the multi-scale nature of the woven reinforcement. The forming simulations using finite element are able to take into account of these specific mechanical properties of the reinforcements.

Finite element forming simulations require a constitutive model that incorporates the specific anisotropic drape behaviour of textiles. In this context, continuous approach has been used more popularly nowadays for composite forming simulations. Although fabrics are discontinuous at lower length scales, the continuous approach has proven to be successful in many forming simulations. Special attention should be given to the constitutive equations, as the fibre directions change upon forming. The stiffness of the fibres is dominant and their orientation should be followed accurately. A continuum description of the reinforced material allows for implementation in standard, commercial FE packages. Many continuum models of

fibre reinforced composites were successfully implemented using the user subroutines available in ABAQUS [HAG05] [CAO05] [BAD08].

The macroscopic drape behaviour is determined by deformation mechanisms at smaller scales and is typically highly non-linear. In order to perform forming simulations at acceptable numerical cost, a multi-scale material approach is applied: material models are being developed at various length scales, such that smaller-scale models predict the mechanical behaviour at the larger length scale. The principal part of the models is being developed at the meso or macro-scale:

Meso-scale models describe in detail the complex structure of a textile (prepreg) unit cell with finite elements (FE) or analytical equations. These models make use of the insight in the physical phenomena and deformation mechanisms at the meso-scale to predict the macro-scale drape behaviour. Meso-scale models have the potential to avoid expensive textile testing for the drape characterization and to virtually design textile prepreg systems.

Macro-scale models are typically implemented in a non-linear FE program to perform forming simulations. These models are generally of elastic or visco-elastic nature and consider a simple equivalent medium, e.g. a homogeneous material or a set of elements (truss, membrane, shell, . . .), displaying similar macro-scale drape behaviour as identified in textile tests of virtual testing on meso-models. Various data exchange formats are being used. Often physical or non-physical constants, that characterize textile force-strain curves, are tabulated.

1.2 Research Objectives and Contributions

Textile woven composites are characterised with their specific mechanical properties and special deformation modes. Therefore their analysis, numerical as well as experimental, requires equally special handling. Numerically, the continuous approach is capable of predicting the mechanical characteristics of the woven composites and considers the fibrous materials as a continuum in average at macroscopic scale. The main objectives of this research work are:

- 1) The exploitation of the continuous approach to analyse woven composites at macro-scale. This includes the finite element analysis by using and validating a suitable

material model that incorporates the typical in-plane drape behaviour (tensile and shear) of bi-axially reinforced textile composites.

- 2) The use of hypoelastic behaviour of fibrous materials in the numerical analysis. The hypoelastic law has been used with an objective derivative based on fibre rotation tensor to update the current fibre axes.
- 3) The forming analysis of woven composite fabrics, both experimentally and numerically, with an international forming benchmark of double dome.

The contributions in this thesis are divided into following major categories which are aimed to meet the above cited objectives.

- 1) The development of a numerical model (a stress computation algorithm for fibrous materials) through a user material subroutine within a commercial finite element code to analyse the woven fabrics at macro-scale. The hypoelastic law based on an objective derivative of fibre rotation tensor, for each of warp and weft fibre direction, has been exploited to trace the specific deformation modes of fibrous materials.
- 2) The implementation of the user material subroutine to analyse the forming of woven composite reinforcements using benchmark geometry of double dome. Finite element forming simulations of double dome have been carried out to analyse woven fabrics. This benchmark study also includes the use of forming process parameters and mechanical behaviour of benchmark study fabrics.
- 3) The in-house development of double dome forming tools and experimental analysis with one the benchmark fabrics. The experimental analysis includes the dry fabric forming experiments and the exploitation of 3D optical strain measurement for measuring the shear angle of fabrics after deformation.

The hypoelastic law has been used over a period of time to analyse numerically the woven fabrics and possesses its established credibility. Originally, its exploitation to analyse the woven fabrics was introduced by Hagège [HAG04]. The analysis was carried out with update of single fibre axis using hypoelastic law. The single fibre axis was mainly used for meso-scale analysis of textile fabrics. However, evidently the woven fabrics have factual form of bi-

directional material data. In this particular research work the hypoelastic law has been applied to take into account the bi-directional fibrous material data.

In this regard, two methods of analysis have been proposed and tested numerically during the present work. The first approach considers only the update of single fibre material but has been supplemented with two superimposed elements sharing the same set of nodes. These elements have different fibre directions and therefore can serve to simulate the deformation of a bi-directional material. The second approach is the standard one and has the bi-directional material data and update of two fibre directions in the same and single element.

The development of double dome forming tools to carry out experimental tests and to validate numerical model has interestingly been a very valuable research application. Although, the exercise of in-house development of forming tools expanded over a hectic time span yet the ultimate results proved to be very useful and are rarely carried out. The successful comparison of simulation results with experimental output has indeed ultimately valued the developed numerical model.

1.3 Outlines of the Thesis

This report has concisely been outlined to focus over the subject and the efforts are made to rationally elaborate the presentation of the work.

Chapter 2 discusses the important textile reinforcement geometries used in textile composites. Then the mechanical properties and deformation modes of textile reinforcements are described in detail along with the tests used to measure these specific mechanical properties are illustrated. The composite forming processes with special emphasis on RTM (Resin Transfer Moulding) is also described in this chapter. The woven reinforcement modelling scales and approaches are presented in depth pertinent to the thesis subject. To the end of this chapter, the recently developed finite element models using continuous approach are discussed in detail.

Chapter 3 specifically treats the detail of numerical model developed and used in this research work. In the start, a few specificities of explicit dynamic scheme are discussed. Then the hypoelastic approach is presented along with its objectivity and its use for fibrous materials. The stress computation algorithm developed for fibrous materials is described explicitly which was used through a user material subroutine in a commercial finite element code. Some important elementary tests were conducted to validate the algorithm output. Two de-facto standard tests of picture frame and bias extension to characterise the in-plane shear behaviour of fabrics conducted numerically for woven composites are presented.

Chapter 4 presents the contributions made for experimental forming analysis of woven composite reinforcements. This introduces the benchmark forum for woven composites, the benchmark fabrics and their shear characterisation study, and derivation of shear modulus. The double dome benchmark geometry is also presented. Afterwards, the in-house development of double dome forming tools is described. The fabric forming experiments carried out using plain weave fabrics of commingled glass/polypropylene are presented in detail. This chapter is concluded by presenting the exploitation of 3D optical strain measurement (OSM) method, using digital image correlation (DIC) system of Vic-3D, for measuring the shear angle of the fabrics is presented.

Chapter 5 deals with the finite element forming simulations of the woven composite reinforcements using the case study of double dome benchmark. The numerical results are compared with the experiments conducted using the same benchmark geometry. This validates the authenticity of the numerical model developed. The parametric sensitivity study is one the important subjects in case of fabric forming simulations. The study has been conducted in order to optimize the process parameters and elaborates their influence within the scope of the continuous approach. Finally, the presentation of some very important conclusions is made as a result of this study.

2

Textile Composites: The Current and Potential Use

2.1 Introduction

The textile composites are used to describe a broad range of materials based on textile reinforcements and polymer matrix (thermoplastic or thermoset). The reinforcement includes woven and non-crimp fabrics to three dimensional textiles. A woven fabric is a planar textile structure produced by interlacing two or more sets of yarns, fibres, rovings or filaments where the elements pass each other usually at right angles and one set of elements is parallel to the fabric axis. Non-crimp fabrics consist of juxtaposed yarn or fibre layers to avoid undulations and maintained together with fine thread stitches. Three-dimensional textiles are the thick knitted yarns produced for specific applications. The fibres are the basic constituents of the textile reinforcement and alone can exhibit essentially tensile properties along their length in the same way as fibres in a rope.

Polymer matrices are usually the resin systems such as epoxies and polyesters have limited use for the manufacture of structures on their own, since their mechanical properties are not very high when compared to most metals. However, they have desirable properties, most notably their ability to be easily formed into complex shapes. It is when the resin systems are combined with reinforcing fibres such as of glass, carbon and aramid that the exceptional properties can be obtained. The resin matrix transfers the load applied to the composite between each of the individual fibres and also protects the fibres from damage caused by abrasion and impact. High strengths and stiffness, ease of moulding complex shapes, high environmental resistance all coupled with low densities, make the resultant composite superior to metals for many applications.

Typical applications of textile composites range from structural parts for high volume cars to high performance aerospace components. The current research activities regarding textile composites are mainly focused on prediction of processing and mechanical properties, process modelling and the interactions between manufacture and performance. For a general textile structure, material models are developed based on a geometric description. These are then implemented within models for draping/forming and subsequent performance. Process modelling for textile composites includes both formability (to eliminate wrinkles and tears) and impregnation (to eliminate dry patches or lengthy fill times). In this chapter, we shall principally confine our study to the textile reinforcement due to the subject requirement.

2.2 Textile Reinforcement Geometry

Textile reinforcements serve as reinforcing constituents to the textile composites. The forming potential and structural performance of reinforcement is determined by its material, shape and fibre configuration. Textile reinforcement is a heterogeneous hierarchical structure: continuous fibres are assembled to fibre bundles, called yarns or tows that are in turn interlaced in a periodic configuration. In the traditional textile industry, yarns are twisted to provide structural integrity and the ability to hold shape. In forming structural composites, in contrast, softer yarns are desirable, since this allows compaction to maximize the total volume fraction or flattening (especially in braids) to maximize coverage. Furthermore, twist would reduce the axial stiffness of yarns, which is paramount in airframe applications. Therefore, yarns with minimal or nominally zero twist (tows) are preferred. Among the family of textile reinforcements for composite materials the notable fabrics are detailed as under.

2.2.1 Woven Fabrics

Woven fabrics are produced by the interlacing of warp (0°) and weft (90°) fibres in a regular pattern or weave style. The fabric's integrity is maintained by the mechanical interlocking of the fibres. Drape (the ability of a fabric to conform to a complex surface), surface smoothness and stability of a fabric are controlled primarily by the weave style. The following is a description of some of the more commonly found weave styles:

a) Plain weave

Plain weave has the warp and weft yarns interlaced alternately in a regular repeated manner as shown in Fig. 2.1. It is also known as one-up-one-down weave or over and under pattern. In the balanced plain weave, the warp and weft yarns are of equal tension and spacing and it is equally visible on the surface. The fabric is symmetrical, with good stability and reasonable porosity. However, it is the most difficult of the weaves to drape, and the high level of fibre crimp imparts relatively low mechanical properties compared with the other weave styles.

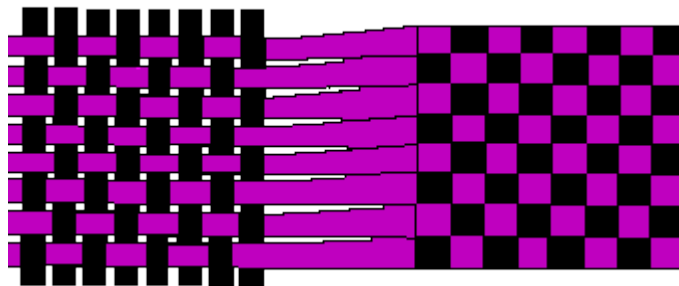


Fig. 2.1 Plain weave fabric

b) Twill weave

This is characterized by producing the visual effect of parallel diagonal ribs formed left-to-right or right-to-left as shown in Fig. 2.2. One or more warp fibres alternately weave over and under two or more weft fibres in a regular repeated manner. The resulting fabric is more pliable and drapable than the plain weave with only a small reduction in stability. With reduced crimp, the fabric has a smoother surface and slightly higher mechanical properties than of plain weave due to increased lengths of straight segments of yarn (float). Twill weave which has more warps than the wefts floating on the face of the fabric is called warp faced and those with wefts predominating is known as weft faced.

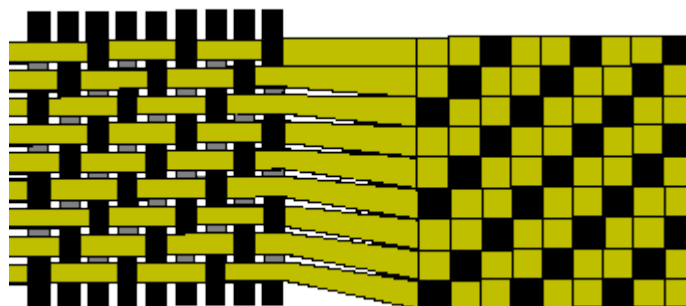


Fig. 2.2 Twill weave fabric (warp-faced)

c) Satin weave

These are fundamentally twill weaves modified to produce fewer interactions of warp and weft. In this weave construction, the interlacing of the yarns is arranged in such a way that the face of the fabric is covered with the warp yarn or filling yarn and no twill line is distinguishable. The ‘harness’ number used in the designation (typically 4, 5 and 8) is the total number of tows/yarns crossed and passed under, before the fibre repeats the pattern. Satin weaves are very flat, have good wet out and a high degree of drape. The low crimp gives good mechanical properties. Individual layers of satin weave fabric are asymmetric. One side of the fabric is predominantly warp yarns; the other fill. Exchange sites also break symmetry because they bend yarns in an asymmetric way. Bending and stretching in a satin weave ply are consequently coupled. There is also coupling between stretching and in-plane shear, because exchange locations are not symmetric about either in-plane axis as shown in Fig. 2.3. Coupling between bending and stretching will tend to cause warping during cure because of thermal strains. Warping can be minimized in a multilayer laminate by considering which side of each ply should face the tool [COX97].

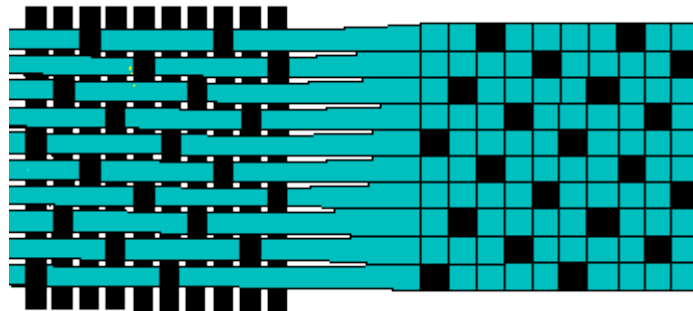


Fig. 2.3 Satin weave fabric

2.2.2 Non Crimp Fabrics (NCF)

The term ‘‘non-crimp’’ implies that the fibres in each lamina are ideally straight and have no or very low waviness perpendicular to the general fibre direction as shown in Fig. 2.4. Multi-axial fabrics which consist of a number of unidirectional plies are arranged in various orientations (Fig. 2.5). The individual plies in these fabrics are kept together by stitching yarns. NCF composites are manufactured from preforms (blankets) with multiple layers of straight fibre bundles with different orientations stitched together by a warp knitting procedure. This manufacturing procedure creates a material which is heterogeneous not only at the micro-scale but also at the meso-scale due to the bundle structure in the layers. NCF

composite has continuous fibres combined in fibre bundles with well defined geometry. One of the features of the NCF composite is that it is an inherently multiscale material. Each layer due to stitching is divided in fibre bundles.

Despite the name - Non-crimp - a certain amount of fibre crimp is present in the fabric and in the final composite. This yarn crimp is defined as the relative difference in length between the yarn and the fabric:

$$C = \frac{L_y - L_f}{L_f} \quad (2.1)$$

Where:

- C is the yarn crimp,
- L_y is the length of the yarn in the fabric and
- L_f is the length of the fabric

NCF composites combine fairly good mechanical properties with low production costs, high deposition rates and virtually unlimited shelf life. In addition to these benefits, NCF composites have also been reported to show high out-of-plane fracture toughness and damage tolerance [MAT08]. Combination of uni-directional placement of fibres in plies with consolidation of the preform by stitching leads to a highly advantageous combination of properties, allowing the possibility to employ an RTM-like process in production and full use of fibre modulus and strength in the ready part.

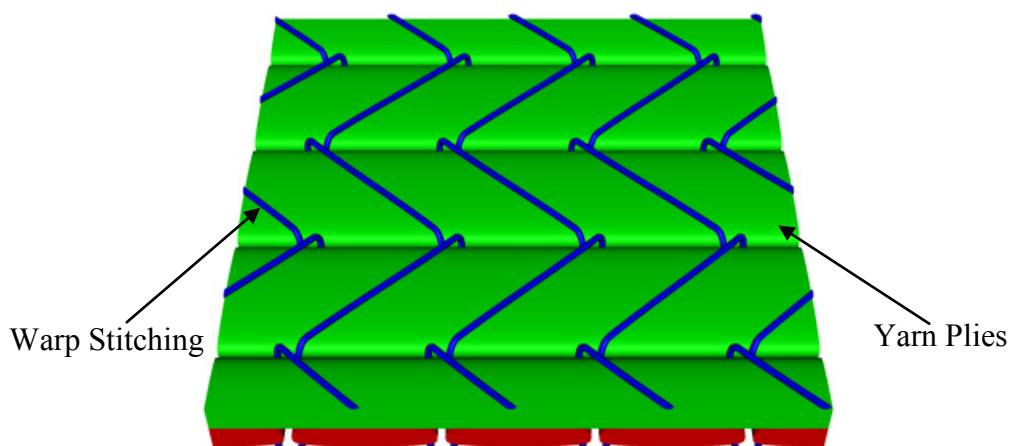


Fig. 2.4 Non-Crimp Fabric (NCF)

The ability to place fibres on 0° , 90° , $+45^\circ$, -45° , (see figure 2.5) means engineers can design composite laminates to handle loads from both the known and unknown directions.

Quadraxial reinforcements are closer to the traditional building materials like steel and aluminium i.e. equal strength in all directions.

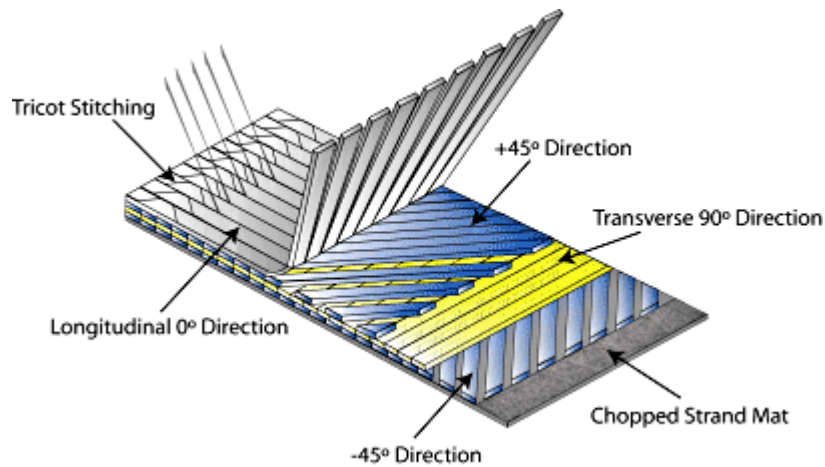


Fig. 2.5 Stitch bonded example, multi-axial. Typical quadraxial ply stack includes 0° , 90° , $+45^\circ$, and -45° plies

2.2.3 3D-Fabrics

When the thickness of a composite part is large, the use of laminated composites is restricted by manufacturing problems and their low resistance to delamination cracking. To overcome these difficulties composites with 3D fibre architecture called ply-to-ply interlock fabric are proposed as shown in Fig. 2.6. Indeed, this material is not fully 3D since there is no third yarn set in the transverse direction but the properties through the thickness are much improved. 3D-fabrics are most commonly manufactured by textile techniques of weaving, braiding, stitching and knitting [MOU99]. Solid 3D woven fabrics, which can be made on commercial machinery either as flat panels or 3D shapes, are of increasing importance in composites. They give a potential for reductions in aircraft weight and have significant applications in military hardware. The stimulus to development given by these uses opens up possibilities in automotive, construction, medical and many other fields. For some forms, braiding is an alternative to weaving. With advances in knitting the whole reinforcement can be produced so that stitching together of separate pieces is eliminated.

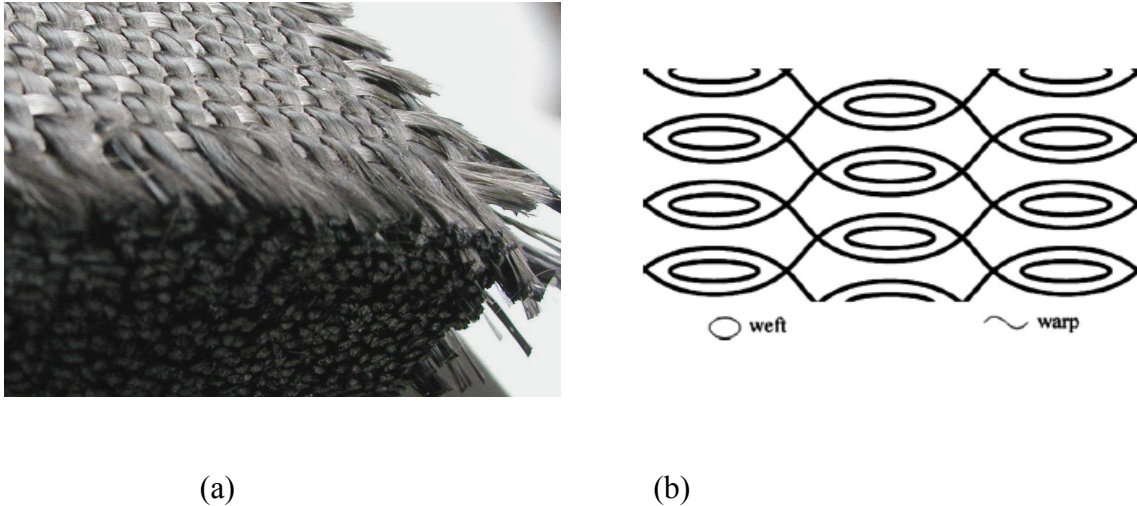


Fig. 2.6 (a) Large thickness (3D) interlock preform, (b) Basic architecture of an interlock preform [DEL09]

2.3 Mechanical Properties of Textile Reinforcements

The textile reinforcement structure is composed of discontinuous matter, relative movement of fibres in yarns, intertwining of yarns and its constitution into a network of textile reinforcement imparts it the specific mechanical properties and deformation mechanisms. In the study of the mechanical behavior of woven reinforcements, there are three levels of observations important for understanding the mechanisms of deformation: the fibres, the yarns and the fabric.

The micro-scale is confined to fibres constituting the yarns and are of the order of 10 μm . These are considered as the basic elements for forming textile reinforcement. The meso-scale is made up of yarns which constitute to form a fabric and are of the order of a few millimeters. This scale represents also the unit cell of the fabric which when repeated continuously makes the whole fabric. The macro-scale is of the fabric itself which has dimensions from a few centimeters to some meters and forms the final shape of the part. The reinforcement at macro level looks like a continuous media which can be bi-dimensional or tri-dimensional. This scale will be treated in detail here as a point of interest for studying the forming processes for textile reinforcements.

2.3.1 Deformation Mechanisms

Since the constitution of the textile reinforcements is special from geometric point of view therefore the deformation mechanisms are also very specific. Some well-known deformation mechanisms of textile reinforcements are detailed as under:

a) In-plane shear

In-plane shear occurs when there is a change in angle between the strong anisotropic directions of the fabric yarns during deformation. For a 2D weave, for example, the change in angle between the warp and weft yarns is called as shear angle γ and is equal to the difference of the enclosed angle ψ between the two yarn directions before and after deformation (Fig. 2.7).

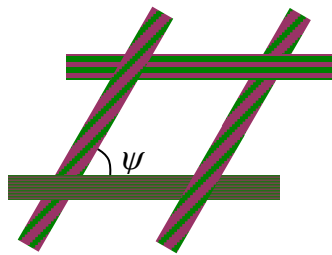


Fig. 2.7 In-plane shear of a fabric with enclosed ψ angle between the yarns

Initially the warp and weft yarns are usually perpendicular to each other, therefore shear angle is:

$$\gamma = \frac{\pi}{2} - \psi \quad (2.2)$$

In-plane shear mechanism of deformation is of a very particular importance which not only affects the subsequent steps of textile composite manufacturing but also determines the strength and performance of final product. The in-plane shear rigidity of textile reinforcement largely depends upon the shear angle between the network of woven yarns. The rigidity is small up to a certain amount of shear, for example 35° to 40° of shear angle, depending upon the nature of weave (Fig. 2.8). After this a stage, the shear angle reaches to a threshold value called “shear locking” where the yarns are under lateral compression and the in plane fabric rigidity enhances rapidly.

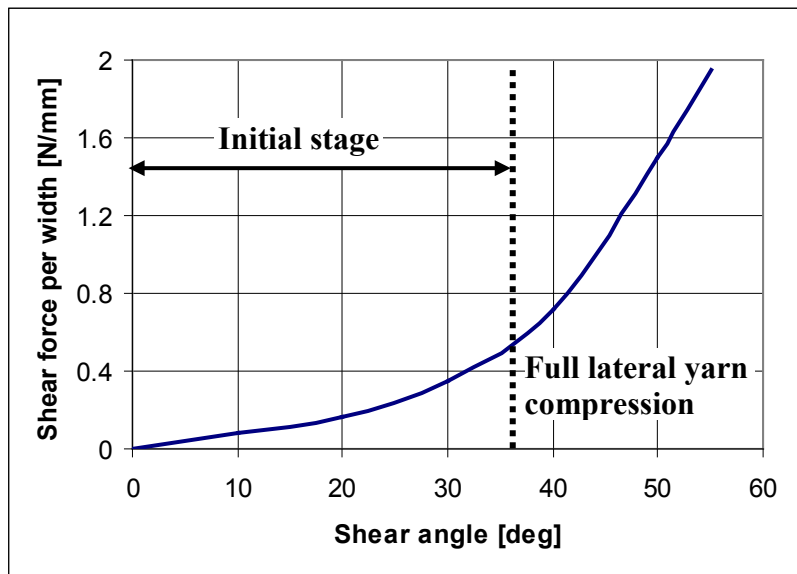


Fig. 2.8 Typical shear behavior stages of a fabric with shear angle evolution

The shear locking eventually leads to out of plane deformation phenomenon called wrinkling or buckling. Wrinkles arise when a non-uniform stress state causes lateral compressive stresses beyond a critical load limit, depending on the material properties and the plate dimensions. The wrinkling is thus an instability phenomenon, governed by the balance between the bending resistance and the membrane deformation resistance. Wrinkles are undesired in textile testing leading to inhomogeneous loading and in composite processing deteriorate mechanical and surface properties.

b) Biaxial tension

The textile reinforcements, for example woven preforms, have yarn undulations because of woven architecture. When a fabric is subjected to a tension, the undulated yarns tend to become straight. That leads to a non-linear tensile behaviour at the beginning of the loading. Because the yarns are woven and undulated in both warp and weft directions, the phenomenon is biaxial. A biaxial tensile device on cross shaped specimens gives the tensile curves for different ratios of strains using biaxial specimens (Fig. 2.9).

The non-linear macroscopic load-strain response is a consequence of the yarn crimp or waviness within the textile, leading to a low initial stiffness zone as long as yarns are being

straightened, but once the straight yarns are being stretched the response changes into a steep linear response.

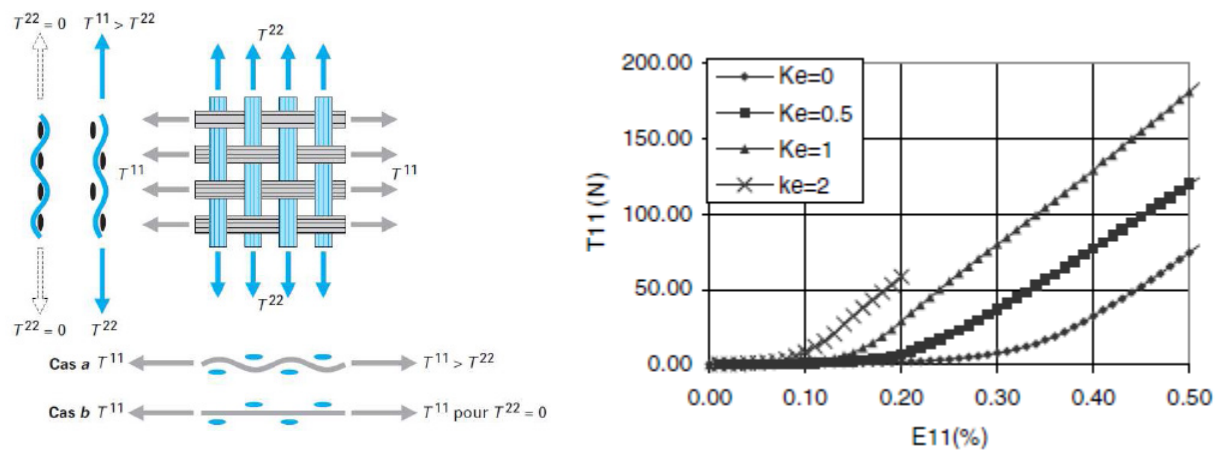


Fig. 2.9 Experimental biaxial tension for a glass plain weave (K_e is the ratio between the weft strain E_{22} and the warp strain E_{11}) [HIV08].

The crimp exchange (i.e. exchange of waviness between the different yarn families) depends on the textile structure, the yarn compressibility and yarn bending stiffness. Due to the crimp exchange the tensile resistance in one yarn direction is affected by the load imposed in the other yarn direction and vice versa, a phenomenon referred to as biaxial tensile coupling. In general, the more tensile load in one yarn direction, the less de-crimping or more crimping occurs in the second yarn direction, leading to a shorter stiffening zone in the second yarn direction as shown in Fig. 2.9.

c) Transverse compaction

Transverse compaction of a textile reinforcement is also a non-linear phenomenon which occurs easily in the start when the yarns are compressed enough (increasing the density of fibres) and it is limited very rapidly. This mode of deformation is important in liquid molding processes because after dry forming the preform is pressed before resin injection in order to increase the fibre volume fraction in the final piece. The textile prepregs are also compacted to reduce the air entrapment or voids. Knowledge of the compaction behavior is necessary to estimate the required pressure to obtain a specific composite thickness or void reduction. For structural applications, it is important to obtain acceptable void content, typically $< 1\%$ for aerospace applications [LIU06].

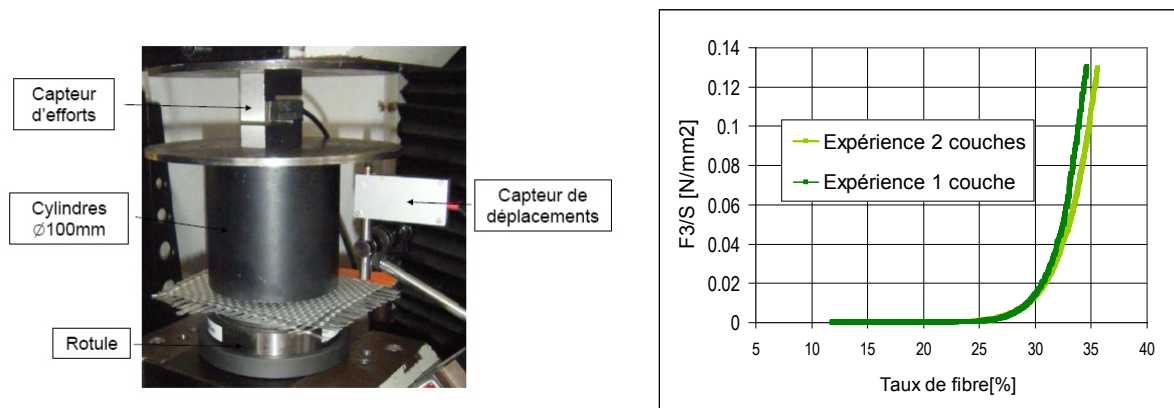


Fig. 2.10 The experimental test setup and results of transverse compression over one and two layers of plain weave fabric [LOA08].

d) Bending

The out-of-plane bending stiffness is typically very low for two dimensional textiles or textile preregs. Therefore the bending stiffness is often neglected in FE forming simulations by selecting membrane elements. However, the tendency to develop thicker 3D textiles or layered sandwiches with textile reinforced skins makes the topic very relevant. When using finite elements with out-of-plane stiffness, like shells, it is important to assign realistic bending resistance values. The out of plane rigidity plays a role important in the development of wrinkles in the forming processes of textile composites. [HAM09] has introduced bending stiffness in a triangular element, without supplementary degree of freedom, by using the positions and displacements of the neighboring nodes to define the curvature. He has shown with an example of airbag simulation that the bending stiffness can better describe the forming of wrinkles as shown in Fig. 2.11.

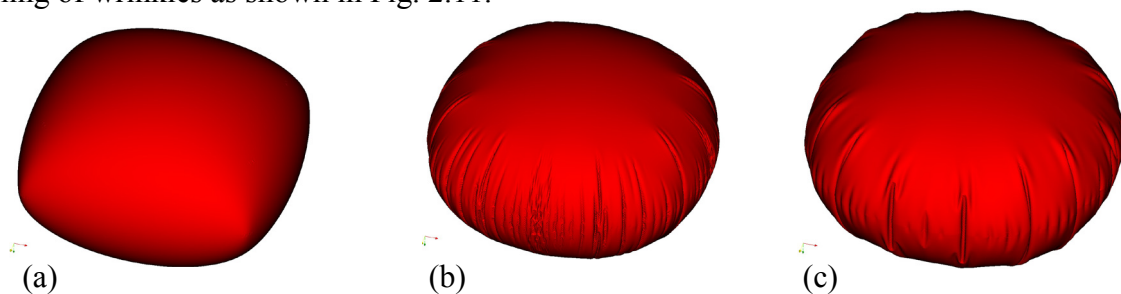


Fig. 2.11 Airbag simulations (a) without shear (b) with shear and (c) with shear and bending stiffness [HAM09]

e) In-plane shear coupled with tensions

In-plane shear behaviour of a fabric changes with tensions induced along the yarn directions. In fact, the shear behaviour of a fabric is largely influenced by the shear resistance that exists between the yarns. Although, the architecture of the textile reinforcement plays an important role yet the rotation of yarns during fabric shear are much affected by the perpendicular pressure at crossovers. The study of the affects of pre-tensions on the in plane shear behaviour of a fabric has recently got attention [LAU08] [WIL08]. The results shown by these studies prove that the shear load is increased by the tension in the yarns especially in the first part of the shear curve (small and medium shear angles). This result is not surprising because the shear rigidity is for a part due to frictions between the yarns (especially in the first part of the curve). When increasing the tension in the yarns, the weaving brings a transverse compressive force, and consequently, the friction loads, and therefore, the shear stiffness increases. This phenomenon is also important in the dry forming of the reinforcements with the use of binder force which increases the membrane tensions of the fabric and consequently its in-plane shear stiffness increases. Another important consequence is to circumvent of wrinkles achieved through binder force which indirectly is related to the membrane tension.

f) Non-sliding between warp and weft

This is one of the hypotheses considered in the deformation mechanisms of woven reinforcements i.e. the warp and weft yarns do not slide with respect to each other when deformed. The tests conducted in case of forming of woven reinforcement indicate that the lines drawn perpendicular to each other over fabric before deformation remain continuous after deformation as shown in Fig. 2.12 This hypothesis is important because it permits utilizing the continuum models for simulation of the woven composite reinforcement forming.



Fig. 2.12 Illustration of non-sliding of warp and weft yarns in a fabric forming experiment

2.3.2 Characterization of Mechanical Properties

The principal mechanical properties both of tensile and shear for the textile reinforcements are non-linear and multi-scale. The characterization of these global properties requires special test methods and test devices detailed hereby.

a) Biaxial tensile device

The mode of biaxial tensile deformation of woven reinforcements, as explained in sec. 2.3.1b, necessitates a special measuring device called biaxial tensile device shown in Fig. 2.13. Since the tension along first direction of yarns is influenced by the deformation along the second direction so it becomes imperative to measure quantitatively the effect of one over other.

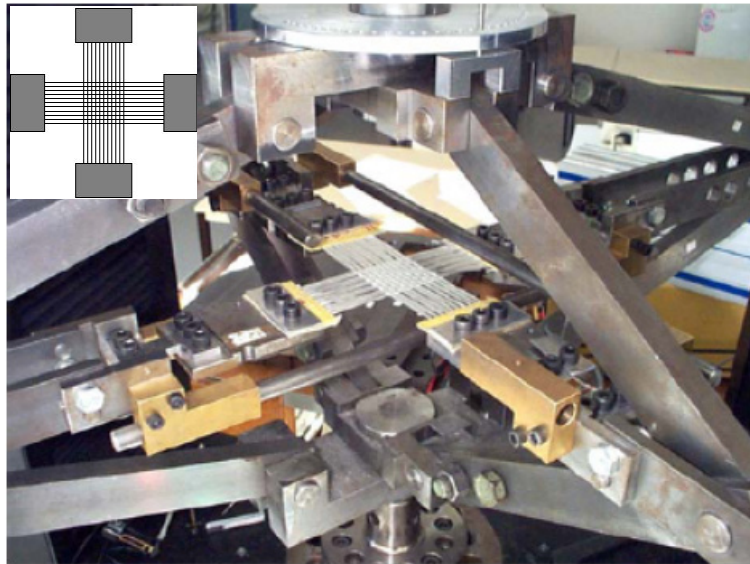


Fig. 2.13 Biaxial tensile device for characterization of tensile properties [BUE01]

The tensile stiffness of a fabric, as it is evidently known, is of the most significant amount compared with other rigidities like shear and bending. Hence, accurate measure of this property is also of a great importance. By using biaxial tensile device it becomes possible to adopt a range of coupled deformations i.e. equal or different ratios of deformations along the two principal directions of yarns. This biaxial tensile effect has been studied in detail by many researchers [BUE01] [WIL08]. When one of the yarn directions is pulled, it tends to de-crimp its waviness and becomes straight if the other direction is left un-stretched. The non-stretched yarns become more undulating and consequently the fabric is under equilibrium. This biaxial effect with different strain ratios along two yarn directions is shown in Fig. 2.9. The

undulation of yarns is due to the geometrical configuration of the yarns and it is a mesoscopic phenomenon. This effect is also related to the re-arrangement of fibres, at least over the points of intersection of yarns, so a microscopic effect is also created. These two phenomena contribute to produce an overall deformation of the fabric called macroscopic effects of biaxial deformation.

b) Shear deformation

Shear deformation of a textile reinforcement is the most significant and important mechanism of material characterisation. The forming processes of a woven fabric induce large in-plane shear angles which enable the reinforcement to conform to complicated contours and non-developable complex shapes. Therefore, it is of vital importance to characterise appropriately this mode of deformation and material property. The shear behaviour characterisation of woven reinforcements is carried out using two de-facto standard tests of picture frame and bias extension. The specificities these tests are presented here in detail.

Picture frame test [NGU99] [PEN04] is one of the two tests used for characterisation of the shear resistance of composite reinforcements measures shear behaviour of the fabric in a wide range of shear angles, up to 50° - 60° , sometimes even up to 75° . The scheme of the test is shown in Fig. 2.14.

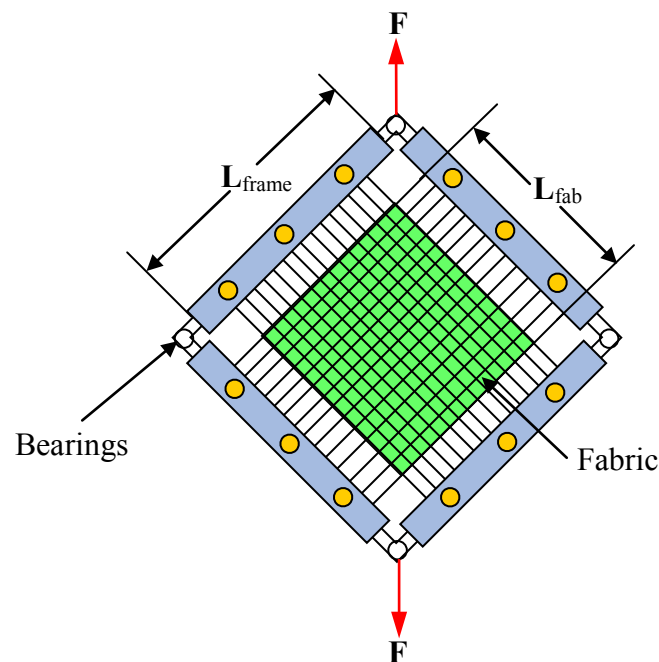


Fig. 2.14 Schematic diagram of picture frame test

In picture-frame test, the fabric sample is initially square and the tows are oriented in the $\pm 45^\circ$ position to start the test. The fabric is clamped in the frame, which is mounted on a tensile machine. The load registered by the load cell of the tensile machine is recalculated into shear force (per unit fabric width) using the kinematic scheme of the frame, equivalence of the mechanical work and the shear deformation energy of the fabric (assuming homogeneous deformation state) and a normalisation method. When processing the results, two assumptions concerning the deformation of the fabric sample are made:

- The shear deformation of the sample is homogeneous.
- The average shear angle of the fabric is the same as the shear angle of the frame.

Geometrically, the shear angle (radians) of the deformed picture frame with a vertical displacement of “d” is calculated as:

$$\gamma = \frac{\pi}{2} - 2 \cdot \cos^{-1} \left(\frac{\sqrt{2} \times L_{\text{frame}} + d}{2 \times L_{\text{frame}}} \right) \quad (2.3)$$

The normalization of the shear force [PEN04][HAR04] is calculated as:

$$F_{\text{nom}} = \frac{F}{2 \cdot \cos \theta} \cdot \frac{L_{\text{frame}}}{L_{\text{fab}}^2} \quad (2.4)$$

The normalization procedure is adopted in order to compare the test results produced from different sample sizes and picture frame dimensions.

Bias extension test [WAN98] [PEN05] is performed with a rectangular test fabric having dimensions of twice or more along length compared with its width. In this test, a tensile test is performed in which the warp and weft directions of the tows are orientated initially at $\pm 45^\circ$ to the direction of the applied tensile load.

When the specimen is stretched from L to $(L + \delta)$ the possible motion between the yarns and their large tensile stiffness lead to a deformed shape as shown Fig. 2.15. In zone A the warp and weft yarns have both a clamped end and there is no deformation in this zone. The zone C is the active zone of the test. The warp and weft yarns have free ends. The non-sliding at crossovers and the global stretching of the specimen leads to a pure shear deformation related to δ : the displacement of the mobile grip. In zone B, one yarn direction is clamped at one end, the other direction is free at both ends. The global stretching of the specimen leads to a shear

strain of a value half of that of the zone C. In this test the zone C is in pure shear. The first advantage of this test with respect to the picture frame lies in its simplicity of implementation. In addition the yarns of the central zone in pure shear are free at their ends. Consequently they are not subjected to tension (or to very weak one). The nature of the test thus leads more naturally to a shear state without tension than the picture frame test.

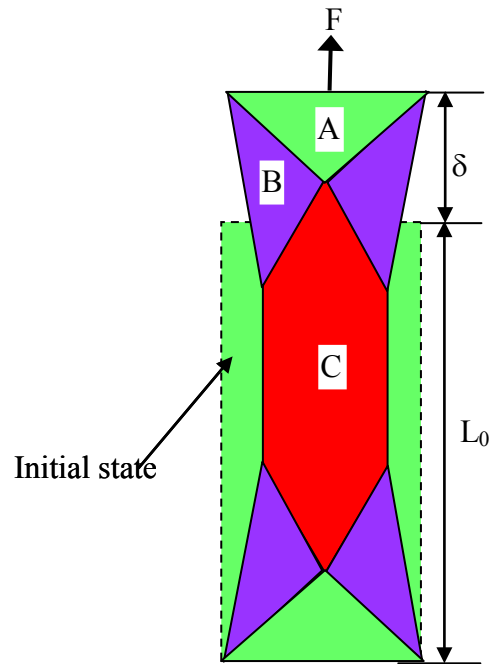


Fig. 2.15 Bias extension test with three zones evolved during deformation

Conversely the intermediate zones B makes the test analysis more delicate because the force measurement on the machine is global and concerns the deformation of all zones at the same time. The measures of both the load on the tensile machine and of the shear angle give the shear load per unit fabric width [CAO08].

The shear angle (radian) in the pure shear zone C, for the end displacement δ , can be calculated as:

$$\gamma = \frac{\pi}{2} - 2 \cdot \cos^{-1} \left(\frac{L_0 + \delta}{\sqrt{2} \times L_0} \right) \quad (2.5)$$

Where, L_0 is the difference between the length and width of the undeformed specimen.

2.4 Composite Forming Processes

The end properties of a composite part produced from different materials (constituents) is not only a function of the individual properties of the resin matrix and fibre but is also a function of the way in which the materials themselves are designed into the part and on the other hand, the way in which they are processed. The high performance domains such as aeronautics require structural components with high load bearing capacity, complex shapes and without defects. Autoclave curing has long been the "gold standard" for aerospace composite parts. However, the capital cost for the autoclave is high, and fibre placement equipment is usually even more expensive. So, there emerged a need for alternative processing methods that can reduce costs while maintaining the high performance of autoclave-cured components. Within the last few years, liquid composite molding (LCM) technologies have advanced to the point where they can provide that alternative. LCM processes are characterized by the injection of a liquid resin into a dry fibre preform, and include resin transfer molding (RTM) and vacuum-assisted RTM (VARTM).

In VARTM, the upper half of the mould is replaced by a vacuum bag. The vacuum pump is installed to expel air from the preform assembly. After the system has been equilibrated and all air leaks have been eliminated, the resin is allowed to flow into the preform. A pressure of usually 1 atm provides both for driving force for the resin to impregnate the reinforcement and the compression force to compact the preform to the desired fibre volume fraction. The vacuum is left on until the resin is completely gelled. The part may then be cured at room temperature or in an oven. VARTM is claimed to have advantages of lower tooling cost, shorter start-up time and for manufacture of large-scale components. Among the disadvantages are: the complex process to perform well, flexible nature of vacuum bag makes it difficult to control the final thickness and thus the fibre volume fraction of the preform.

2.4.1 Resin Transfer Moulding (RTM)

Resin Transfer Moulding [POT99] process begins with a two-part, matched, closed mold, made of metal or composite material. Dry reinforcement (typically a preform) is placed into the mold, and the mold is closed. The polymeric resin is then pumped into the mold under low

to moderate pressure (of the order of a few Bars, 1-5) through injection ports, following predesigned paths through the preform. Resin injection pressure depends on the resin viscosity, permeability of the porous media, mould fill time needed and cure kinetics of the resin. Vent ports, connected to a vacuum pump, evacuate trapped gases and excess resin. Extremely low-viscosity resin is used in RTM applications for thick parts, to permeate preforms quickly and evenly before cure. Epoxy resins have been the predominant matrix in textile composites manufactured by RTM or RFI for commercial aircraft structures. Epoxies meet the requirement of having a low-viscosity state (100-500 cps), which is crucial for flow through a low permeability preform with complete wetting of the fibres. Both mould and resin can be heated, as necessary, for particular applications. RTM produces parts that do not need to be autoclaved. A curing reaction is initiated, either after completely filling the mould cavity, or possibly at some stage during impregnation. After the piece is sufficiently cured, the finished composite product can be removed from the mould. However, once cured and demolded, a part destined for a high-temperature application usually undergoes post-cure. Low injection pressure, coupled with vacuum, allows the use of less-expensive, lightweight two-part moulds.

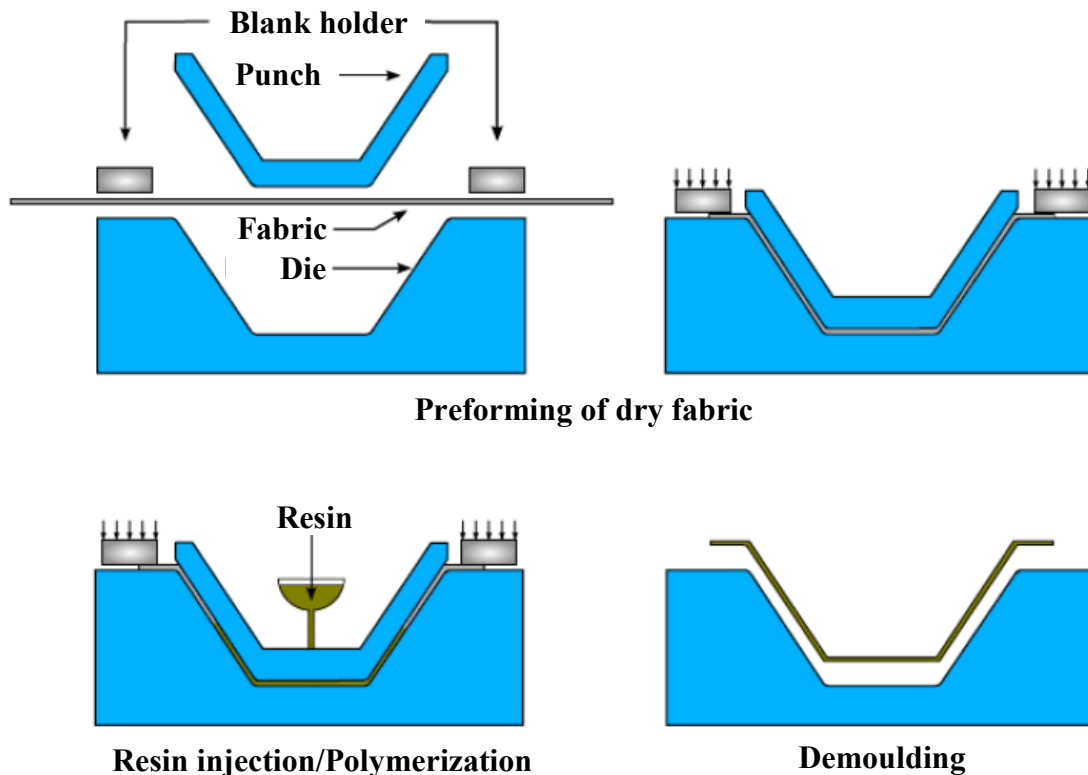


Fig. 2.16 Schematic stages of Resin Transfer Moulding (RTM) process

In a successful RTM process, the preform is fully wetted with resin, but achieving full wetting can be challenging in a complex part. Resin flow is controlled by the permeability of the fibre preform and the viscosity of the resin. Permeability is higher for low fibre volume fractions, but of course high fibre volume is usually demanded to maximize structural performance. Despite this conflict, high quality parts have been made with fibre volume fractions exceeding 60% [GIL09]. Success often depends on having good process models to identify the optimum location of injection and venting ports.

The benefits of RTM are impressive. Generally, dry preforms for RTM are less expensive than prepreg material and can be stored at room temperature. The process can produce thick, near-net shape parts, eliminating most post-fabrication work. It also yields dimensionally accurate complex parts with good surface detail and delivers a smooth finish on all exposed surfaces. It is possible to place inserts inside the preform before the mould is closed, allowing the RTM process to accommodate core materials and integrate "moulded in" fittings and other hardware into the part structure during the moulding process. Moreover, void content on RTM'd parts is low, measuring in the 0 to 2 percent range. Finally, RTM significantly cuts cycle times and can be adapted for use as one stage in an automated, repeatable manufacturing process for even greater efficiency, reducing cycle time from what can be several days, typical of hand layup, to just hours - or even minutes.

Fig. 2.16 shows different stages of the RTM process. The first stage is the preforming of the dry fabric and this is very important stage in prediction of mechanical properties of the final structure. In the present study, we shall mainly focus our work on this first stage of RTM process. This stage determines the orientation and density of fibres which significantly influences the subsequent stage of resin injection [HAM96] [HEA01] and knowing the orientation of fibres means predicting the mechanical characteristics of the product because the second stage does not alter the orientation of fibres or yarns.

2.5 Woven Reinforcement Modelling

The constitution of the woven reinforcements requires special FE modelling methods. The simulation tools assign the product quality to textile formability and process conditions

support the design and process optimization. Hence, the modeling of composite forming processes leads to significant cost reduction. The prediction of local textile deformations (fibre orientation, fibre density, fibre volume fraction, thickness etc) on the product during/after forming via drape forming simulation is an essential task.

To predict the final structural performance of the product (stiffness, strength, fatigue etc), knowledge of the local fibre orientations and its distribution density is essential. Furthermore, local deformations during drape forming affect the final product quality. For instance, in a LCM process the local fibre volume fraction governs the permeability during resin injection [SON06], while in a matched die molding process the local thickness determines the pressure distribution, hence friction and consolidation conditions. Therefore FE forming analyses using constitutive models that incorporate the specific macroscopic textile drape behavior are performed to support process optimization. These strive to suggest process conditions that ensure a product without failures (wrinkles, fibre breakage, etc). The ultimate goal is to virtually design the textile (prepreg) system by pursuing a multi-scale material approach that links the macroscopic textile behavior to the textile microstructure and component properties.

Two approaches are used for the drape forming simulation: the mapping approach and the finite element analysis (FEA). The mapping approach is mainly used in industry for fast predictions, but has limited accuracy and can not support process optimization or virtual material design. The more accurate FEA incorporates a constitutive model in a nonlinear FE code, and it may employ a multi-scale material approach.

2.5.1 The Scales of Modelling

There exist three different scales of composite forming analysis [LOM07]. All of them are intended to investigate the mechanical responses of the textile reinforcements during deformation. The scales of reinforcement depend over the nature of its constitution and categorised in order of smallest component to global element. These scales are studied in detail by different researchers and hold their own significance. All three scales will be presented here in order of size.

a) Micro-scale models

The micro-scale is the smallest of three scales designated for the textile reinforcements. This is confined to the smallest constituents of the reinforcement called fibres. The fibres diameter ranges from 5 μm to 50 μm depending upon the type of material. These fibres are

manufactured using the special manufacturing techniques. For example, the present invention of glass fibres includes charging a raw glass batch to a melting zone and forming fibres from the melt. The molten glass is extruded to the bushing, small metal surface containing nozzles, to be formed into fibres. As the fibres are drawn from the bushing, a light water spray is applied so that the fibres are generally cool to the touch, before they pass over the sizing application roller, and then are wound onto a cardboard collection spool to form what is called a package. There exist some modelling studies at this scale [VAN96] [ZHO04] [DUR08] [YUY08] and the problem lies in the very large number of contact elements and computational time.

Fig. 2.17 shows the simulation of the weaving process, based on the microscopic scale approach, considered necessary to determine the unknown initial configuration of the weaving structure. Initially, all yarns are straight and penetrate each other at crossings and their separation is made through contact at normal direction. The forces and displacement applied are then relaxed to obtain an equilibrium configuration of the woven structure.

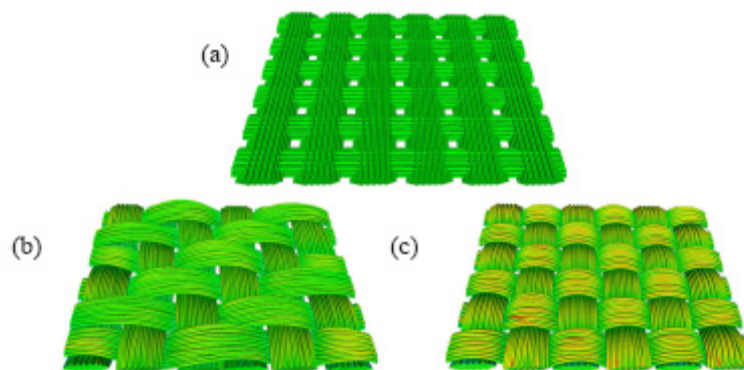


Fig. 2.17 Simulations of the weaving process: (a) configuration before weaving (b) computed configuration for twill weave and (c) for plain weave [DUR08]

b) Meso-scale models

The meso-scale consists of yarns or tows which are made up of a few thousands of fibres (3k to 48k per yarn). This is the scale of a repeat, studying resin-yarn and yarn-yarn interactions; typically 0.5–10 mm. The meso-scale sometimes ranges up to the unit cell of the fabric which is repeated continuously to make a fabric. Textile architectures of greater complexity need to be modelled: as three-axial and three-dimensional weaves and braids, non-crimp fabrics with complex stitching patterns. The meso-level models define the internal structure of the

reinforcement subdivided into interlacing of the yarns (weave, braiding pattern, stitching structure), variations of the yarn direction and the fibre volume fraction inside the yarns and the fibrous plies within a representative volume element (RVE). Finite element (FE) modelling of textile composites on the meso-level (meso-FE) aims at determining the maximum detail of both the reinforcement geometry and the stress–strain state.

The main features of meso-FE are: (1) meshing of a realistic geometrical model of the reinforcement internal geometry, which represents actual volumes of the yarns, (2) application of micro-homogenisation to calculate local (per finite element) properties of the impregnated yarns, accounting for local fibre volume fraction and orientation and (3) definition of boundary conditions, representing the periodic nature of the reinforcement [BAD07] [LOM08b].

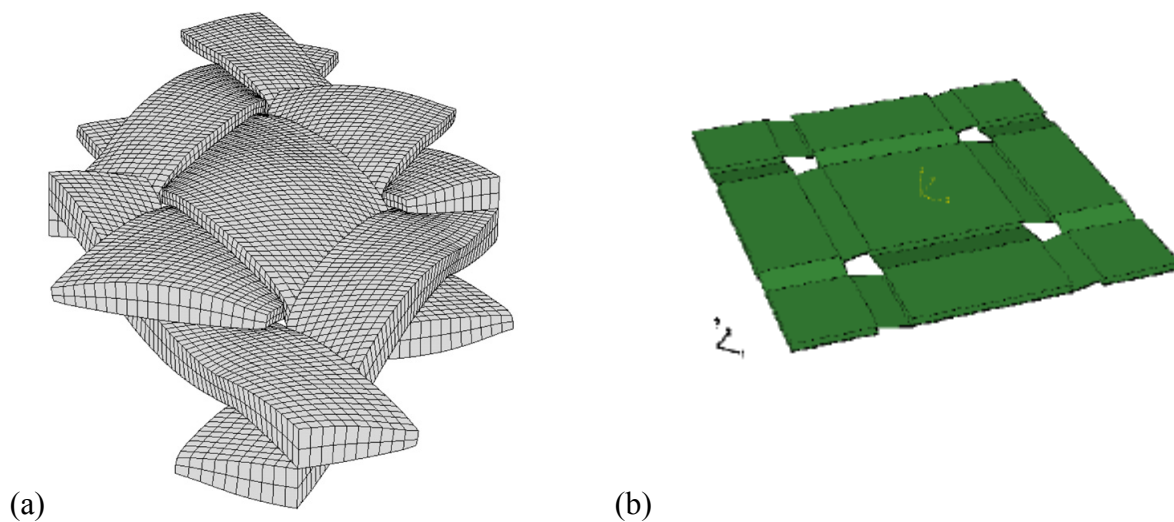


Fig. 2.18 Deformed geometry of a meso-scale in-plane shear test: (a) [BAD07], (b) [GAT09]

Meso-scale models use numerical (FE) or analytical methods to generate a predictive geometrical-mechanical model of a unit cell. In an analytical model the energy contributions due to various meso- (or micro-) mechanisms are summed up and a heuristic energy minimization procedure is used to calculate the macroscopic stress-strain equilibrium [SAG03]. In an FE model the yarn and resin volumes within a unit cell are usually imported from a dedicated textile pre-processing program and consequently solid mesh is generated. Finally boundary conditions and frictional contact are assigned along with an appropriate constitutive law for the yarn and resin [LOM07]. These models require geometrical data of

the textile architecture, yarn mechanical data (tensions, lateral compression, bending) and resin viscosity data (for preregs). The FE meso-model enables the incorporation of more complex yarn geometries, but suffers from mesh penetration difficulties and requires more CPU time. The forming simulations using meso-scale models developed recently at LaMCoS, INSA-Lyon shown in Fig. 2.18b [GAT09], on the other hand reduce significantly the computational time. These models use shell elements and take into account the contact and friction behaviour of the reinforcement at meso-scale which serves to act as in-plane shear property of the fabric. The reduced number of dof in the model makes the computation fast.

Despite a few inconveniences, meso-scale models describe in detail the complex structure of a textile (prepreg) unit cell with finite elements (FE) or analytical equations. These models make use of the insight in the physical phenomena and deformation mechanisms at the meso-scale to predict the macro-scale drape behaviour. Therefore, deeper understanding of mesoscopic behaviour forms a basis for adequate macro-models, used for simulation and optimisation of draping. Meso-scale models have the potential to avoid expensive textile testing for the drape characterization and to virtually design textile prepreg systems. Meso-mechanics can be applied in numerous areas to explain the composite response under forming conditions. Friction between plies and between the laminate and the tooling are the important phenomenon that can be investigated.

Experimental methods of registration of mesoscopic deformations

The mesoscopic deformation mechanisms have also been recorded through full field strain registrations. This is very important to validate the assumed deformation mechanisms with the experimentally observed behaviour on the mesoscopic level. Recent advances in full-field registration of strain using digital image correlation (DIC) in textiles under shear and biaxial tension have made such comparison possible and created confidence in the models [DUM03], [LOM08].

The DIC optical measurement can be performed on a smaller domain and especially on a woven yarn. The main interest of such analysis is to address internal deformation mechanisms of fabrics. It permits to show that the strain in the yarn may be different from the global macroscopic strain in the fabric. The optical strain measurement performed on a smaller domain i.e. a yarn or a unit cell of a fabric is called a meso-scale deformation analysis. Meso-scale DIC allows studying meso-scale deformation mechanisms. Fig. 2.19 shows a DIC analysis performed at the mesoscopic level and presents the incremental displacement field vectors over a specimen under shear.

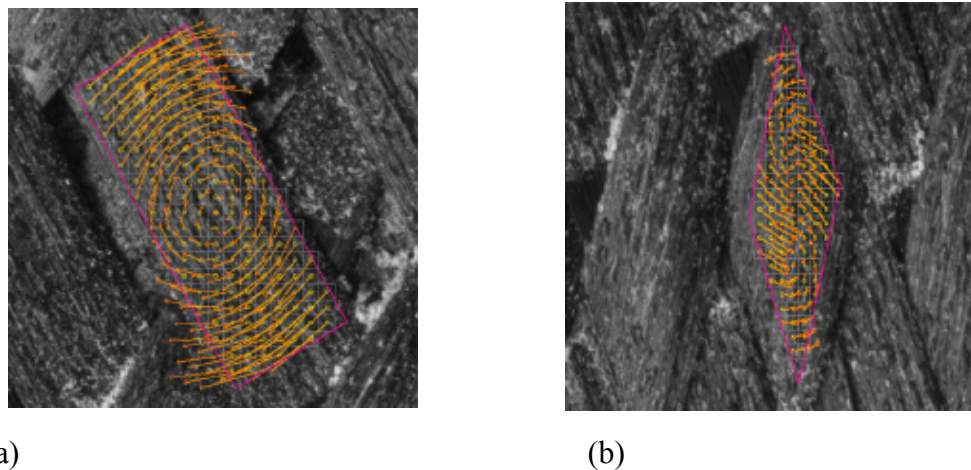


Fig. 2.19 Mesoscopic analysis: displacement fields within a yarn (a) shear angle=35°
(b) shear angle=56° [LOM08b]

c) Macro-scale models

The macro-scale is the full scale of the reinforcement and ranges from few centimetres up to decimetres or even metres. The macro-level models study the phenomenon at the scale of a composite product. Macro-scale models consider a simple equivalent media, i.e. a homogeneous media or a set of elements. The analysis of composite forming processes comes under the category of macro-scale modelling of textile drape behaviour. The macroscopic behaviour is much dependent of possible motion and interactions of yarns at meso-scale (scale of the woven unit cell) and at the micro-scale (level of the fibres constituting yarns). The macroscopic drape behaviour is therefore determined by deformation mechanisms at smaller scales and is typically highly non-linear. Generally a macro-scale material model is implemented in a nonlinear explicit FE package (ABAQUS, LS-DYNA, PAMFORM, etc), and formability predictions are generated via textile testing or via mesoscale models.

The measures at macroscopic scale consider the fabric as a continuum material and mechanical behaviour is measured in shear, tension etc. Macro-scale DIC enable to verify boundary conditions and loading homogeneity. Fig. 2.20 shows the images over macroscopic scale of a bias test and analysis performed with image correlation software ICASOFT developed at LaMCoS, INSA-Lyon by Fabrice Morestin [<http://icasoft.insa-lyon.fr>]. This analysis verifies the existence and position of three different zones evolved during a bias extension test.

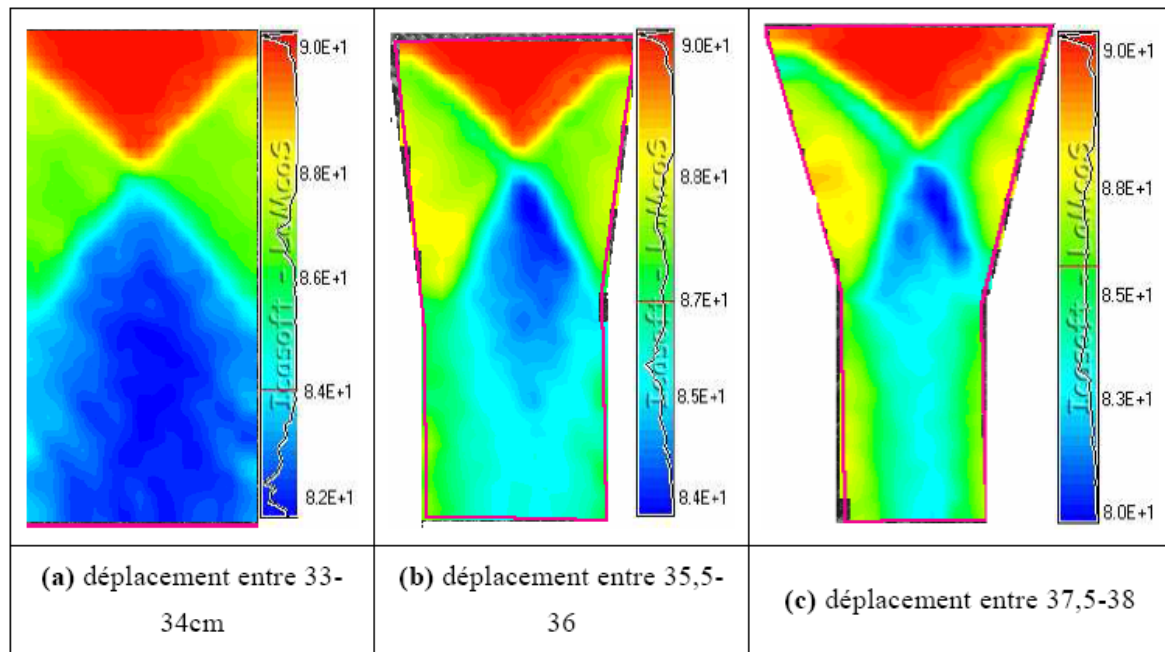


Fig. 2.20 Shear angle measurements in a bias test by image correlation [DEL09]

2.5.2 The Modelling Approaches

There exist different modelling approaches from almost last 4 decades.

a) Kinematic approaches

The kinematic approach also called “geometrical draping approach” is commonly used to predict the resulting fibre re-orientation for double curved fabric reinforced products. In the kinematic models, [ROB84] [VAN91] [POT01], developed to simulate fabric forming, the yarns are assumed to be pinned together at the crossover points of the weave and the yarns are inextensible, incompressible and free to rotate around the pin-joints. Typically, draping starts from an initial point and two initial fibre directions. Further points are then generated at a fixed equal distance from the previous points. By applying strategies, different drape solutions can be found. The model simply predicts the change in the angle between the warp and weft yarns in deformation conforming to different contours. They permit to compute the angle between warp and weft yarns in order to compare this value to a limit angle over which the forming is no more possible without wrinkles. In these methods the fabric is placed progressively starting from an initial line and they provide a close enough resemblance to hand operated draping of classic fabrics and prepregs.

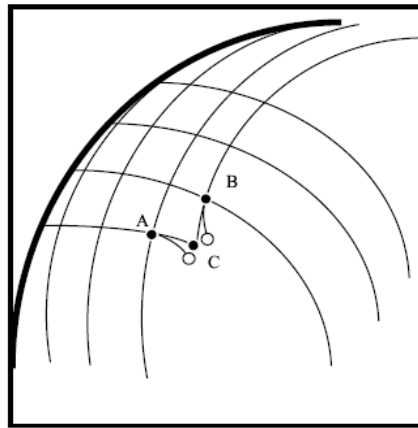


Fig. 2.21 Kinematic approach: the determination of point C with known positions of A and B with the fishnet algorithm.

Fig. 2.21 representing a kinematic approach based on fishnet algorithm shows that the position of node C can be determined if its neighbouring points A and B are with known positions. Segments AC and BC have the known lengths. C is defined as the intersection of two geodesic issues of A and B which cut at C by verifying their lengths. This generates a small problem of non-linear nature which can be solved very rapidly.

This method is fast and fairly efficient but the models do not account for the mechanical behaviour of the woven reinforcement. Therefore, the result will be identical for different type of fabric materials used. Whereas, the results of forming for dry fabrics of prepregs depend largely on material characteristics. The kinematic models are also unable to take into account the loads generated during forming, tool-fabric interactions and binder force effects. Geometrical draping methods therefore are not capable of modelling process specific boundary conditions. To incorporate these boundary conditions FE simulations are used to predict the fibre re-orientation.

b) Discrete approaches

The discrete approaches use FE models of the components of fibrous reinforcement at low scale. These components can be yarns, woven cells or stitching, and also sometimes fibres. Because these elements are usually at the mesoscale, the approach is also known as meso-mechanical modelling. Some analyses have been proposed where all fibres are modelled (microscale modelling) [DUH06], but the number of fibres in a composite structure limits these computations to small sub-domains, for instance a woven cell or a few braided or

knitted loops. A major difficulty lies in the description of the components at mesoscopic scale, usually the woven yarns.

In the discrete approach, the analysis is usually carried out at unit cell level where each yarn or fibre is modelled. The discrete models of fabrics are based on modelling the woven yarns usually described by simplified elements such as trusses or beams connected by torsional or rotational springs [DUR05] [BEN07]. The approach used by Ben Boubaker is to connect nodal masses and rigid trusses via tensile, bending and torsional springs. The model incorporates elastic bending, torsional, shear and tensile resistance. In discrete models the elements are generally connected via common nodes (Fig. 2.22), but sometimes via springs or frictional contact. In [CHE01], the prepreg FE analysis is obtained by the combination of two complementary FE families: elastic (or viscoelastic) 3D membrane FE representative of the resin behaviour and elastic non-linear 3D truss finite element representative of the fibre behaviour. This model has been used to simulate hemispherical dome draping.

The difficulty in accounting for the complex behaviour of woven cells: the large number of components and the contacts with friction confines this approach. The global structure deformation during a forming process will be expensive from the computation point of view and a balance must be established between the precise description and the simplicity of the model used for local components. One of the solutions for forming textile reinforcements with discrete modelling has been proposed in [GAT09].

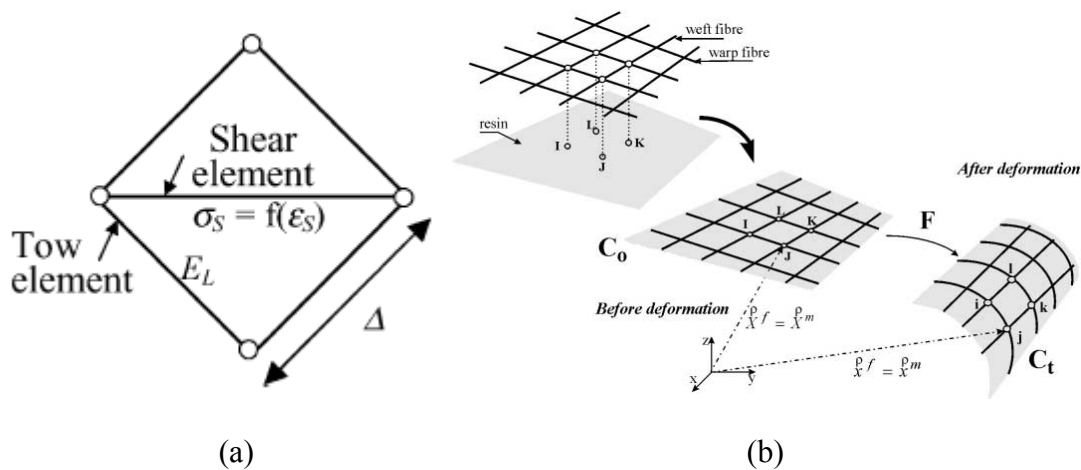


Fig.2.22 Discrete modelling: (a) Unit cell made of four trusses for tows and one truss for shear stiffness [SHA04], (b) Truss elements used for fibres and membrane elements represent the resin [CHE01]

c) Continuous approaches

FE analysis of composite forming requires modelling of the different aspects involved in the process and especially a constitutive mechanical model of the fibrous reinforcement. The multiscale nature of the composite and of its fibrous reinforcement permits different possible approaches. The continuous approach considers the fibrous reinforcement as a continuum. As we have seen in the preceding sections (for example in sub-section 2.5.1), the reinforcement is not continuous at lower scales but it is usually continuous in average and a continuous material superimposed to the fibrous material can be considered. The advantage of the continuous approach is that it can be used in commercial FE codes. Nevertheless, the constitutive model of this continuum will have to convey the very specific mechanical behaviour of the fibrous reinforcement. Especially this behaviour is mainly depending on the fibre directions that are strongly changing during forming. Most of the proposed continuous approaches for FE draping simulations are based on rate constitutive equations (or hypoelastic approaches). This permits to develop the models in user subroutine such as VUMAT in ABAQUS/Explicit. The stresses are cumulated in a rotated frame. In [HAG04] [CAO05] [BOI07] and [TEN07], different approaches within the domain of continuous approach using finite element codes have been proposed. In some cases such as [PEN05], it is the GN frame (the average material rotation frame of ABAQUS) is used and the constitutive matrix is deduced in this basis from behaviour in the fibre basis for two non orthogonal directions of fibres after deformation. Others, [HAG04] and [BOI06], employ a specific objective derivative defined from the fibre rotation. In the subsequent sections we shall present these approaches in detail. Moreover, it is pertinent to clarify at this stage that the approach used within this dissertation is based on the objective derivative using fibre rotation tensor based on each of warp and weft direction.

The main difficulty in using the continuous approach is capturing the effects of the fibre architecture and its evolution during forming processes. There are many models and most of them assume that the fibrous reinforcement is elastic while forming. That is usually true for extensions in the fibre directions, but not obvious in the other directions, such as in-plane shear, bending, and transverse compression. Nevertheless, the forming process is a more or less monotonous operation and making this assumption doesn't change the result of the analysis greatly.

d) Semi-discrete approach

The semi-discrete approach [BOI01] [HAM07] is a compromise between the above continuous and discrete approaches. A finite element method is associated to a mesoscopic analysis of the woven unit cell. Specific finite elements are defined that are made of a discrete number of woven unit cells. The mechanical behaviour of these woven cells is obtained by experimental analyses or from 3D F.E. computations of the woven cell. The nodal interior loads are deduced from this local behaviour and the corresponding strain energy in the element deformation. The objective of the approach is to use a description of the yarns (or woven cells) at mesoscopic level while keeping a limited number of degrees of freedom. This description of the fabric by finite elements needs to assume that two points of a weft and a warp yarns initially superimposed remain superimposed after forming. i.e. there is no translation sliding between the yarns (see sec. 2.3.1f). That has been experimentally shown in most cases. Nevertheless, the model will have to describe the specificities of textile reinforcement mechanical behaviour, especially:

- the non-linear tensile behaviour due to crimp interchange
- shear locking angle and the in-plane shear behaviour which is different before and after this angle.

The textile composite reinforcement is seen as a set of a discrete number of unit woven cells submitted to membrane loadings (i.e. biaxial tension and in-plane shear) and bending [HAM09].

In any virtual displacement field $\underline{\eta}$ such as $\underline{\eta} = 0$ on the boundary with prescribed loads, the virtual work theorem relates the internal, exterior and acceleration virtual works:

$$W_{\text{ext}}(\underline{\eta}) - W_{\text{int}}(\underline{\eta}) = W_{\text{acc}}(\underline{\eta})$$

with

$$W_{\text{int}}(\underline{\eta}) = W_{\text{int}}^t(\underline{\eta}) + W_{\text{int}}^s(\underline{\eta}) + W_{\text{int}}^b(\underline{\eta})$$

Where: $W_{\text{int}}^t(\underline{\eta})$, $W_{\text{int}}^s(\underline{\eta})$, $W_{\text{int}}^b(\underline{\eta})$ are the internal virtual works of biaxial tension, in-plane shear and bending respectively with :

$$W_{\text{int}}^t(\underline{\eta}) = \sum_{p=1}^{\text{ncell}} {}^p \varepsilon_{11}(\underline{\eta}) {}^p T^{11} {}^p L_1 + {}^p \varepsilon_{22}(\underline{\eta}) {}^p T^{22} {}^p L_2$$

$$W_{\text{int}}^s(\underline{\eta}) = \sum_{p=1}^{\text{ncell}} {}^p \gamma(\underline{\eta}) {}^p M^s$$

$$W_{\text{int}}^b(\underline{\eta}) = \sum_{p=1}^{\text{ncell}} {}^p\chi_{11}(\underline{\eta}) {}^pM^{11} {}^pL_1 + {}^p\chi_{22}(\underline{\eta}) {}^pM^{22} {}^pL_2$$

Where “ncell” is the number of woven cell. L_1 and L_2 are the length of unit woven cell in warp and weft directions. $\varepsilon_{11}(\underline{\eta})$ and $\varepsilon_{22}(\underline{\eta})$ are the virtual axial strain in the warp and weft directions. $\gamma(\underline{\eta})$ is the virtual angle between warp and weft directions. $\chi_{11}(\underline{\eta})$ and $\chi_{22}(\underline{\eta})$ are the virtual curvatures of warp and weft yarns. $\varepsilon_{11}(\underline{\eta})$, $\varepsilon_{22}(\underline{\eta})$, $\chi_{11}(\underline{\eta})$, $\gamma(\underline{\eta})$, $\chi_{11}(\underline{\eta})$ and $\chi_{22}(\underline{\eta})$ are function of the gradient of the virtual displacement field. T^{11} and T^{22} are the tensions on the unit woven cell in warp and weft directions. M^{11} and M^{22} are the bending moments on the woven cell respectively in warp and weft directions. M^s is the in-plane shear moment. The mechanical behaviour of the textile reinforcement defines a relation between the loads $T^{\alpha\alpha}$, M^s , $M^{\alpha\alpha}$ and the strain field. Experimental tests specific to textile composite reinforcements are used to obtain these mechanical properties. The biaxial tensile test gives the tensions T^{11} and T^{22} in function of the axial strain ε_{11} and ε_{22} [BUE01], the picture frame or the bias extension test gives the shear moment M^s in function of the angle change γ between warp and weft yarns [CAO08] and the bending tests give the bending moments M^{11} and M^{22} in function respectively of χ_{11} and χ_{22} [DEB08].

2.6 Mechanical Behaviour Models

The mechanical behaviour of fibrous materials is an important point in the model development by finite element analysis. Proper knowledge of the specific deformation modes of the fibrous yarns or tows are among those special behaviours which enable to build proper numerical models. This is attributed to the constitution of the long fibres in the yarns and assemblage of the yarns to make a fabric. High tensile and low transverse rigidities, possible sliding and rearrangement of fibres during deformation are among the specific properties of fibrous materials.

Most recently, the constitutive models have been developed in order to treat the scientific problems of the strong anisotropic of the fibrous materials. The majority among them consider the case of reinforcements along two fibre directions in order to simulate the forming

of thin composites. We present here three methods among them and the approach used in this thesis which was first presented by [HAG04] but on a different scale. The two approaches cited in [YU02] and [TEN07a] are close to the principle and allow treating correctly the contributions of tensions only. The state of stress is determined from the calculations of strains in the material directions of the yarns and Young's modulus in these directions.

2.6.1 Approach of Yu

The approach of Yu [YU02] is based on the kinematics of the deformation of the reinforcement. The principle is based on the hypothesis of relative non-sliding of the network of warp and weft yarns. This is largely admitted in case of FE analysis using continuous approach (section-2.3.1f).

An element of the fabric is composed of n_α yarns of warp (network α , in which the direction is common with the side of the finite element) and n_β the weft yarns (network β) as shown in Fig. 2.23. The deformation along the directions of the fibres (α and β) is calculated from the deformation tensor expressed in the local frame $\{\underline{x}, \underline{y}\}$ of the element. These strains can be traced back to the tensions in each of the network of yarns which are then ordered to determine the forces on each side of the element. These forces are then written in terms of stresses using the thickness of the reinforcement and the dimensions of the element.

It is important to note that these calculations are used as relations between the geometrical characteristics of the initial and deformed networks mainly vector quantities $\underline{\mathbf{a}}$ and $\underline{\mathbf{b}}$ defining the geometry of the mesh reinforcement (see Fig. 2.23). The relationship between these quantities is known by deformation gradient tensor $\underline{\underline{\mathbf{F}}}$. The stiffness matrix of the element made of yarns is finally obtained from the stress tensor in the local frame of the element and as a function of imposed deformations and known rigidities of the yarns.

In short, the constitutive tensor of reinforcement (it contains only two rigidities) is expressed in the given basis that is linked to the element and of which one side corresponds to α . It should be noted that at each instant the directions of the yarns are updated from the deformation gradient tensor which guaranties to follow the correct material directions. All the geometric quantities used in writing the constitutive tensor thus utilize the material directions and which make an important aspect.

To conclude, we note that the alternative proposed for handling the follow up of anisotropy directions works well as a description of the reinforcement behavior that is simplified to tensions only. Later on, Yu has also proposed to superpose shear behavior in addition to tension [YU05].

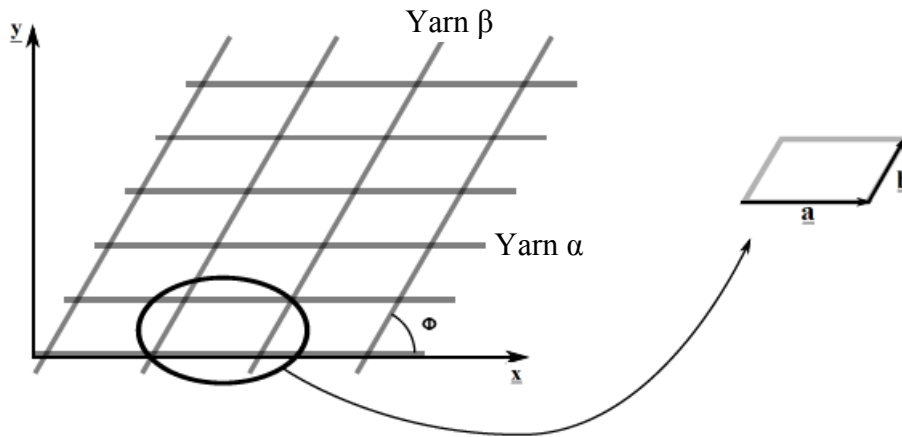


Fig. 2.23 The geometric elements used in the modelling approach of Yu [YU02]

2.6.2 Modelling Approach of Ten Thije

The modelling approach proposed by Ten Thije [TEN07a] and Huetink [HUE06] is a hyper-elastic approach.

The starting point is an elastic potential (free energy) given as a function of right Cauchy-Green tensor, $\Psi = \Psi(\underline{\underline{\mathbf{C}}})$ of which second Piola Kirchhoff tensor is derived as $\underline{\underline{\mathbf{S}}} = 2 \frac{\partial \Psi}{\partial \underline{\underline{\mathbf{C}}}}$

[BAS00]. Afterwards, Cauchy stress tensor $\underline{\underline{\boldsymbol{\sigma}}}$ is determined from the relation

$\underline{\underline{\boldsymbol{\sigma}}} = 2\rho \underline{\underline{\mathbf{F}}} \cdot \frac{\partial \Psi}{\partial \underline{\underline{\mathbf{C}}}} \cdot \underline{\underline{\mathbf{F}}}^T$ where ρ represent the current density. The definition of elastic potential is

an important point for this type of method: it is a purely elastic potential in the direction of fibres given by: $\psi = \frac{1}{2\rho} E_f \varepsilon^2$ where E_f is the elastic tensile modulus of fibres and

$\varepsilon = \frac{1}{2} \frac{l^2 - l_0^2}{l_0^2} = \frac{1}{2} \underline{\underline{\mathbf{a}}}_0 \underline{\underline{\mathbf{a}}}_0 : (\underline{\underline{\mathbf{C}}} - \underline{\underline{\mathbf{1}}}) / l_0^2$ is the strain in the direction of fibres (initially noted as $\underline{\underline{\mathbf{a}}}_0$).

The potential Ψ (free energy function) extended to arbitrary anisotropic case becomes:

$$\Psi = \frac{1}{8\rho_0} (\underline{\underline{\mathbf{C}}} - \underline{\underline{\mathbf{1}}}) : \underline{\underline{\mathbf{E}}} : (\underline{\underline{\mathbf{C}}} - \underline{\underline{\mathbf{1}}}) \text{ where } \underline{\underline{\mathbf{E}}} \text{ is the invariant and constant fourth order material tensor.}$$

The method proposed in [TEN07a] uses a constant orthotropic tensor, written in initial material configuration. In this case, it would be imperative to use a total Lagrangian movement description. In the updated Lagrangian formulation chosen by the authors, constitutive tensor can not be constant because it becomes non-orthotropic. For this type of formulation, the proposed solution should consist to calculate individual contributions of each direction and then accumulate it. The shear behavior is undertaken by the superposition of an isotropic material additionally. However, this solution is tantamount to generate parasitic tension in the directions of fibres. This problem has been dealt with more detail by Aimen [AIM07].

In conclusion, this approach is well suited to the case of a unidirectional fibrous materials and extension in several directions is done by superposition as it has been done in the present work. An interesting alternative to using a hyperelastic approach for the purpose of simulation of forming of reinforced composites is proposed in [AIM07] [AIM08]. The hyper-elastic potential is constructed by adding three terms (supposedly decoupled): two energies of tension and one of shear. This choice is motivated by the principal modes of deformation of the woven reinforcements that are elongation (low) in the directions of the yarns and large variations of angle in the plane of reinforcement (shear). The expression of the proposed potential is a function of right Cauchy Green tensor and of tensor invariants of structures; the latter characterizes the material directions. The traction and shear tests on woven reinforcements are used to identify the various terms of proposed potential. This method shows satisfactory results on different reference tests under large transformations. Forming simulations also offer the relevant qualitative results and allow the description of fabric layers.

2.6.3 Non-orthogonal Approach

This approach was first proposed by Dong [DON01] and has been developed by Pr. J. Cao [PEN05] naming it to non-orthogonal approach.

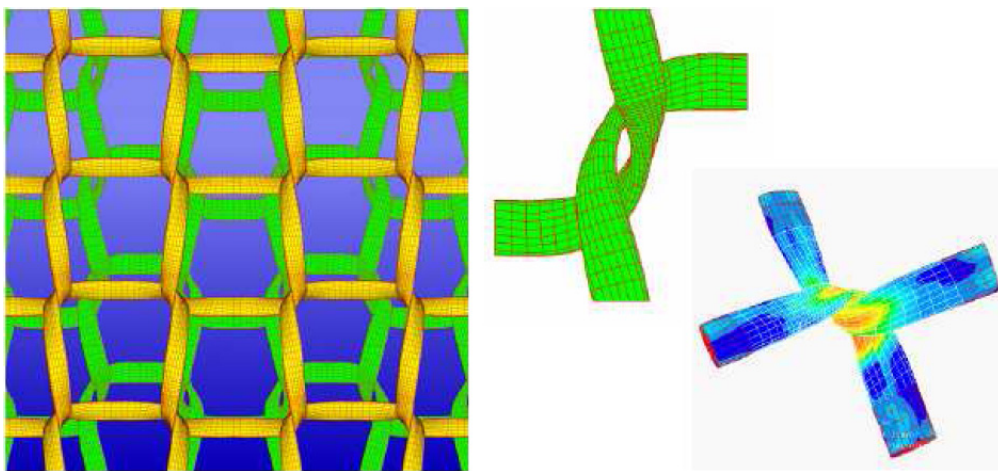
These models use a hypoelastic behavior based on utilization of classical objective derivatives of Green-Naghdi and Jaumann. The popularity of this method comes from the constitutive tensor which is projected in the code work frame as a function of the transformation of

material axes (yarn directions). The objective is to use an updated constitutive tensor taking into account the follow-up of the anisotropy directions.

This method is more close to what we propose in chapter-3. Badel [BAD08] has explored it in more detail and also indicated the problems generated in certain situations. However, this method proposes the handling of more than one material direction and also the inclusion of shear behavior. The work presented in this thesis is also of the same objectives but the difference lies in the use of objective derivative based on the fibre rotation tensor for unidirectional fibres confined to treat fibrous materials at meso-scale. We extend it to bi-directional material data which is suitable for forming analysis of fibrous materials.

2.6.4 Hypoelastic Approach developed by Hagège

The work presented in this manuscript is based on the approach developed by Hagège [HAG04] [BOI05] [HAG05] which was used in the mesoscopic study of knitted reinforcements (see illustrations in Fig. 2.24). The approach uses an objective tensor based on the fibre rotation. This rotation is used to update the current constitutive axes based on the initial constitutive axes and the deformation gradient tensor. The heart of the present study however focuses on use of a hypo-elastic behavior for two material directions (i.e. a fabric of composite reinforcement). The objective derivative proposed by Hagège based on the fibre rotation tensor has been extended to take into account the second direction of fibres. Therefore, the two material directions can be followed during deformation. This permits to perform analysis of a woven reinforcement at macroscopic scale.



(a) biaxial traction, initial and deformed mesh (b) Initial and deformed mesh for an FEM test

Fig. 2.24 Examples of mesoscopic calculations over a knitted reinforcement [HAG04]

Conclusions of Chapter-2

In this chapter we have presented the current position of research related to textile composite reinforcement deformation and the use of textile technology to produce textile composite fabrics. The specific mechanical properties and the deformation modes inherited by the textile reinforcements have been presented in detail. These properties distinguish the textile composites from the traditional metallic structures. Therefore, their analysis necessitates adopting special techniques in order to simulate properly the mechanical behavior of fibrous materials.

Among the composite forming processes, the specificities of RTM process were presented and discussed in detail. The current research work is attributed to dry forming stage RTM process which is indeed very important to determine the mechanical characteristics of a textile composite part and also affects the subsequent stage of resin injection. The analysis of woven composites is of the multi-scale nature. The scales of numerical modeling are also discussed to highlight their importance. The study carried out in this research work is based on macroscopic scale. The mechanical models based on this scale are also presented briefly to the end of this chapter. The continuous approach has been adopted in these models and the same will be exploited in this work. However, the forming analysis of composite reinforcement has been carried out using a hypoelastic behavior based on the fibre rotation tensor is used.

In the next chapter, the formulations developed in the stress computation algorithm are based on hypoelastic behavior in order to trace the deformation of two material directions i.e. warp and weft direction of fibres. In addition, the same model developed by predecessors in this domain has been used to do analysis for two material directions. This consisted of using the single material directions in an element but superposed with another having common nodes. The new material direction can extend it to bi-directional material data. The numerical model is also extended to two material directions in the single element. The model with two material directions is used to do forming simulations of the composite reinforcements. It will be shown that the elementary tests, in-plane shear tests and then the forming tests all support to produce correct results.

3

Numerical Modelling of Woven Composite Reinforcements

3.1 Introduction

In this chapter, an effort based on the macro-scale modelling technique, precisely the exploitation of a continuous approach using hypoelastic law based on the fibre rotation tensor, for continuous woven reinforcements has been carried out. The numerical modelling is based on the explicit dynamic scheme which is usually adopted for sheet forming processes. Then, a hypoelastic approach used in many FE codes at large strains [XIA00] [BEL00] and adopted by researchers, [HAG04] [BOI06] and [BAD07], for analysis of fibrous materials will be presented. Subsequently, stress computation algorithm for fibrous materials and formulations developed for forming analysis using bidirectional material data will be demonstrated explicitly in this chapter. This algorithm will be used through a user material subroutine VUMAT to conduct numerical forming analysis of textile reinforcements. Then, the two analysis techniques named “unidirectional fibres with two superimposed elements” (1DF2E) having common nodes and “bidirectional fibrous material data within one element” (2DF1E) usually treated as a standard procedure will be explained. Based on these two methods the important elementary tests considered necessary to evaluate fibrous material behaviour will be presented. Subsequently, in this chapter, two de-facto standard tests to characterise in-plane shear behaviour of textile fabrics i.e. bias extension and picture frame will be presented in detail along with the numerical results. Afterwards, a recently introduced user material subroutine VFABRIC within the commercial FE code ABAQUS/Explicit for analysis of woven fabrics will be discussed.

To the end of this chapter, the numerical modelling of composite preregs will be proposed. This analysis is based on utilisation of two superimposed elements with common nodes. One

of the two elements is assigned a bi-directional fibrous material data using VUMAT and the second one is allocated with resin material properties.

3.2 Explicit Dynamic Scheme of Analysis

Most of the efficient industrial numerical codes of sheet forming processes are based on explicit dynamic methods although sheet forming and especially fabric forming are quasi-static processes. The explicit dynamic procedure is ideally suited for analyzing high-speed dynamic events, but many of the advantages of the explicit procedure also apply to the analysis of slower (quasi-static) processes. A good example is sheet metal forming, where contact dominates the solution and local instabilities may form due to wrinkling of the sheet.

The explicit dynamics analysis procedure is based upon the implementation of an explicit integration rule together with the use of diagonal element mass matrices. The general equation of motion in the set of degrees of freedom is:

$$\mathbf{M}\ddot{\mathbf{u}}_n = \mathbf{F}_{\text{ext}} - \mathbf{F}_{\text{int}} \quad (3.1)$$

Where \mathbf{M} is the mass matrix, \mathbf{F}_{ext} is the externally applied load vector and \mathbf{F}_{int} is the internal force vector. The equations of motion for the body are integrated using the explicit central-difference integration rule. The explicit central-difference operator satisfies the dynamic equilibrium equations at the beginning of the increment, t ; the accelerations calculated at time t^i are used to advance the velocity solution to time $t + \Delta t / 2$ and the displacement solution to time $t + \Delta t$. The central-difference integration operator is explicit in the sense that the kinematic state is advanced using known values of $\dot{\mathbf{u}}_n^{i-1/2}$ and $\ddot{\mathbf{u}}_n^i$ from the previous increment

$$\dot{\mathbf{u}}_n^{i+1/2} = \dot{\mathbf{u}}_n^{i-1/2} + \frac{\Delta t^{i+1} + \Delta t^i}{2} \ddot{\mathbf{u}}_n^i \quad (3.2)$$

On a time step Δt^i , from t^i to t^{i+1} , the central difference scheme gets the solution u_n^{i+1} from u_n^i by

$$u_n^{i+1} = u_n^i + \Delta t^{i+1} \dot{u}_n^{i+1/2} \quad (3.3)$$

Where u_n^i is a degree of freedom (a displacement or rotation component) and the superscript i refers to the increment number in an explicit dynamic step. The accelerations at the beginning of the increment are computed by

$$\ddot{u}_n^i = \mathbf{M}_D^{-1} (\mathbf{F}_{\text{ext}} - \mathbf{F}_{\text{int}}) \quad (3.4)$$

Where \mathbf{M}_D is the diagonal mass matrix. The diagonal mass matrix is used because of the simplicity to compute its inverse. This is also advantageous because the vector multiplication of mass inverse by the inertial force requires n operations, where n is the number of degrees of freedom.

An approximation to the stability limit is often written as the smallest transit time of a dilatational wave across any of the elements in the mesh.

$$\Delta t \approx \frac{L_{\min}}{C_d} \quad (3.5)$$

Where L_{\min} is the smallest element dimension in the mesh and C_d is the dilatational wave speed defined below:

$$C_d = \sqrt{\frac{\lambda + \mu}{\rho}} \quad (3.6)$$

Where ρ is the density of the material. λ and μ are Lamé's constants defined in terms of Young's modulus E , and Poisson's ratio ν for an elastic material.

The explicit dynamic procedure performs a large number of small time increments efficiently. The use of small increments (dictated by the stability limit) is advantageous because it allows the solution to proceed without iterations and without requiring tangent stiffness matrices to be formed. It also simplifies the treatment of contact.

The method is computationally attractive for problems where the total dynamic response time that must be modelled is only a few orders of magnitude longer than the stability limit; for example, wave propagation studies or some “event and response” applications. The key to the computational efficiency of the explicit procedure is the use of diagonal element mass matrices.

The yielding of very small time-steps in an explicit dynamic analysis would result in extremely lengthy computations of the real draping process. In order to accelerate the numerical computations, the forming process is simulated at artificially higher draping rates (increased punch speed) which increases artificially the inertia effects in Eq. (3.4) and might generate high frequency numerical oscillations. To control these oscillations, a small amount of artificial damping is introduced in the dynamic analysis. The effects of higher draping rates and damping will be discussed in the chapter-5 dedicated to forming simulations of woven composite reinforcements.

3.3 Hypoelastic Approach

Keeping in view the geometrical texture and specific deformation modes of textile reinforcements, the proposed model must meet the theory of large transformations. The phenomenon to be modelled should include both material and geometric non-linearities due to large displacements and large deformations of the yarns. It is the advertant choice of this study to adopt hypoelastcity which can meet these requirements while remaining close to the physical problem. It should be noted at the outset that the model is setup purely elastic, which seems adequate in view of the deformation phenomena and processes, most often monotonous, which we want to simulate. However, one of the interests with the use of hypo-elastic laws concerns the possible extension and simple behaviours such as non-linear visco-elasticity, visco-plasticity whereas maintaining a relatively simple formulation. The possible extension to this kind of behaviour is one of the interests of using this type of law for the material which we consider.

The hypoelastic laws, written as rate constitutive equations and widely used in finite element codes [HUG80] [CRI97] [XIA97], are of the following form:

$$\underline{\underline{\underline{\sigma}}}^{\nabla} = \underline{\underline{\underline{C}}} : \underline{\underline{\underline{D}}} \quad (3.7)$$

Where, $\underline{\underline{\underline{\sigma}}}$ and $\underline{\underline{\underline{D}}}$ are the eulerian tensors of Cauchy stress and the strain rate respectively. $\underline{\underline{\underline{C}}}$ is also a eulerian constitutive tensor orientated by a unit vector in the material directions. $\underline{\underline{\underline{\sigma}}}^{\nabla}$ is an objective derivative of $\underline{\underline{\underline{\sigma}}}$ defined to avoid stress change due to rigid body rotations in $\underline{\underline{\underline{\dot{\sigma}}}} = d\underline{\underline{\underline{\sigma}}}/dt$. An objective derivative can be considered as a derivative for an observer who is fixed with respect to the material.

The constitutive laws used in this work are elastic and thus reproducing the case of fibrous reinforcement forming. However, it is possible to extend these constitutive equations to plasticity which could have been interesting in the complex loading conditions. This extension of hypoelastic model to plasticity is classically used in the domains of sheet metal forming as shown in [CRI97] and [BOU97].

3.3.1 Objectivity of Hypoelastic Laws

a) The principle of objectivity

The principle of objectivity demands that the constitutive equations involve objective tensors only. Needless to say, because of the arbitrary time dependence, many tensors in the ordinary sense are not objective tensors. The objectivity principle yields to define the invariance of quantities in large rotations. Thus, the objectivity ensures that certain quantities, such as Cauchy stress, remain same for all observers irrespective of the frame of reference.

Objective tensors can be defined in close connection with the rotation of the configuration from initial configuration B to actual configuration B* as:

- A scalar valued function ψ is said to be objective if it remains unchanged in the new configuration:

$$\psi^* = \psi$$

- A vector valued function $\underline{\underline{\underline{\psi}}}$ is objective if it transforms:

$$\underline{\underline{\underline{\psi}}}^* = \underline{\underline{\underline{Q}}} \cdot \underline{\underline{\underline{\psi}}}$$

- A Eulerian second order tensor $\underline{\underline{\psi}}$ is also objective if the equality holds for an arbitrary orthogonal tensor $\underline{\underline{Q}}$

$$\underline{\underline{\psi}}^* = \underline{\underline{Q}} \cdot \underline{\underline{\psi}} \cdot \underline{\underline{Q}}^T \quad (3.8)$$

The material rotation can be accounted correctly by using an objective rate of stress tensor, also called as frame invariant rate. Fig. 3.1 shows that the stress state remains unchanged with the material rotation. Thus we can say that an objective material law leaves the stress components unchanged if the actual state B^* has been subjected to a rigid body rotation [BAS00].

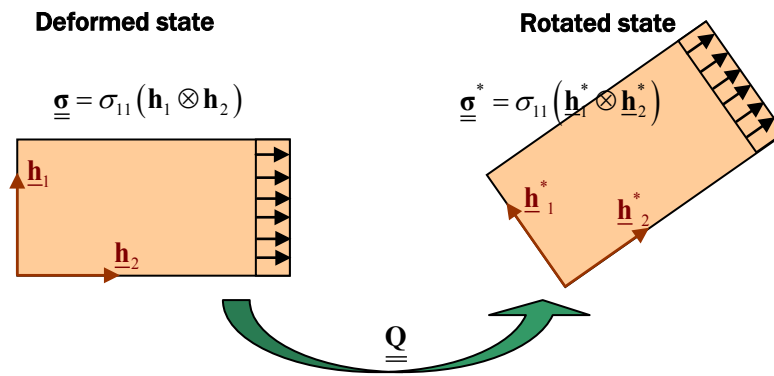


Fig. 3.1 Objectivity of the material law through traction subjected to rigid body rotation

The hypoelastic model adopted for fibrous materials should obey the principle of objectivity and it will be demonstrated in the section-3.5 with elementary tests through numerical examples.

b) Objectivity of rate constitutive equations

In the hypoelastic law, used as a rate constitutive equation, the stress rate is linearly related to rate of deformation. To achieve the requirement of objectivity for Cauchy stress, many objective stress rates are introduced, notably: Truesdell rate, GN rate and Jaumann rate of the Cauchy stress. The Truesdell rate includes the spin related terms as of Jaumann and additionally the terms which depend on the rate of deformation [BEL00]. The GN rate differs from the Jaumann rate only in using a different measure of the rotation of the material. The first one considers orthogonal rotation matrix $\underline{\underline{\Omega}} = \dot{\underline{\underline{R}}} \cdot \underline{\underline{R}}^T$, where $\underline{\underline{R}}$ is the orthogonal rotation

matrix obtained from the polar decomposition of deformation gradient $\underline{\underline{\mathbf{F}}} = \underline{\underline{\mathbf{R}}}\underline{\underline{\mathbf{U}}}$. Whereas, the Jaumann rate uses skew symmetric spin tensor of velocity gradient as its rotation matrix, $\underline{\underline{\mathbf{W}}} = \frac{1}{2}(\underline{\underline{\nabla}}\underline{\underline{\mathbf{v}}} - \underline{\underline{\nabla}}\underline{\underline{\mathbf{v}}}^T)$, where $\underline{\underline{\nabla}}\underline{\underline{\mathbf{v}}}$ is the velocity gradient tensor. The rotational objective derivatives are the most commonly used for simplicity reasons such as in the commercial FE code ABAQUS only Jaumann and GN stress rates are used [ABA68]. ABAQUS/Explicit, adopted as a work code in this study, uses GN rate as its objective stress rate when used with a user material subroutine.

Here, we calculate the time derivative of $\underline{\underline{\boldsymbol{\sigma}}}$ whose components are associated with spatial directions with a set of base vector, $\underline{\underline{\mathbf{e}}}_i$, $i=1,2,3$. Since the above cited two stress rates use rotational objective derivatives, therefore the set of base vectors can not stretch but are defined to spin with the material.

The concept of the rotations of base vectors for Jaumann rate is $\underline{\underline{\mathbf{e}}}_i = \underline{\underline{\mathbf{W}}}\cdot\underline{\underline{\mathbf{e}}}_i^0$ whereas for GN rate is $\underline{\underline{\mathbf{e}}}_i = \underline{\underline{\boldsymbol{\Omega}}}\cdot\underline{\underline{\mathbf{e}}}_i^0$

$$\begin{aligned}\underline{\underline{\boldsymbol{\sigma}}} &= \sigma_{ij}\underline{\underline{\mathbf{e}}}_i \otimes \underline{\underline{\mathbf{e}}}_j \\ \dot{\underline{\underline{\boldsymbol{\sigma}}}} &= \dot{\sigma}_{ij}\underline{\underline{\mathbf{e}}}_i \otimes \underline{\underline{\mathbf{e}}}_j + \sigma_{ij}\dot{\underline{\underline{\mathbf{e}}}}_i \otimes \underline{\underline{\mathbf{e}}}_j + \sigma_{ij}\underline{\underline{\mathbf{e}}}_i \otimes \dot{\underline{\underline{\mathbf{e}}}}_j \\ \dot{\underline{\underline{\boldsymbol{\sigma}}}} &= \dot{\sigma}_{ij}\underline{\underline{\mathbf{e}}}_i \otimes \underline{\underline{\mathbf{e}}}_j + \sigma_{ij}(\underline{\underline{\boldsymbol{\Omega}}}\cdot\underline{\underline{\mathbf{e}}}_i) \otimes \underline{\underline{\mathbf{e}}}_j + \sigma_{ij}\underline{\underline{\mathbf{e}}}_i \otimes (\underline{\underline{\boldsymbol{\Omega}}}\cdot\underline{\underline{\mathbf{e}}}_j) \\ \dot{\underline{\underline{\boldsymbol{\sigma}}}} &= \underline{\underline{\boldsymbol{\sigma}}}^{\nabla\text{GN}} + \underline{\underline{\boldsymbol{\Omega}}}\cdot\underline{\underline{\boldsymbol{\sigma}}} + \underline{\underline{\boldsymbol{\sigma}}}\cdot\underline{\underline{\boldsymbol{\Omega}}}^T \\ \dot{\underline{\underline{\boldsymbol{\sigma}}}} &= \underline{\underline{\boldsymbol{\sigma}}}^{\nabla\text{GN}} + \underline{\underline{\boldsymbol{\Omega}}}\cdot\underline{\underline{\boldsymbol{\sigma}}} - \underline{\underline{\boldsymbol{\sigma}}}\cdot\underline{\underline{\boldsymbol{\Omega}}}\end{aligned}$$

Therefore;

$$\underline{\underline{\boldsymbol{\sigma}}}^{\nabla\text{GN}} = \dot{\underline{\underline{\boldsymbol{\sigma}}}} - \underline{\underline{\boldsymbol{\Omega}}}\cdot\underline{\underline{\boldsymbol{\sigma}}} + \underline{\underline{\boldsymbol{\sigma}}}\cdot\underline{\underline{\boldsymbol{\Omega}}} \quad (3.9)$$

and similarly,

$$\underline{\underline{\boldsymbol{\sigma}}}^{\nabla\text{J}} = \dot{\underline{\underline{\boldsymbol{\sigma}}}} - \underline{\underline{\mathbf{W}}}\cdot\underline{\underline{\boldsymbol{\sigma}}} + \underline{\underline{\boldsymbol{\sigma}}}\cdot\underline{\underline{\mathbf{W}}} \quad (3.10)$$

We see in the above relations that objective rate is a function of material response. The material derivative of the Cauchy stress then depends on two parts: the rate of change due to material response, which is reflected in the objective rate, and the change of stress due to rotation, which corresponds to the last two terms in equations (3.9) and (3.10). The

differences between the two stress rates (Jaumann and GN) are significant only if the finite rotation of a material is accompanied by finite shear. Conversely, the two stress rates are identical for a deviatorically undeformed continuum.

3.4 Hypoelastic Model for Fibrous Materials

The approach used in this study, in case of fibrous materials, exploits an objective derivative based on the fibre rotation tensor, $\underline{\underline{\Delta}}$. It is used to define a strain measure of the fibrous medium and to define the evolution of the strong anisotropic direction that strictly follows the fibre direction. This approach is different from the commonly used approaches in finite element codes of Jaumann corotational formulation (based on corotational frame rotation, $\underline{\underline{Q}}$) or GN approach (based on polar rotation, $\underline{\underline{R}}$). The objective derivative of the Cauchy stress tensor with respect to fibre rotation tensor is:

$$\underline{\underline{\dot{\sigma}}} = \underline{\underline{\Delta}} \cdot \left(\frac{d}{dt} (\underline{\underline{\Delta}}^T \cdot \underline{\underline{\sigma}} \cdot \underline{\underline{\Delta}}) \right) \cdot \underline{\underline{\Delta}}^T \quad (3.11)$$

Where $\underline{\underline{\Delta}}$ is the rotation from the initial frame to the frame of fibre. In case of bidirectional material data, it is based on each of warp and weft direction of fibres. It will be shown later on (section 3.4.1) that the fibre rotation tensor takes the form $\underline{\underline{\Delta}} = \underline{\underline{f}}_1 \otimes \underline{\underline{e}}_1 + \underline{\underline{f}}_2 \otimes \underline{\underline{e}}_2$ using two fibre directions. Where $\underline{\underline{f}}_1$ and $\underline{\underline{f}}_2$ are the current fibre directions and, $\underline{\underline{e}}_1$ and $\underline{\underline{e}}_2$ are the current orientations of GN axes.

3.4.1 Stress Computation Algorithm for Fibrous Materials

Since the constitutive tensor $\underline{\underline{C}}$ is oriented along the fibre direction, therefore it is mandatory to update the current fibre directions so that the constitutive laws could be used properly. Once the current fibre directions are rationalized, it becomes possible to transform the strains from the GN axes (the work basis of ABAQUS/Explicit when used with user subroutine and

where the default output of material state tensors is available) to the current fibre axes. The rotation tensor $\underline{\underline{\mathbf{R}}}$ is obtained from polar decomposition of deformation gradient tensor $\underline{\underline{\mathbf{F}}}$.

$$\underline{\underline{\mathbf{R}}} = \underline{\underline{\mathbf{F}}}\underline{\underline{\mathbf{U}}}^{-1} \quad (3.12)$$

Where $\underline{\underline{\mathbf{U}}}$ is the right stretch tensor. The GN axes $\underline{\mathbf{e}}_\alpha$ in the current configuration (the average rotation of the material axes) are updated using orthogonal rotation matrix $\underline{\underline{\mathbf{R}}}$ and the initial orientation of GN axes $\underline{\mathbf{e}}_\alpha^0$ as:

$$\underline{\mathbf{e}}_\alpha = \underline{\underline{\mathbf{R}}}\underline{\mathbf{e}}_\alpha^0 \quad (3.13)$$

The index α takes the values of 1 and 2.

Since the interest lies here to do modelling for the thin reinforcements and for that membrane elements are used, therefore, the axis-3 is common for both GN and fibre frames and it is perpendicular to the plane 1-2.

Whereas the current fibre directions $\underline{\mathbf{f}}_\alpha$ are obtained using the deformation gradient tensor $\underline{\underline{\mathbf{F}}}$ and the initial fibre orientation $\underline{\mathbf{f}}_\alpha^0$:

$$\underline{\mathbf{f}}_\alpha = \frac{\underline{\underline{\mathbf{F}}}\underline{\mathbf{f}}_\alpha^0}{\|\underline{\underline{\mathbf{F}}}\underline{\mathbf{f}}_\alpha^0\|} = \frac{\underline{\underline{\mathbf{F}}}\underline{\mathbf{e}}_\alpha^0}{\|\underline{\underline{\mathbf{F}}}\underline{\mathbf{e}}_\alpha^0\|} \quad (3.14)$$

Where $\underline{\mathbf{f}}_\alpha^0$ and $\underline{\mathbf{e}}_\alpha^0$ are assumed to coincide initially. Once, both directions of current GN axes and fibre axes are determined, it becomes possible to transform the strain components from the code work basis (GN basis) to the fibre bases. The two fibre axes ($\underline{\mathbf{f}}_1$ and $\underline{\mathbf{f}}_2$) usually do not remain orthogonal after deformation. Therefore, we construct two orthogonal frames where each one is based on one of the two fibre axes.

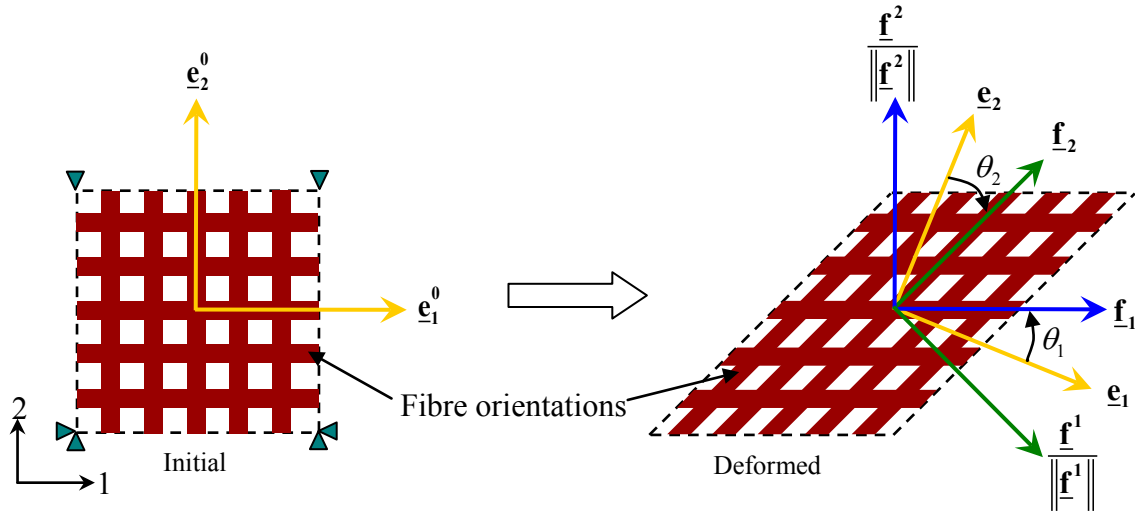


Fig. 3.2 Orientation of GN axes, \underline{e}_α and fibres axes, \underline{f}_α before and after deformation during a simple shear test. Initially both frames are superimposed; $\underline{f}_\alpha^0 = \underline{e}_\alpha^0$, where $\alpha = 1, 2$

Let θ_1 be the angle between the GN frame and the first orthogonal frame constructed from the first fibre axis \underline{f}_1 and the orthogonal normalized vector $\underline{f}^2 / \|\underline{f}^2\|$ in the deformed position (Fig. 3.2) with $\underline{f}^\alpha \cdot \underline{f}_\beta = \delta_\beta^\alpha$, where δ_β^α is 1 if $\alpha = \beta$ and 0 otherwise. Note that the covariant vectors (with subscripts) are parallel to their respective fibre or yarn directions while the contravariant vectors (with superscripts) are orthogonal to the directions of the other fibre or yarn (Fig. 3.2). The transformation matrix $[\mathbf{T}_1]$ formed between the two frames is:

$$[\mathbf{T}_1]_{(e, f_1)} = \begin{bmatrix} \cos \theta_1 & -\sin \theta_1 \\ \sin \theta_1 & \cos \theta_1 \end{bmatrix} \quad (3.15)$$

Where $e(\underline{e}_1, \underline{e}_2)$ stands for GN frame and $f_1(\underline{f}_1, \underline{f}^2 / \|\underline{f}^2\|)$ refers to an orthogonal frame having first fibre direction \underline{f}_1 and where:

$$\cos \theta_1 = \frac{\|\underline{e}_1 \cdot \underline{f}_1\|}{\|\underline{e}_1\| \cdot \|\underline{f}_1\|} \quad \sin \theta_1 = \frac{\|\underline{e}_1 \times \underline{f}_1\|}{\|\underline{e}_1\| \cdot \|\underline{f}_1\|} \quad (3.16)$$

Similarly, let θ_2 be the angle between the vector \underline{e}_2 of GN frame and the second orthogonal

frame formed by the second fibre direction $\underline{\mathbf{f}}_2$ and the orthogonal normalized vector $\underline{\mathbf{f}}^1/\|\underline{\mathbf{f}}^1\|$ (Fig. 3.2). So, the transformation matrix $[\mathbf{T}_2]$ based on the change in angle between the GN frame and the second orthogonal frame is:

$$[\mathbf{T}_2]_{(e,f_2)} = \begin{bmatrix} \cos\theta_2 & -\sin\theta_2 \\ \sin\theta_2 & \cos\theta_2 \end{bmatrix} \quad (3.17)$$

And $f_2(\underline{\mathbf{f}}^1/\|\underline{\mathbf{f}}^1\|, \underline{\mathbf{f}}_2)$ refers to the second orthogonal frame having second fibre direction $\underline{\mathbf{f}}_2$ and where:

$$\cos\theta_2 = \frac{\|\underline{\mathbf{e}}_2 \cdot \underline{\mathbf{f}}_2\|}{\|\underline{\mathbf{e}}_2\| \cdot \|\underline{\mathbf{f}}_2\|} \quad \sin\theta_2 = \frac{\|\underline{\mathbf{e}}_2 \times \underline{\mathbf{f}}_2\|}{\|\underline{\mathbf{e}}_2\| \cdot \|\underline{\mathbf{f}}_2\|} \quad (3.18)$$

The strain increment $[\underline{\mathbf{d}}\boldsymbol{\varepsilon}]_e$ is available in the GN frame in each calculation loop (as a code's output) and is extracted in the user subroutine. The strain tensor to be expressed in the first orthogonal frame containing the first true fibre direction is obtained using the first transformation matrix $[\mathbf{T}_1]$ of Eq. (3.15). The fibre strain increments are defined as:

$$[\underline{\mathbf{d}}\boldsymbol{\varepsilon}]_{f_1} = [\mathbf{T}_1]^T [\underline{\mathbf{d}}\boldsymbol{\varepsilon}]_e [\mathbf{T}_1] \quad (3.19)$$

Where, $[\mathbf{T}_1]^T$ is the transpose of $[\mathbf{T}_1]$. The strain increments expressed in the second orthogonal frame having the updated second fibre directions are calculated using the second transformation matrix $[\mathbf{T}_2]$ of Eq. (3.17):

$$[\underline{\mathbf{d}}\boldsymbol{\varepsilon}]_{f_2} = [\mathbf{T}_2]^T [\underline{\mathbf{d}}\boldsymbol{\varepsilon}]_{f_1} [\mathbf{T}_2] \quad (3.20)$$

The first component of the direct strains $d\varepsilon_{11}^{f_1}$ which acts along the first fibre direction is calculated from the Eq. (3.19) and is the increment of strain in the first fibre direction. The second direct strain component $d\varepsilon_{22}^{f_2}$ along the second fibre direction is obtained from Eq.

(3.20) and it is the increment of strain in the second direction. Whereas, the in-plane shear strain increment $d\gamma$ is defined to be the change in the angle between the warp and weft yarns and specifically here, it is equal to sum of the components of shear strain increments calculated from the Eqs (3.19) and (3.20) i.e.:

$$d\gamma = d\varepsilon_{12}^{f_1} + d\varepsilon_{12}^{f_2} \quad (3.21)$$

While operating the constitutive tensor the above mentioned two components of shear strain increments will be used independently and only the summation of stresses will be made while transformation to the code work basis.

Stresses along fibre directions are computed using the constitutive matrix in the fibre direction $[\mathbf{C}]_f$ in conjunction with Eqs (3.19) and (3.20):

$$[d\boldsymbol{\sigma}]_{f_1} = [\mathbf{C}]_{f_1} [d\boldsymbol{\varepsilon}]_{f_1} \quad (3.22)$$

$$\text{and,} \quad [d\boldsymbol{\sigma}]_{f_2} = [\mathbf{C}]_{f_2} [d\boldsymbol{\varepsilon}]_{f_2} \quad (3.23)$$

Considering the elastic tensile modulus (E_1 and E_2) and the shear modulus G_{12} as the only non-zero material data, the Eqs. (3.22) and (3.23) can explicitly be written as:

$$\begin{bmatrix} d\sigma_{11}^{f_1} \\ d\sigma_{22}^{f_1} \\ d\sigma_{12}^{f_1} \end{bmatrix} = \begin{bmatrix} E_1 & 0 & 0 \\ 0 & 0 & 0 \\ 0 & 0 & G_{12} \end{bmatrix} \begin{bmatrix} d\varepsilon_{11}^{f_1} \\ d\varepsilon_{22}^{f_1} \\ d\varepsilon_{12}^{f_1} \end{bmatrix} \quad (3.24)$$

and,

$$\begin{bmatrix} d\sigma_{11}^{f_2} \\ d\sigma_{22}^{f_2} \\ d\sigma_{12}^{f_2} \end{bmatrix} = \begin{bmatrix} 0 & 0 & 0 \\ 0 & E_2 & 0 \\ 0 & 0 & G_{12} \end{bmatrix} \begin{bmatrix} d\varepsilon_{11}^{f_2} \\ d\varepsilon_{22}^{f_2} \\ d\varepsilon_{12}^{f_2} \end{bmatrix} \quad (3.25)$$

The stress increments computed in Eq. (3.24) and (3.25) are accumulated in each fibre frame

following the incremental formulation of Hughes and Winget [HUG80]. This approach is commonly used in finite element codes at large strains. It is consistent with the objective derivative in Eq. (3.7) and employs the mid-point integration scheme to compute stress state at time step t^{n+1} knowing at t^n .

$$[\boldsymbol{\sigma}^{n+1}]_{f_1^{n+1}} = [\boldsymbol{\sigma}^n]_{f_1^n} + [d\boldsymbol{\sigma}]_{f_1^{n+1/2}} \quad (3.26)$$

$$[\boldsymbol{\sigma}^{n+1}]_{f_2^{n+1}} = [\boldsymbol{\sigma}^n]_{f_2^n} + [d\boldsymbol{\sigma}]_{f_2^{n+1/2}} \quad (3.27)$$

This scheme has the advantage of being simple and efficient needing only to compute the corrective term since the first has been known from the previous increment.

The stresses computed in the two fibre frames using Eqs. (3.26) and (3.27) are then expressed in the GN frame as:

$$[\boldsymbol{\sigma}]_e = [\mathbf{T}_1][\boldsymbol{\sigma}]_{f_1} [\mathbf{T}_1]^T + [\mathbf{T}_2][\boldsymbol{\sigma}]_{f_2} [\mathbf{T}_2]^T \quad (3.28)$$

Thus, the stress tensor in the code work basis (GN frame) is the sum of the transformed stresses calculated in the two orthogonal frames containing fibre directions.

The algorithm used for the stress computation of woven textiles is summarized in Fig. 3.3. The working code is ABAQUS/Explicit and the formulations developed for stress computation algorithm are written in FORTRAN code and implemented through a user material subroutine VUMAT. The working of the algorithm occurs in the form of a loop. This is evident from the flow chart shown in Fig. 3.3 that three tensor quantities are calculated by the FE code i.e. deformation gradient tensor $\underline{\underline{\mathbf{F}}}$, right stretch tensor $\underline{\underline{\mathbf{U}}}$ and incremental strains $[d\boldsymbol{\varepsilon}]_e$ in the default basis of the code. All other tensor quantities, shown in the flow chart, are calculated using above formulations of the algorithm. The important aspect of this algorithm is about the use of two orthogonal frames and addition of correct tensor quantities finally transformed to the single orthogonal frame of the working code.

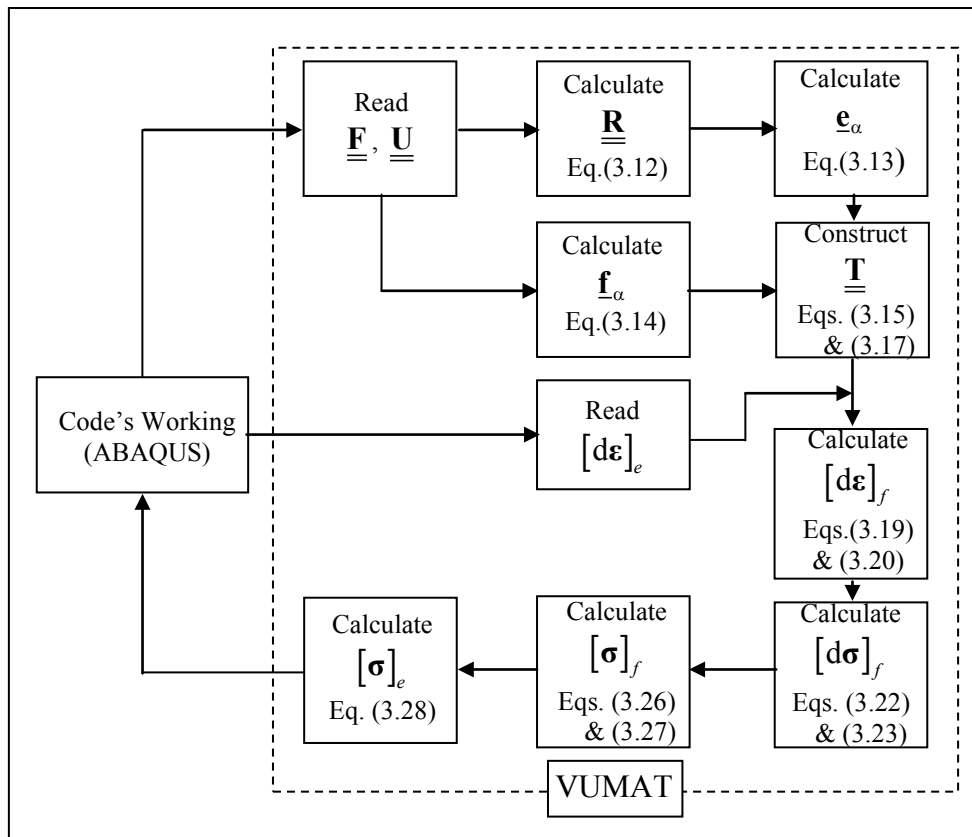


Fig. 3.3 Flow chart of VUMAT algorithm of stress computation
adopted for analysis of fibrous materials

3.4.2 Modelling Methods for Fibrous Media

In the present study, two methods have been proposed and adopted for analysis of fibrous materials within the domain of continuous approach. Indeed, both methods use hypoelastic formulation and are implemented within commercial FE code with standard elements. The difference lies in the formulations adopted and the technique used for analyzing the special behaviour of fibrous materials. Additionally, the state of affairs becomes very interesting when compared the results generated by the two methods.

a) Unidirectional fibres with two superimposed elements (1DF2E)

In the first method, two sets of superimposed elements are created which share the same single set of nodes [KHA08]. Each set of element has unidirectional fibre properties. However, the initial orientation for the two unidirectional sets of fibres has been selected differently and,

in this particular study, it is chosen perpendicular to each other. The formulations described in section-3.4.1 for updating only the first direction of fibres are used for both orientations (i.e. $\alpha=1$). This method is schematized in Fig. 3.4. In the element-1, the fibres are oriented horizontally and first axis of the local orthogonal frame defined in this element takes the fibre direction. Whereas, the fibre directions in the second element are oriented vertically and the orthogonal frame defined for element-2 is rotated through 90° so that axis-1 takes again the fibre directions. Therefore, only the use of common nodes for both elements simplifies the problem to analyse the bidirectional material behaviour.

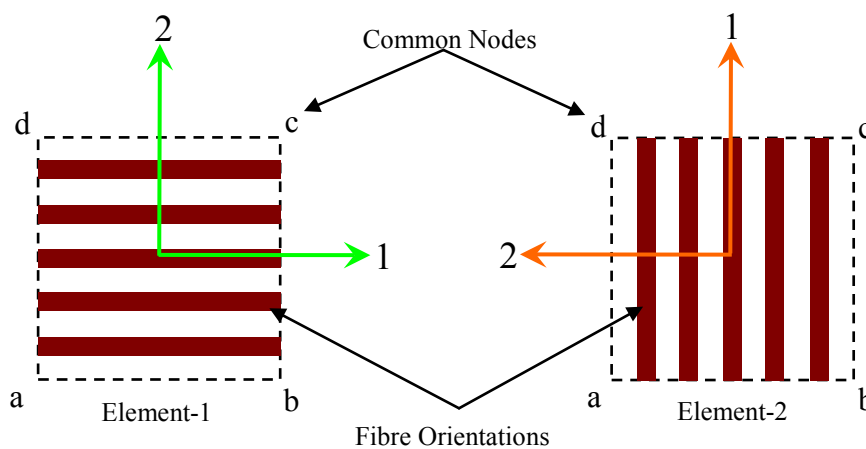


Fig.3.4 A schematic diagram demonstrates the method using two superimposed elements with common nodes but with different orientation of fibres to represent and analyse woven fabrics

The single direction of fibres in a single set of elements using hypoelastic laws has already been used in previous research works [HAG04] [BOI07], [BAD07] as predecessors of the same research group. The update of single direction of fibres using hypoelastic model has been used for analysing the fabrics at meso-scale (unit cell level). In order to analyse woven fabrics at macro-scale, and which have factual form of bidirectional fibres, the update of single fibre direction in the algorithm developed formulations has been used and only the analysis technique of common nodes using superimposed elements has been adopted.

b) Bidirectional fibres within single element (2DF1E)

The second method takes into account the bidirectional fibre properties in the single set of elements. The two directions of fibres are updated independently with the formulations

suggested in section-3.4.1 (i.e. $\alpha=1$ and 2). Moreover, the computations of the stress states for the two directions of fibres have also been made separately in the two orthogonal bases illustrated in Fig.3.2. However, the stress states from the two orthogonal bases are transformed to a single orthogonal basis of the code work (e. g. GN basis for ABAQUS/Explicit used here). Fig.3.2 describes the orientation of the two directions of fibres during a simple shear test. It is shown that the GN axes ($\underline{\mathbf{e}}_\alpha$) are transformed under orthogonal rotation tensor $\underline{\mathbf{R}}$ with an average rotation of material axes. Whereas, the fibre directions ($\underline{\mathbf{f}}_\alpha$) are transformed followed by the deformation gradient tensor $\underline{\mathbf{F}}$. It will be further shown in the subsequent sections, that two distinct methods proposed for fibrous media analyses hold equally correct.

3.5 Validating the Algorithm Formulations

3.5.1 Elementary Tests

In order to validate the developed formulations, some important elementary tests were performed and compared with the theoretical results. 3-D quadrilateral membrane elements with reduced integration (M3D4R) have been selected for numerical analysis. Three different methods and each method with three types of tests have been adopted to compare the outputs.

The details of the elementary test methods are as under:

- 1) Single element with unidirectional fibres
- 2) Single element with bidirectional fibres
- 3) Two superimposed elements with unidirectional fibres

Each above method has been tested with following three types of tests:

- i) 45° simple shear test (Fig. 3.2)
- ii) Traction followed by 45° simple shear (Fig. 3.5)

iii) Traction followed by rigid body rotation (Fig. 3.6)

Each one of the three tests has been explored with a plane stress case. The tensile rigidity of the fibres being only the non-zero material data having unidirectional fibres as $E_1 = 35,400$ MPa and in addition as $E_2 = 35,400$ MPa for bidirectional fibres.

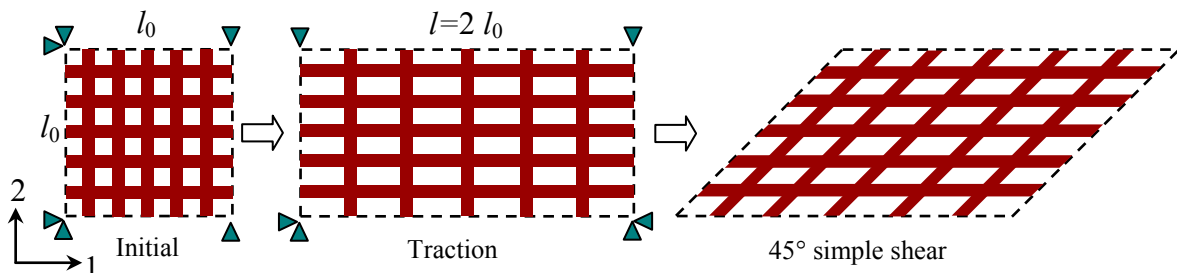


Fig. 3.5 The traction ($l/l_0 = 2$) followed by 45° simple shear test showing the positions of fibres

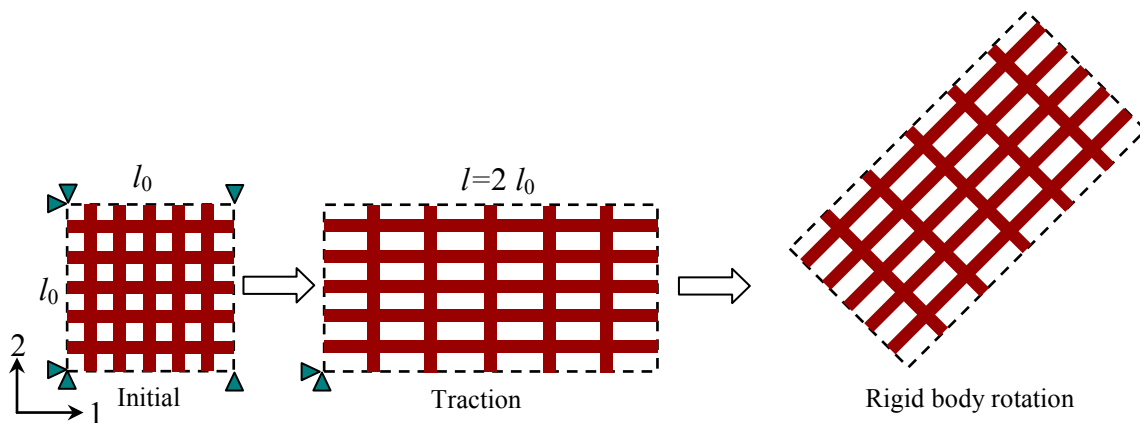


Fig. 3.6 The traction ($l/l_0 = 2$) followed by rigid body rotation showing the possible positions of fibres

The numerical results of stress computations given in the fibre frame are detailed below:

- ❖ Stress output in a simple shear test with unidirectional fibres initially aligned horizontally.

$$[\sigma]_f = \begin{bmatrix} \sigma_{11} \\ \sigma_{22} \\ \sigma_{12} \end{bmatrix} = \begin{bmatrix} 0 \\ 0 \\ 0 \end{bmatrix}$$
- ❖ Stress output in a simple shear test with unidirectional fibres initially aligned vertically

$$[\sigma]_f = \begin{bmatrix} 1.23E+04 \\ 0 \\ 0 \end{bmatrix}$$
- ❖ Stress output in a 45° simple shear test with methods 2 and 3(Fig 3.2)

$$[\sigma]_f = \begin{bmatrix} 0 \\ 1.23E+04 \\ 0 \end{bmatrix}$$
- ❖ Stress output in a traction test followed by 45° simple shear test with methods 2 and 3 (Fig 3.5)

$$[\sigma]_f = \begin{bmatrix} 2.45E+04 \\ 1.23E+04 \\ 0 \end{bmatrix}$$
- ❖ Stress output in a traction followed by rigid body rotation with all three methods (Fig.3.6)

$$[\sigma]_f = \begin{bmatrix} 2.45E+04 \\ 0 \\ 0 \end{bmatrix}$$

All above tests have come up to the expected solutions and conform to the theoretical results. Moreover, it has been shown with comparison of results in [BAD08] that this is not the case for alternate approaches such as GN approach used in [PEN05].

3.5.2 Discussion and Analysis: Elementary Tests

The test (i) is a single step analysis while tests (ii) and (iii) are two steps analyses. In the test (i), the possible deformation of fibres exists along direction-2 (vertical fibres) while direction-1 is undeformed. In the first step of the tests (ii) and (iii), the direction-2 is constrained and the deformation exists only in the direction-1. While, for the second step of test (ii) the deformation exists in the direction-2 only, as in the case of test (i), and it keeps the stresses along direction-1 unchanged during the second step. This fulfils the requirement and is the real characteristic and true output of the fibrous media. The results shown for test type (iii) are of the same magnitude at the end of first step and remained unchanged in the test with the second step. The objective of the test (iii) is primarily to show the true result of the element in

tension and then to see the objectivity of the behaviour i.e. to prove that a large rotation under tension does not lead to spurious stresses. So, the true computation of the fibre direction plays a major role in the hypoelastic approach whereas the classical rotated frames (GN or Jaumann rotations) can not be used for large strain simulation of fibrous material.

An important aspect of this algorithm is the independent transformations of two direct strains from GN axes to the two fibre axes. For that two orthogonal fibre frames (as detailed in section 3.4.1) have been defined where each one contains one of the fibre directions. Similarly, the shear strains in each of the fibre frames is computed and taken into account. The computation of correct stresses in these frames is an important stage and only the true quantities are finally transformed to the single orthogonal frame of the code work basis (i.e. GN basis). This makes the formulations simplified and the results for the two directions of fibres are extracted explicitly. The use of two superimposed elements is also an important aspect of this work. The use of 1DF2E method is equally valuable which accommodates the two fibre directions and produces equally correct results as with 2DF1E method. With these schemes, we can say that the mechanical behaviour of woven fabric can be extracted accurately with the algorithm adopted, formulations used and methods suggested.

3.6 Picture Frame Test

Picture frame test is one of the two de-facto standard in-plane shear tests adopted to characterise the shear behaviour of textile reinforcements. Based upon the results of elementary tests using the developed formulations and the algorithm adopted, the tests are extended to validate the developed model numerically for the in-plane shear deformation of a fabric based upon the experimental results. The numerical tests of picture frame are performed based on the experimental results of two benchmark fabrics of commingled glass/polypropylene i.e. balanced plain weave (BPW) and balanced twill weave (BTW) [CAO08]. The benchmark study has already been conducted experimentally to characterise the shear behaviour of these fabrics.

Numerically the picture frame test is performed using bidirectional fibres parallel to the external edges and $\pm 45^\circ$ to the loading direction. The model, used here, consists of 5×5

quadrilateral membrane elements. The velocity amplitudes have been applied to the external nodes only to produce pure shear deformation. The nodal reaction forces (Fig. 3.7b) are perpendicular to the fibre directions. This indicates that there is no extension in the fibres and therefore, they are in a state of pure shear.

The test is performed using the in-plane shear properties of a BPW fabric taken from a benchmark study conducted recently [CAO08]. The available test data is in the form of normalized shear force (N/mm) versus shear angle (degrees). This data is first converted in the form of a curve between shear stress versus shear angle (radians). By assigning the curve a polynomial regression equation results in the form of shear stress as a function of shear strain (radians). Then, by taking derivative of this polynomial may result in the form of shear rigidity as a function of shear angle (radians). The in-plane shear rigidity “ G_{12} ” of the glass/polypropylene BPW fabric has been deduced as a function of shear angle “ γ ” in radians.

$$G_{12}(\gamma) = 8.48\gamma^4 - 12.0972\gamma^3 + 6.1275\gamma^2 - 0.83\gamma + 0.051 \quad (3.29)$$

The picture frame test output has been deduced as normalized shear force as a function of shear angle (degrees). The shear force normalization is defined as proposed in [PEN04] and [HAR04] when fabric length is equal to the frame length:

$$F_{\text{normalized}} = \frac{F}{2 \cos \theta \cdot L_{\text{fab}}} \quad (3.30)$$

$$\text{where,} \quad \theta = \frac{\pi}{4} - \frac{\gamma}{2}$$

Where F is the total force required to produce shear and L_{fab} is the fabric length and γ is the shear angle (of the frame or fabric) in radians.

The numerical results of normalized force are obtained through shear stress output during the test as:

$$F_{\text{normalized}} = t_{\text{fabric}} \cdot \sigma_{12}^f \quad (3.31)$$

Where t_{fabric} is the thickness of the fabric. The numerical results of normalized force versus

shear angle (degrees) are plotted in Fig.3.8 to validate the numerical model output using experimental results of shear characteristics of plain weave (BPW) fabric. The experimental tests were partly conducted at LaMCoS, INSA-Lyon for benchmark study [CAO08]. The numerical results validate very well the experimental output.

The numerical test using BTW data of shear behaviour has also been validated in the same manner as of BPW fabric. The numerical results of normalized force along with experimental input data are shown in Fig. 3.9. The shear rigidity extracted for BTW fabric is:

$$G_{12}(\gamma) = -15.90225\gamma^4 + 34.858\gamma^3 - 19.9065\gamma^2 + 3.7098\gamma - 0.0458 \quad (3.32)$$

The detailed procedure for determination of shear modulus for a fabric using experimental data is presented in chapter 4.

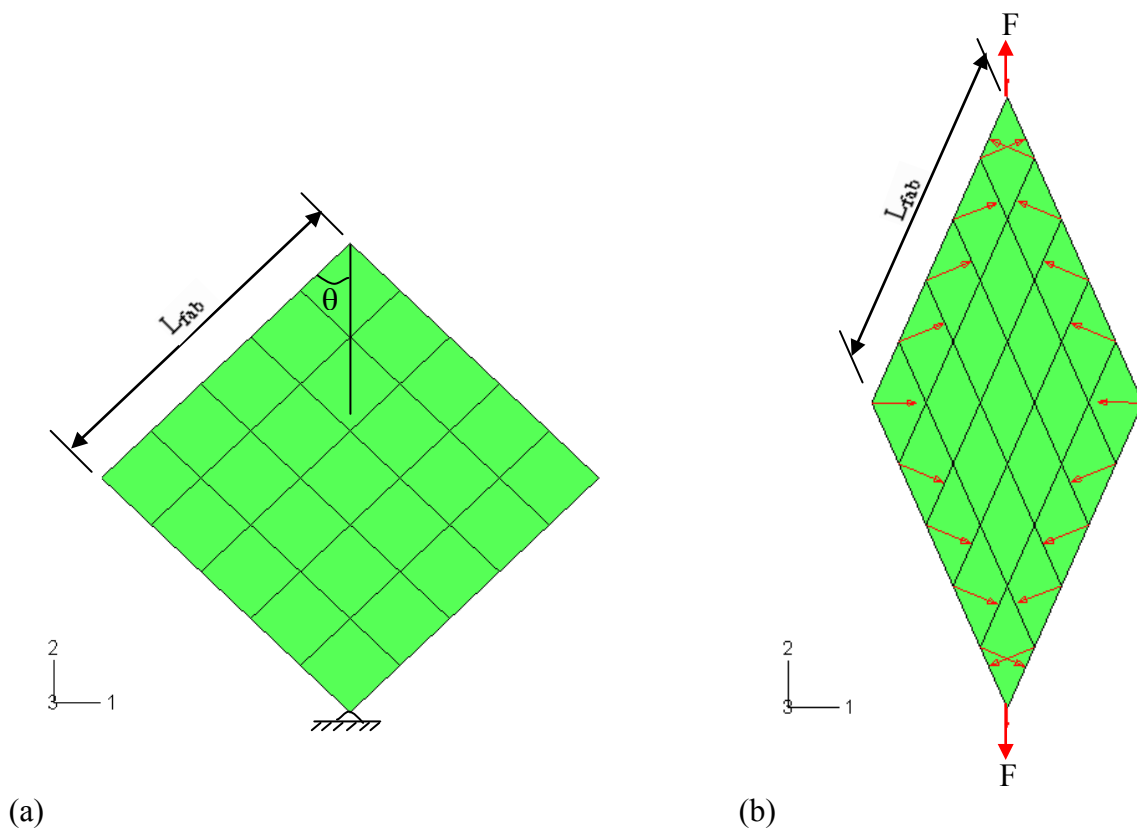


Fig.3.7 Picture Frame test with 5×5 elements, (a) initial state and, (b) deformed state showing nodal reaction force symbols: a testimony of pure shear phenomena.

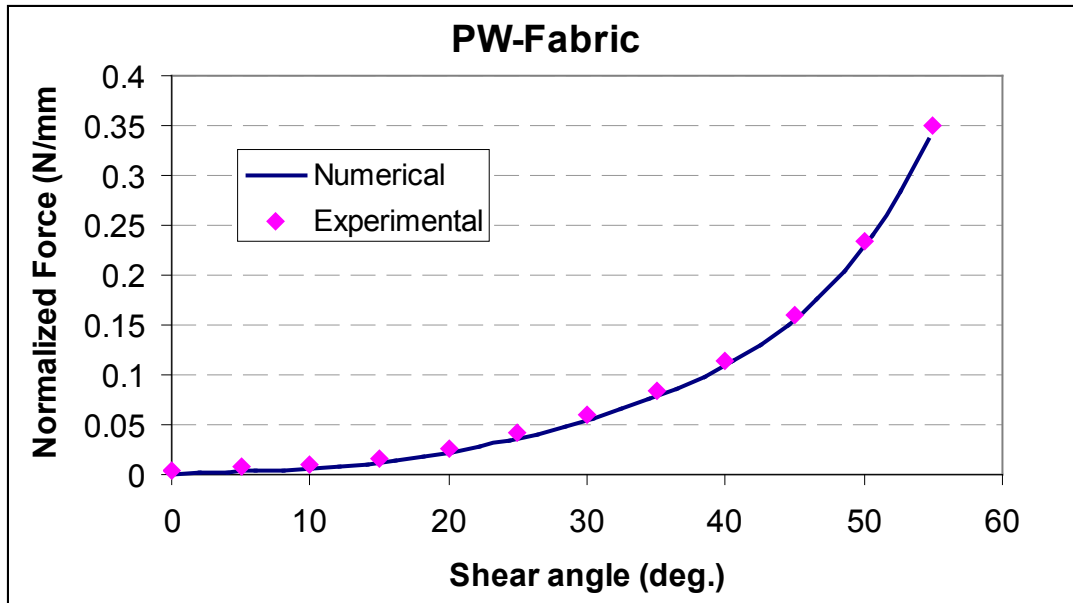


Fig.3.8 The validation of numerical test for normalized force vs shear angle (deg.) through experimental test results in case of BPW fabric

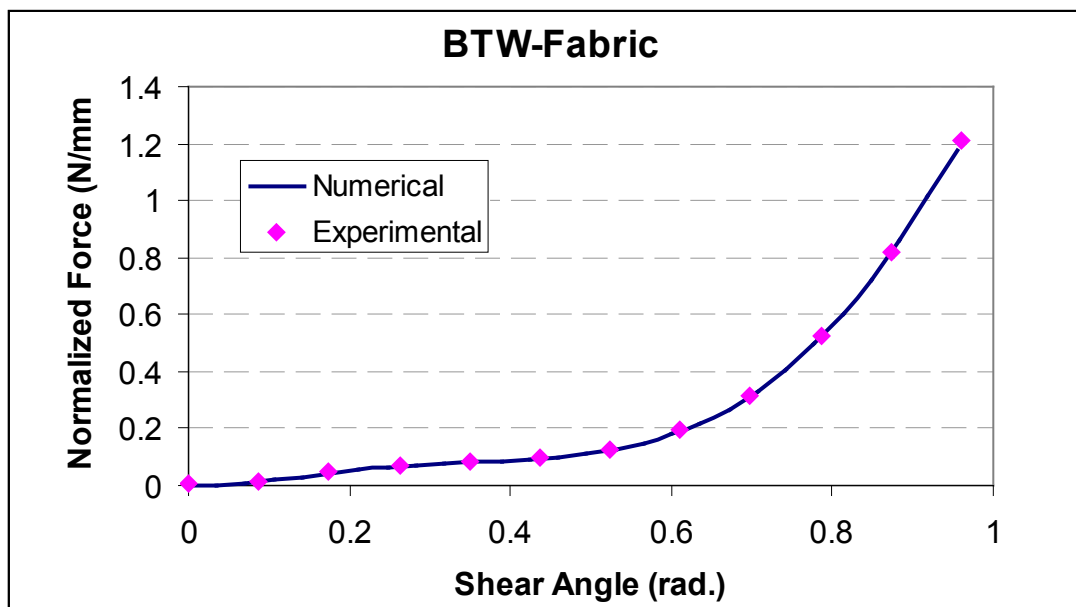


Fig. 3.9 The validation of numerical test for normalized force vs shear angle (deg.) through experimental test results in case of BTW-fabric

In order to validate the numerical output of 1DF2E method, we have performed a simulation

of picture frame test using the same material input data for both types of test methods (i.e. also for 2DF1E). The boundary conditions used for the two tests have also been similar. It should be known that mostly the standard method (2DF1E) with single element having bidirectional fibrous material data has been used in the numerical simulation especially in forming simulation tests presented in chapter 5.

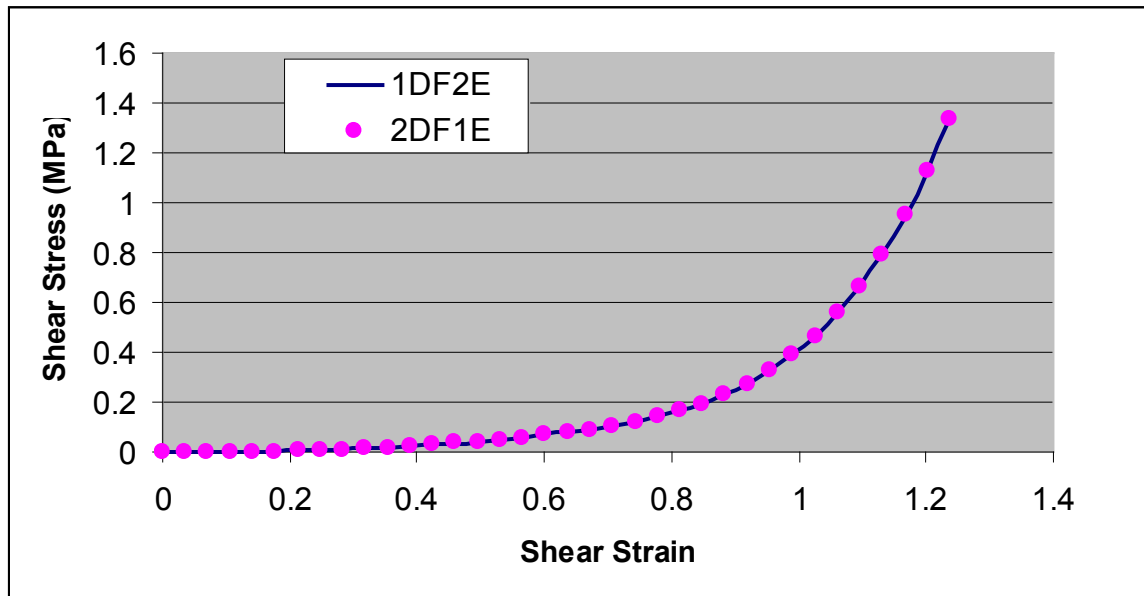


Fig. 3.10 The shear stresses vs shear strain numerical outputs to compare the 1DF2E and 2DF1E methods.

Fig. 3.10 shows the shear stress versus shear strain outputs of the two test methods (1DF2E and 2DF1E). This is evident from the results that two methods hold equally correct in tracing the mechanical behaviour of fibrous materials. This should also be known that the shear rigidity used for these fabrics depends on the evolution of shear angle of the fibre directions during deformation. Therefore, shear rigidity used is a function of kinematic property of the fabric. The correct computation of shear angle during deformation is therefore very important because it imparts shear modulus data to the fabric under test.

3.7 Bias Extension Test

Bias extension test is adopted to characterise the shear behaviour of a fabric with a length equal to or greater than twice its width. The test presented in this work consists of a length 2.5 times its width. The test is performed for both types of weaves (BPW and BTW) with uni-axial displacement along its length where one end is held constrained. The fibres are oriented at $\pm 45^\circ$ to the loading direction. Three basic distinct zones that develop within the fabric after deformation can be identified, and are shown in Fig. 3.11 Zone-I is formed by two isosceles triangles, one at each end of the deformed fabric with the base being the width of the specimen that is held constant. There is no significant deformation in this zone and is considered undeformed zone. The shear angle stays the same in this zone. Zone-II consists of four identical triangular regions, neighbouring Zone-I. In this zone the deformation is a combination of both scissoring and sliding deformation. There is some change in the shear angle in this zone. The sliding deformation is most appreciable at the edges, even though there is some sliding throughout this zone. Zone-III is the remainder of the preform located between Zone-I and Zone-II. The former forms a shape that resembles a hexagon. This zone is free from the constrained ends boundary effects and most of the deformation of the fabric occurs in this zone. The main mode of deformation in this zone is scissoring/shear. There is pure shearing in the middle of the preform. However, there is a considerable amount of sliding that occurs at the free edge of the preform. The shear rigidity “ G_{12} ” has been used as a function of shear angle defined in Eq. (3.29).

The analytical relationship used to predict the evolution of shear angle in the pure shear zone is defined as:

$$\gamma = \frac{\pi}{2} - 2 \cdot a \cos\left(\frac{D+d}{\sqrt{2} \cdot D}\right) \quad (3.33)$$

Where ‘D’ is the difference in length and width of the rectangular specimen in the undeformed state and ‘d’ is the overall extension applied along length of the fabric.

The model used to perform numerical test of bias extension consists of 3D quadrilateral membrane elements (M3D4R). The nodal positions of elements are deliberately defined to produce the three distinct shear zones as shown in Fig. 3.11. The numerical results are

compared with the theoretical output of the shear angle evolution in the pure shear zone i.e. zone-III.

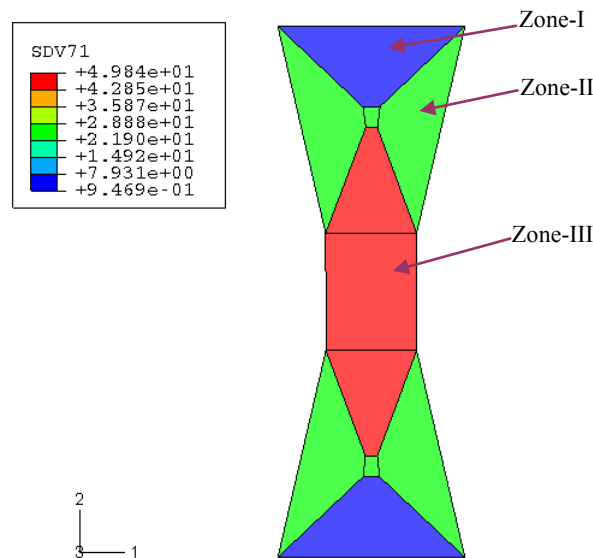


Fig. 3.11 Bias extension test with three distinct zones emerged after deformation.

SD71 is the shear angle in degrees.

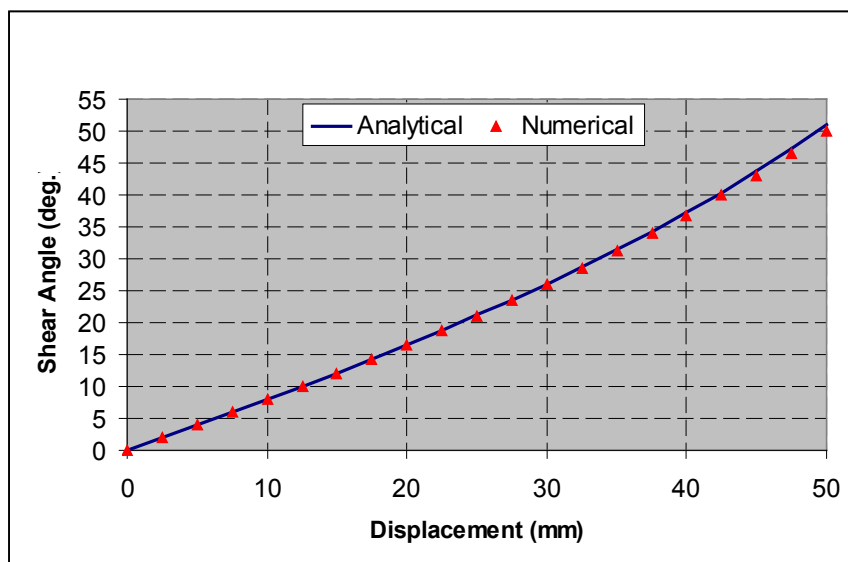


Fig. 3.12 Numerical and analytical comparison of the shear angle with longitudinal displacement.

Fig. 3.11 shows the evolution of shear angle in the central zone (pure shear) with extension of the rectangular specimen. The numerical results confirm the theoretical output in case of BPW fabric material data.

3.8 Fabric Material Behaviour with VFABRIC

In the latest version (V-6.8) of ABAQUS/Explicit, a user subroutine named VFABRIC has been introduced to analyse numerically the woven fabrics specifically at macro-level. It is presented here for the purpose of comparison of results obtained through direct application of user subroutine VFABRIC and by using the stress computation algorithm developed for fibrous materials (Section-3.4) implemented through the user subroutine VUMAT. However, the advantage of the developed algorithm using hypoelastic behaviour lies in its generalization to be implemented in any commercial FE code. Thus, fibrous materials analysis can be carried out using standard elements in a generalized FE code.

Essentially, some significant features of the user material subroutine VFABRIC in conjunction with fabric material behaviour [ABA68] are presented here.

- VFABRIC captures the mechanical constitutive behaviour of the fabric material (anisotropic and nonlinear) in the plane of fabric and therefore, used with elements under plain stress condition.
- It takes into account the materials exhibiting two structural directions that may not be orthogonal to each other before and/or after deformation.
- Nominal stresses are updated using nominal strains along the yarns (measured as stretch ratios λ_1 and λ_2) whereas the engineering shear strain is measured as the change in angle (in radians) between the two directions going from reference to deformed configuration (B to B*).

Moreover, it is claimed that:

- The user material subroutine VFABRIC allows for building a complex material model taking into account both the fabric structural parameters such as yarn spacing, yarn cross-section shape, and the yarn material properties.

Since the local directions may not remain orthogonal with deformation, ABAQUS updates the local directions with deformation. There is not enough algorithm detail applied for tracing the fibre directions with deformation however, it can be presumed that the two structural directions are traced based on deformation gradient as the stress computation algorithm

presented in Section-3.4 has been using in VUMAT.

By using VFABRIC, ABAQUS computes the nominal strains along fibre directions based on stretch ratios (λ_1 and λ_2). Moreover, it seems in contradiction to ABAQUS/Explicit default scheme of strain computations (i.e. based on logarithmic strains) [ABA68a]. However, the angle in radians between current fibre directions is correctly translated as fabric shear strain.

The stretch ratio λ and the nominal strain $\varepsilon_{\text{nom}}(\lambda)$ are computed as:

$$\lambda = \frac{1}{L} \quad \varepsilon_{\text{nom}}(\lambda) = \lambda - 1 \quad (3.34)$$

The constitutive behaviour for the fabric defines the nominal stresses in the local system in terms of the fabric strains which is transformed to Cauchy stresses in the GN orthogonal basis at material points.

3.8.1 Elementary Tests using VFABRIC

Material input data: $E_1=35,400$ MPa, $E_2=35,400$ MPa, $\nu_{12}=0$

(a) 45° simple shear test (Fig 3.2)

$$[\boldsymbol{\sigma}]_f = \begin{bmatrix} \sigma_{11} \\ \sigma_{22} \\ \sigma_{12} \end{bmatrix} = \begin{bmatrix} 1.56 \neq 0 \\ 1.466\text{E} + 04 \\ 0 \end{bmatrix}$$

(b) Traction followed by rigid body rotation (Fig 3.6)

$$[\boldsymbol{\sigma}]_f = \begin{bmatrix} 3.54\text{E} + 04 \\ 0 \\ 0 \end{bmatrix}$$

Remarks

The elementary test outputs conducted numerically clearly indicate that the nominal strain was used to compute stresses. The output of simple shear test endorses that there exists some discrepancy in true stress state computations for fibrous materials since the magnitude of stresses along first fibre direction is of the order of a few MPa. Whereas the same output, with

exactly identical material input and boundary conditions, using hypoelastic behaviour algorithm for fibrous materials with VUMAT is of the order of 10^{-6} MPa which is far more accurate than VFABRIC output. However, the second elementary test output indicates that algorithm behind VFABRIC comes true to the principle of objectivity: with rigid body rotation there are no spurious stresses generation.

3.9 Numerical Modelling for Composite Prepreg

Prepreg is an important composite material form of the “pre-impregnated” fabric. The fibres in prepreg usually take the form of a weave or are uni-directional laminate. The fabric reinforcement is saturated with partially cured resin. The prepreps are mostly stored in cooled areas since polymerization activation is most commonly done by heat. Hence, composite structures built of prepreps will mostly require an oven or autoclave to cure out. Pre-preps have the advantage of possessing more controlled fibre-resin ratio.

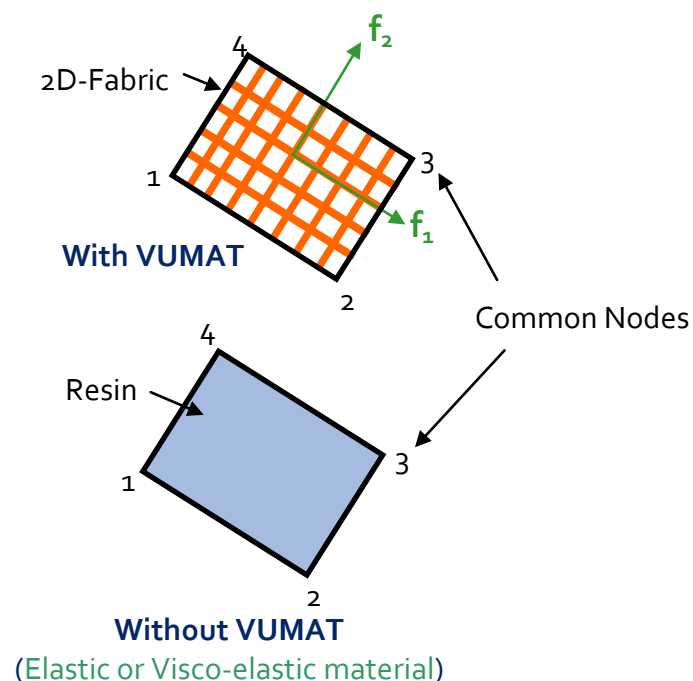


Fig. 3.13 The representation of a numerical technique to analyse composite prepregs using two superimposed elements with common nodes

Here we suggest a numerical technique to analyse the composite preregs. The algorithm adopted is the same that developed for fibrous media analysis. However, the technique used is of unidirectional fibres with two superimposed elements (1DF2E) presented in section-3.4.2.a. Fig. 3.13 shows numerical technique adopted for prepreg analysis. Two 3D quadrilateral membrane elements with common nodes have been selected. One element contains 2D fabric material data and is analyzed with VUMAT subroutine built with stress computation algorithm of hypoelastic behaviour for fibrous materials. The second element possesses resin material properties which have elastic or visco-elastic material behaviour.

The nodal displacements in case of superimposed elements with common nodes are:

$$\mathbf{U}_{(x,y,z)}^{\text{fibers}} = \mathbf{U}_{(x,y,z)}^{\text{resin}}$$

The deformation gradient tensor will also be same for both fibres and resin:

$$\mathbf{F}^{\text{fibers}} = \mathbf{F}^{\text{resin}} = \frac{\partial \mathbf{x}}{\partial \mathbf{X}}$$

The strain tensor computed by working code (ABAQUS/Explicit) will be same when expressed in the default output basis (GN frame). However, due to application of fibrous algorithm via VUMAT, the strain tensor expressed in fibre bases will differ.

$$\boldsymbol{\varepsilon}_{(f_1 \otimes f_2)}^{\text{fibers}} \neq \boldsymbol{\varepsilon}_{(e_1 \otimes e_2)}^{\text{resin}}$$

The stress computation will also be different for the element containing fabric material data. This fabric stress is computed in the fibre bases and is based on the strains in the fibres and change in angle (radians) between fibres during deformation. Also, the material input data is different for both resin and fibres. Therefore;

$$\boldsymbol{\sigma}_{(f_1 \otimes f_2)}^{\text{fibers}} \neq \boldsymbol{\sigma}_{(e_1 \otimes e_2)}^{\text{resin}}$$

The main mode of deformation in a pre-preg numerical analysis will due to fabric deformation and resin material will add enhanced shear rigidity to fabric. Here, a numerical

example of bias extension test for pre-preg analysis is presented and compared with fabric without resin. The fibres are aligned with edges of the elements and both are at $\pm 45^\circ$ to the loading direction initially. The material properties for dry fabric are same as of bias extension test presented earlier. The resin is supposed to have elastic isotropic properties with tensile modulus of 150 MPa. Both models are loaded to the same extension.

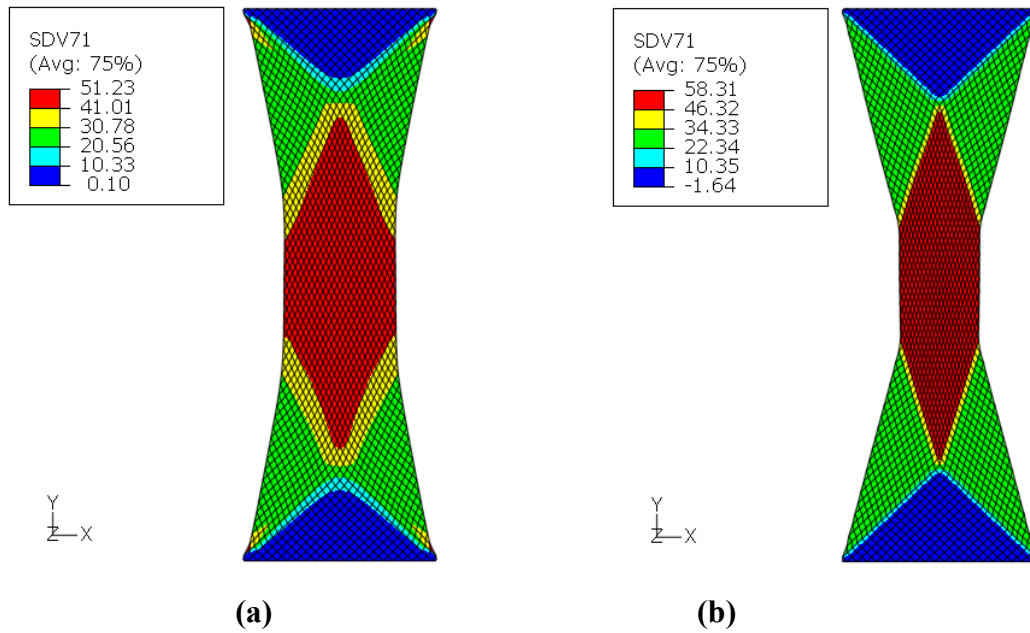


Fig.3.14 The shape and shear angle (degrees) evolution in bias extension tests:

(a) Prepreg (b) Dry fabric (SDV71 is shear angle in degrees)

Fig. 3.14 shows the evolution of shear angle in degrees. It is noted that the model having resin material data in addition to the fabric properties produces less shear angle evolution when compared with the dry woven fabric for the same extension of the specimens under test. This can be attributed to the fact that the resin introduces enhanced shear rigidity to the specimen. However, the test has not been verified through experiments.

Conclusions of Chapter-3

The major focus in this chapter has remained over the development of an algorithm for fibrous material analysis using a hypoelastic model. At first this model was developed for single direction of fibres which was used mainly for meso-scale analysis of woven fabrics. Importantly, the model is based on the continuous approach and has been formulated in a user material subroutine VUMAT of the commercial FE code i.e. ABAQUS/Explicit. Specifically in this study, the hypoelastic model has been applied to the macro-scale analysis of woven composites. The key point presented in this chapter lies in section-3.4 where the unidirectional formulation of the already developed hypoelastic model has been extended to the factual form of woven fabrics i.e. bidirectional material data. The bidirectional formulation has been developed to incorporate 2D material data of both tensile and in-plane shear. The stress computation algorithm developed is based on selection of two orthogonal frames where each one contains one set of fibre orientation along one of its axes. To the end of algorithm formulation, stress output is transformed to the single orthogonal frame of the code work basis. Moreover, an interesting and equally accurate technique for 2D fabric analysis has been presented. This is based on the unidirectional formulation of hypoelastic law already built. However, it was extended to analyse 2D fabrics implementing the idea of superimposed elements having common nodes.

The two methods of analysis have been tested numerically through verification tool of elementary test output conforming accurately to the theoretical results. A short analysis of the recently introduced user material subroutine VFABRIC presented in comparison to the developed algorithm output shows its capability limits. Finally, two widely used de-facto standard tests for in-plane shear characterisation of woven fabrics have been numerically tested using the hypoelastic model, needless to say, with both methods of fabric analysis (1DF2E and 2DF1E). Undoubtedly, the results obtained numerically with the algorithm developed using hypoelastic model and validated through theoretical and experimental output establish the legitimacy and accuracy of this algorithm to a great extent.

4 Experimental Forming Analysis of Woven Composites

4.1 Introduction

This chapter deals with the experimental forming analysis of woven composite reinforcements. As explained in the preceding chapters that our major focus in this study will remain over RTM process among the widely used contemporary composite forming processes. Specifically, the first stage of RTM process called “preforming of dry fabric” will be considered in the experimental study. The model studied for fabric forming is an international forming benchmark for woven composites called “double dome” [WC08]. In this chapter, the in-house development of forming tools and hence, the fabric forming experiments performed will be presented and discussed in detail. In this project of PhD study, the benchmark geometry of double dome will be a “preforming case study” either for experimental tests or for numerical simulations.

The textile fabrics used for preforming experiments are mostly those used in the benchmark study for material characterisation of woven composites. The benchmark study of woven composites mainly consists of two stages: a material characterisation stage with three types of woven fabrics and the stamping operations using double dome geometry with same fabrics. The first stage has recently been accomplished by the participants [CAO08]: the researchers of six different universities of the world (composite forming group headed by Pr. Philippe Boisse at LaMCoS, INSA de Lyon is among the participants), expanded over some years since its origin in 2003. The types of fabrics and material characterisation will be briefly introduced in this chapter as a reference. The second stage of benchmark study mainly demands the numerical modelling using already published material characterisations [CAO08] and hence the output data comparison among the group of researches. However, in

this particular study of PhD thesis, the experimental forming analysis has been considered to be a part and parcel of numerical modelling. The major focus in this chapter will be the fabric forming experiments and also the exploitation of 3D optical strain measurement (OSM) method using Vic-3D system of digital image correlation (DIC) for measurement of shear angles over the draped fabrics.

4.2 Benchmark Study Fabrics

4.2.1 Types of Fabrics

There are three types of commingled glass/polypropylene woven fabrics selected for benchmark study of woven composites namely:

- 1) Balanced Plain Weave (BPW)
- 2) Balanced Twill Weave (BTW)
- 3) Un-balanced Twill weave (UBTW)

The benchmark fabrics, shown in Fig. 4.1, are manufactured with commingled glass and polypropylene fibres with a certain ratio. The fabric material selections are based on the objective to perform thermo-stamping operation of woven composite forming. Yet, it should be known that the recent published benchmark effort [CAO08] based on shear characterisation of above cited fabrics is experimented without preheating. These fabrics were initially distributed to different research groups to test and report the fabric material specifications, the test procedures used and most importantly the shear properties obtained [WC08].

Among these benchmark fabrics, we have used BPW fabric as to perform fabric forming experiments. It will be shown in section-4.3 that availability of CAD model and the development of forming tools constraints have limited us to use only BPW fabrics.

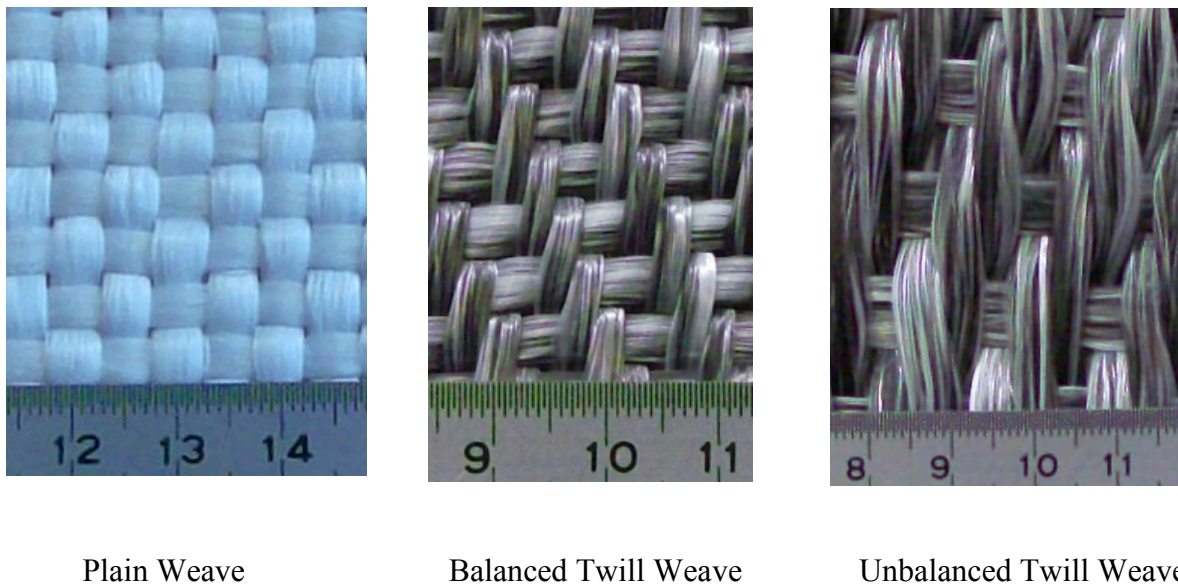


Fig. 4.1 Three types of fabrics used for benchmark study of woven composites

4.2.2 Material Characterisation and Specifications

The material characterisation mainly concerns the “shear behaviour characterisation” of the benchmark fabrics. Indeed, the shear deformation behaviour is a specific feature and distinguished mode of deformation of textile fabrics. There have been many other important parameters of benchmark fabrics reported by different research groups available on benchmark forum such as: fabric thicknesses, areal densities, volumetric densities, yarn linear densities, coefficient of friction.... also shown in Table 4.1.

The shear behaviour of benchmark fabrics have been tested using well-known de-facto standard tests of picture frame and bias extension. The shear properties reported by different research groups of each fabric have been compared separately. Since different groups used varied sizes of fabric test samples so before comparison of the material characteristic data obtained through these two tests, therefore, they have been normalized with agreed normalization methods.

Table. 4.1 Important material specifications of the benchmark fabrics reported on [WC08]

Manufacturer's style	TPEET22XXX	TPEET44XXX	TPECU53XXX
Weave type	Plain	Balanced Twill	Unbalanced Twill
Yarns	Glass/PP	Glass/PP	Glass/PP
Weave	Plain	Twill 2/2	Twill 2/2
Area density, g/m ²	743	1485	1816
Yarn linear density, tex	1870	1870	2400
Thickness*, mm	1.2 (NU)	2.0 (NU)	3.3 (NU)
Yarn count, picks/cm or ends/cm			
Warp	1.91 (KUL) 1.93 (HKUST) 1.95 (NU)	5.56 (KUL)	3.39 (KUL)
Weft	1.90 (KUL) 1.93 (HKUST) 1.95 (NU)	3.75 (KUL)	1.52 (KUL)
Yarn width in the fabric, mm (**standard deviation)			
Warp	4.18±0.140** (KUL) 4.20 (HKUST) 4.27 (NU)	1.62±0.107** (KUL)	2.72±0.38** (KUL)
Weft	4.22±0.150** (KUL) 4.20 (HKUST) 4.27 (NU)	2.32±0.401** (KUL)	3.58±0.21** (KUL)

* ASTM Standard D1777 (Applied Pressure = 4.14 kPa)

HKUST: Hong Kong University of Science and Technology, Hong Kong

KUL: Katholieke Universiteit Leuven, Belgium

NU: Northwestern University, USA

The picture frame test is normalized using different “frame and fabric lengths” [PEN04] and using “energy method” [HAR04] when frame and fabric lengths are equal as under:

The shear force F_s (Fig.4.2) is calculated as:

$$F_s = \frac{F}{2 \cos \theta} \quad (4.1)$$

Where F is the total force required to deform the fabric.

The normalized force F_n using frame and fabric lengths is as under:

$$F_n = F_s \cdot \frac{L_{\text{frame}}}{L_{\text{fabric}}^2} \quad (4.2)$$

Where L_{frame} and L_{fabric} are lengths of the frame and fabric specimens, respectively, used in case of picture frame test.

The normalized force F_n when frame and fabric lengths are equal reduces to:

$$F_n = F_s \cdot \frac{1}{L_{\text{fabric}}} \quad (4.3)$$

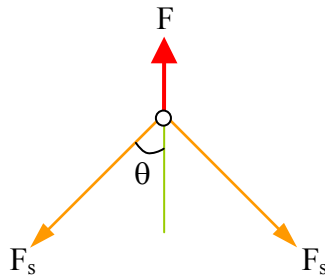


Fig. 4.2 Schematic free body diagram for the applied force F and the shear force F_s of the picture frame test

The important test results of shear behaviour of benchmark fabrics with picture frame and bias extension tests are referred hereby. These test results will be exploited in the numerical simulations in the succeeding chapter.

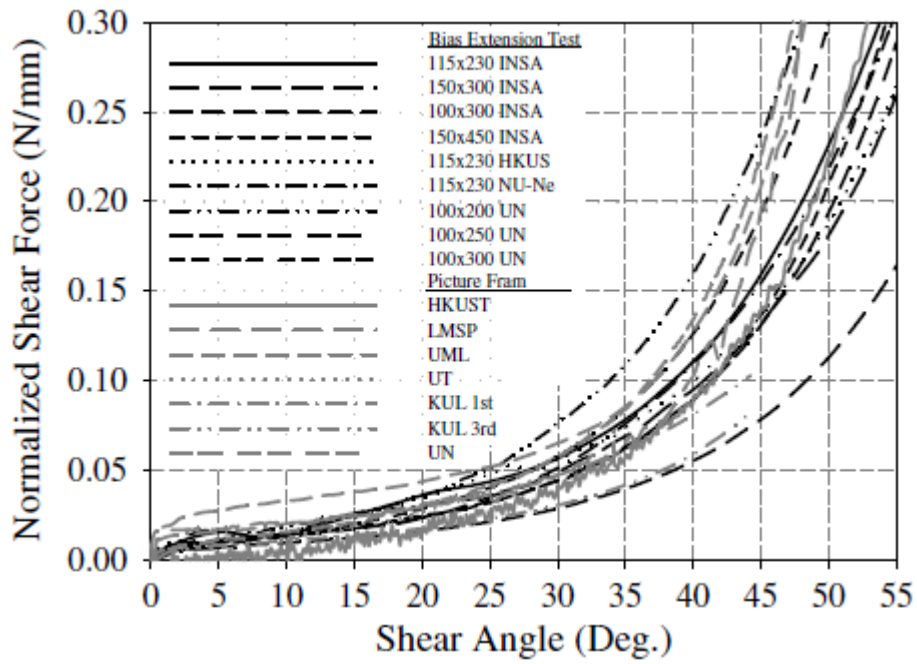


Fig. 4.3 Normalized shear force vs. shear angle from picture frame and bias extension tests for BPW fabric [CAO08]

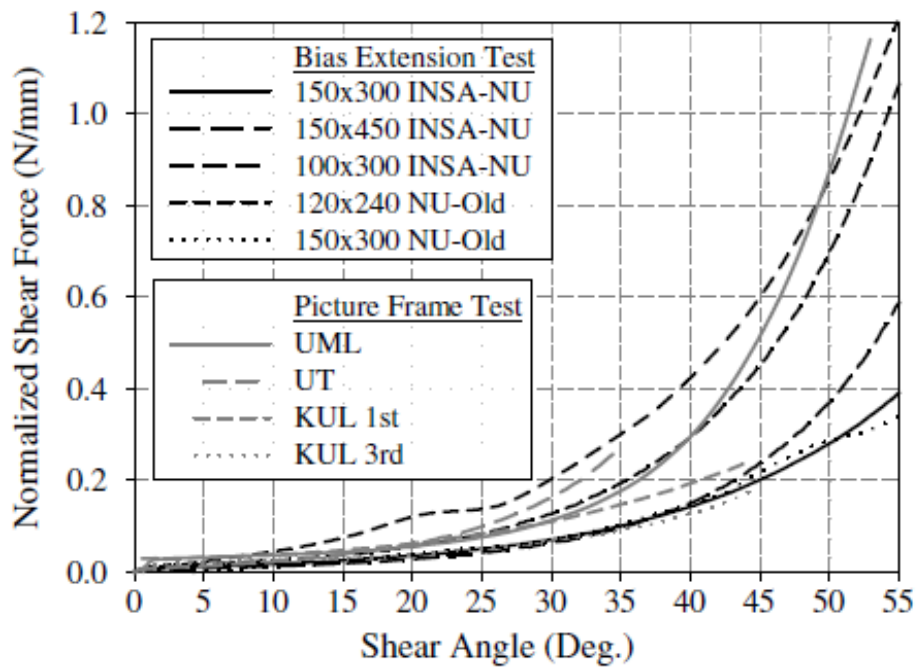


Fig. 4.4 Normalized shear force vs. shear angle (degrees) from picture-frame and bias extension tests for BTW fabric [CAO08]

4.2.3 Shear Modulus Determination

Shear rigidity of the fabrics are determined from the normalized shear force data as a function of shear angle. The normalized shear force results are hereby assigned with an approximated curve with reference the curves shown in Figs. 4.3 and 4.4. The data for this curve is first converted into normalized shear force versus shear angle in radians.

Considering the case of picture frame test and as shown in Fig. 4.2 the shear force acts along the side of the frame. So, when it is divided by the cross-sectional area “A” along the side of the fabric, it defines the shear stress given by:

$$\tau = \frac{F_s}{A} = \frac{F_s}{L_{\text{fabric}} \cdot t_{\text{fabric}}} \quad (4.4)$$

Where t_{fabric} is the thickness of the fabric. By using Eq. (4.3), when fabric and frame length are equal, and when the shear data of the fabric is available in the form of normalised shear force, the shear stress τ can also be written as:

$$\tau = \frac{F_n}{t_{\text{fabric}}} \quad (4.5)$$

Therefore, just by dividing the normalised shear force with thickness of the fabric it gives the shear stress in case of a picture frame test having same fabric and frame lengths. The shear stress is plotted against shear angle in radians as shown in the Fig. 4.5. Now this curve is assigned a polynomial regression equation that appropriately traces the path of this curve. The derivative of this curve (the regression equation) can provide us the shear rigidity as a function of shear angle in radians.

a) BPW fabrics

The polynomial regression equation selected passing through normalised shear force data curves for “BPW fabric” as shown in Fig. 4.3 is:

$$F_n(\gamma) = 2.035\gamma^5 - 3.6291\gamma^4 + 2.451\gamma^3 - 0.498\gamma^2 + 0.06121\gamma + 0.005 \quad (4.6)$$

Here γ is in radians. By using Eq. (4.5) in conjunction with Eq. (4.6), i.e. dividing the data points with thickness of the fabric, the shear stress come out as:

$$\tau(\gamma) = 1.696\gamma^5 - 3.0243\gamma^4 + 2.0425\gamma^3 - 0.415\gamma^2 + 0.051\gamma + 0.0042 \quad (4.7)$$

Taking derivative of the polynomial Eq. (4.7) as a function of shear angle (radians) γ , this gives us the shear rigidity of the fabric:

$$G_{12}(\gamma) = 8.48\gamma^4 - 12.0972\gamma^3 + 6.1275\gamma^2 - 0.83\gamma + 0.051 \quad (4.8)$$

This procedure of shear modulus determination for the BPW fabric is plotted in the form a graphic representation as shown in Fig. 4.5. The shear angle is taken in radians and there are two vertical scales. The scale on left is with units of MPa and serves a common scale for shear stress and shear rigidity. The right hand scale is for normalised shear force with units of N/mm. All three curves are drawn as a function of shear angle in radians as an independent quantity. Figs. 4.5 is just the graphical representation of Eqs. (4.6)-(4.8).

Shear Modulus Determination-PW

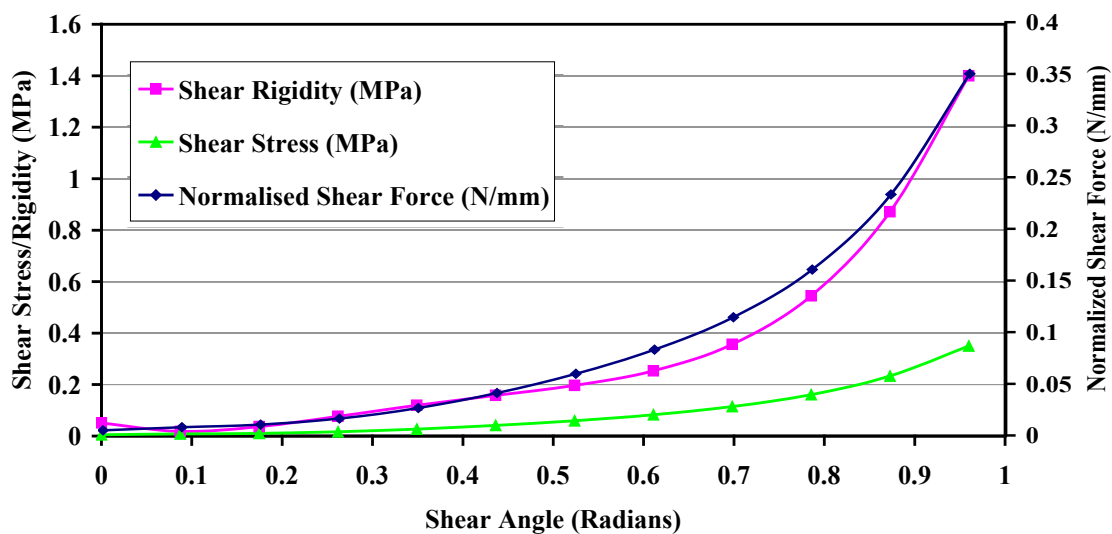


Fig. 4.5 Normalised shear force, shear stress and shear rigidity curves for BPW fabric

The shear rigidity determined here for BPW fabric will be used in the numerical tests of 3D fabric forming in the subsequent chapter. The same has also been used in the numerical tests of picture frame and bias extension presented in chapter-3. The shear rigidity of BTW fabric has already been exploited in case of picture frame test conducted numerically (chapter-3).

b) BTW fabrics

Similarly, the polynomial regression equation selected passing through normalised shear force data curves for “BTW fabric” as shown in Fig. 4.4 is:

$$E_n(\gamma) = -6.3609\gamma^5 + 17.429\gamma^4 - 13.271\gamma^3 + 3.7098\gamma^2 - 0.0916\gamma + 0.0041 \quad (4.9)$$

Where γ is the shear angle in radians. By using Eq. (4.5) in conjunction with Eq. (4.9), i.e. dividing the data points with thickness of the fabric, the shear stress come out as:

$$\tau(\gamma) = -3.18045\gamma^5 + 8.7145\gamma^4 - 6.6355\gamma^3 + 1.8549\gamma^2 - 0.0458\gamma + 0.0021 \quad (4.10)$$

And finally, the shear rigidity obtained for BTW-fabric is:

$$G_{12}(\gamma) = -15.90225\gamma^4 + 34.858\gamma^3 - 19.9065\gamma^2 + 3.7098\gamma - 0.0458 \quad (4.11)$$

A graphical representation of Eqs. 4.9-4.11 is shown in fig. 4.6.

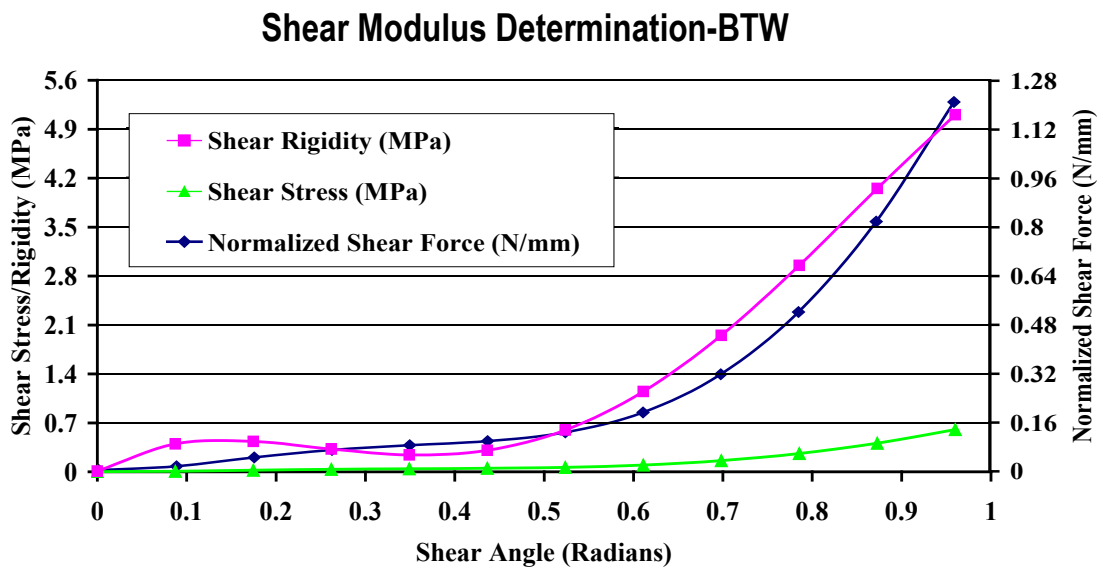


Fig. 4.6 Normalised shear force, shear stress and shear rigidity curves for BTW fabric

4.2.4 Double Dome Benchmark

As mentioned earlier, the double dome benchmark geometry is selected for preforming the dry reinforcements with benchmark study fabrics within the scope of present study related to forming of woven composites. The CAD rendering surfaces of the punch, binders and die are illustrated in Fig. 4.7. This benchmark geometry is provided by Ford Motor Company (Dearborn, Michigan, U.S.A.). CAD models of the punch, die and holder are available on the woven composite benchmark forum website [WC08]. Note that the binders are segmented so that each segment can be controlled independently. However, in this particular study, all binder segments will be used together to equally displace vertically. This tooling geometry is symmetric about the x-y plane at $z=0$ and about the y-z plane at $x=0$. The gap between the punch and die can be adjusted to either 1 or 2 or 3 mm. In practice, this adjustment is achieved by using three different punches that are mounted to the upper tool to create the desired cavity thickness. However, the cavity gap of 1mm has been used here to perform forming tests.

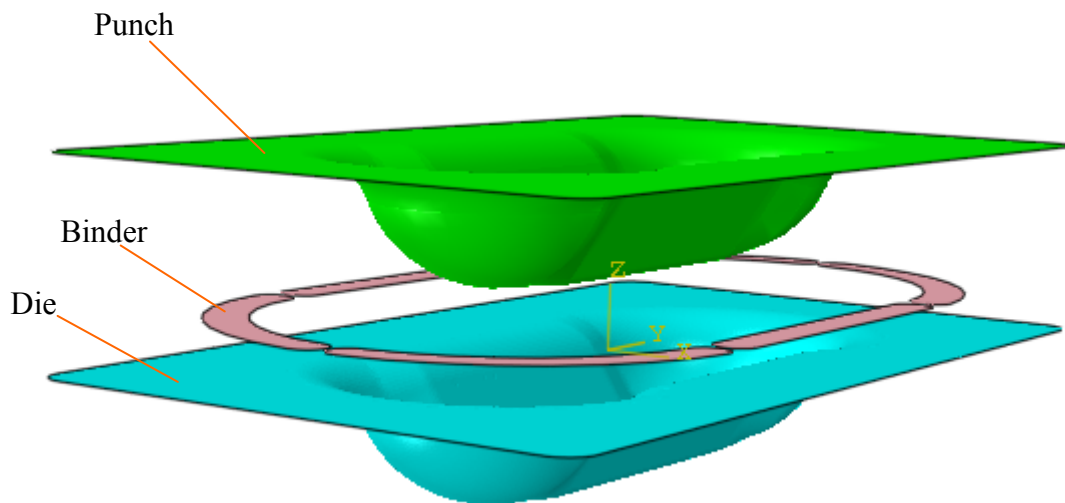


Fig. 4.7 The surface rendering of the stamping model of double dome geometry

4.3 Composite Forming Experiments

The first stage of “dry fabric forming” is one of the two major stages of RTM process. It influences a lot over the subsequent stage of the resin injection and consequently, the mechanical properties of final composite part are much dependent on this stage. It has already been pointed out that the first stage of RTM process is of our main interest in this study. The experimental study carried out for 3D forming of double dome model consists of two main steps: the development of double dome forming tools and the execution of experiments.

4.3.1 Development of Forming Tools

The CAD model of double dome geometry is obtained from the benchmark forum [WC08]. The development stage of forming tools was a hectic task expanded over a couple of months. The model was exported to CAM software Esprit-2006. The latter was exploited to simulate the machining of double dome according to different strategies of the moving cutting tool. The optimized strategy yielding to a good machined surface quality was retained and post-processed to create the G-code program useful for double dome machining. The latter was performed on a 5-axis machining centre (HURON K2X8 FIVE). The material used for developing forming tools was Prolab-65; selected keeping in view producing rapid prototyping and has sufficient mechanical properties with respect to the present forming tests. The cavity gap between punch and die was retained 1mm.



Fig. 4.8 The binder (six-pieces) assembled with cylindrical pins passing through punch and groove on punch to accommodate the binder segments.

Figs. 4.8 and 4.9 show the detailed assembly of the six piece blankholder used. The six segments of the binder are assembled in such a manner that they move vertically with the same displacement. Fig. 4.9 shows that on the top of the punch they are joined through a ring. This ring is also used to carry the dead weights during forming operation which act to insert binder force over the fabric. The binder force applied is constant throughout the test. The vertical pins can move through the pin-holes in the punch and thus punch displaces to deform the fabric whereas the blankholder stays at its position during the test. At the completion of the punch stroke, the segmented holder takes its position in the groove beneath the punch so that punch flat region and binder may come at the same level.

The challenges faced during machining of the tools were those which are normally faced in prototype development such as the machining strategy and the clamping systems.

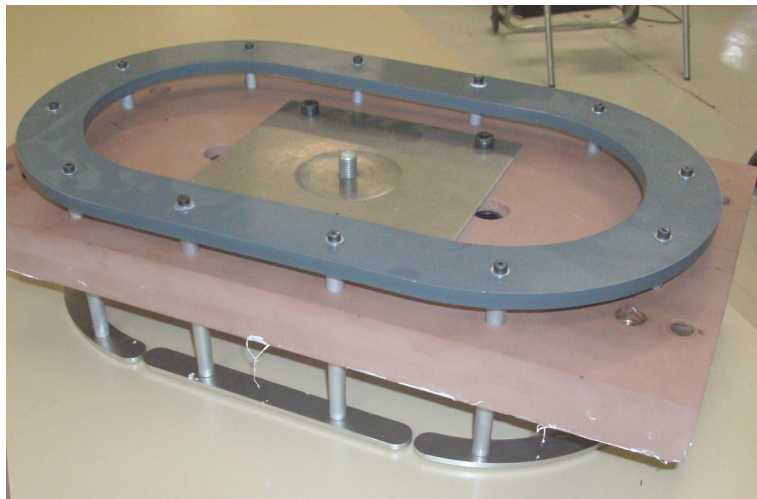


Fig. 4.9 The top ring assembled to the binder segments through pins and former is used to carry dead weights

4.3.2 Double Dome Forming Tests

The experimental tests have been performed with a local development of the experimental setup shown in Fig. 4.10. These tests are performed using benchmark model called “double dome” with forming tools developed as detailed above.

A constant binder force of 100 N was applied during the forming of all experimental tests. The blankholder (binder) used consists of six segmented pieces and each one has a width of 20 mm and thickness of 5 mm. The binder segments are evenly loaded with the binder force

and are constrained to displace vertically during forming process which was carried out with a constant punch velocity of 200mm/min. The forming tests were performed over a tensile testing machine (RSA 250 KN Schenk-mechanical). Indeed, one main objective of these tests is to qualify the numerical model developed for composite reinforcement forming. It is interesting to note that the tests were preceded by delicate position adjustments between the punch and the die. The aim was to ensure a constant gap between the convex and the concave imprints.

The experimental tests have been carried out using the benchmark study fabric of commingled glass/polypropylene with BPW shown in Fig. 4.1. Rectangular blank sizes of 470 mm × 270 mm have been used. The blanks are prepared with the yarn orientations of 0°/90° and ±45° with respect to the sides of the rectangular blank. Since the blanks are cut out of the large fabric sheet manually there could be some possibility of misalignment and human error contribution, although it was made sure with a transparent sheet containing angles and straight lines to avoid significant errors. The blanks were applied with a very slight layer of a commercially available hardening agent mixed with resin prior to forming operation. This treatment virtually does not affect mechanical properties of the fabric and enable the formed fabric to maintain its new shape after the forming operation.

The results obtained of the experimental forming tests of fabric reinforcements are shown in Figs. 4.11 and 4.12. The procedure adopted for experimental fabric forming tests has been advantageous in the sense that yarn orientations of the fabrics are clearly visible after draping. It will be shown in the section-4.4 that this visibility of the yarns has helped a lot to measure the shear angle of the draped fabrics.

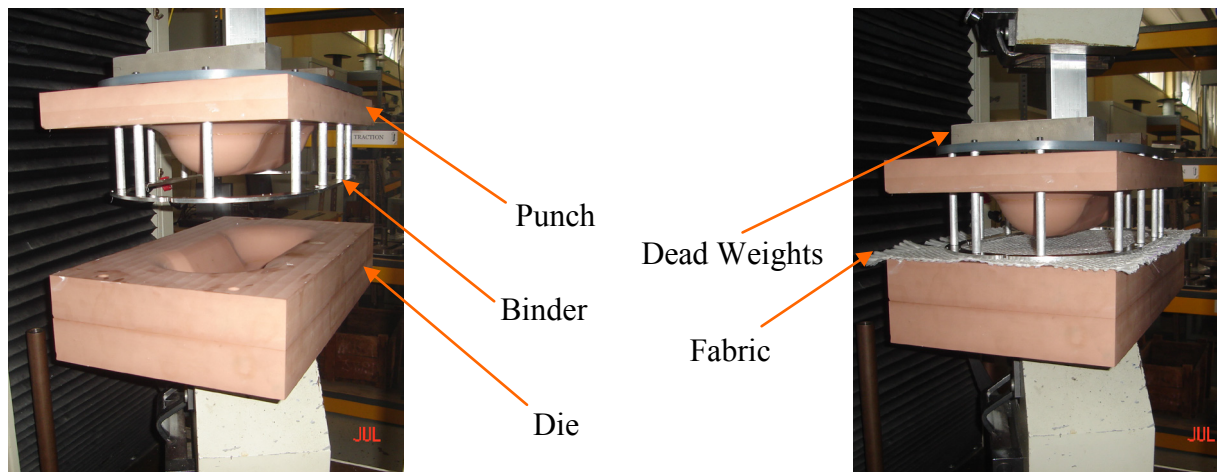


Fig. 4.10 Experimental setup forming of the double dome benchmark



Fig. 4.11 Experimental test output of double dome benchmark tests with 0°/90° fibre orientations

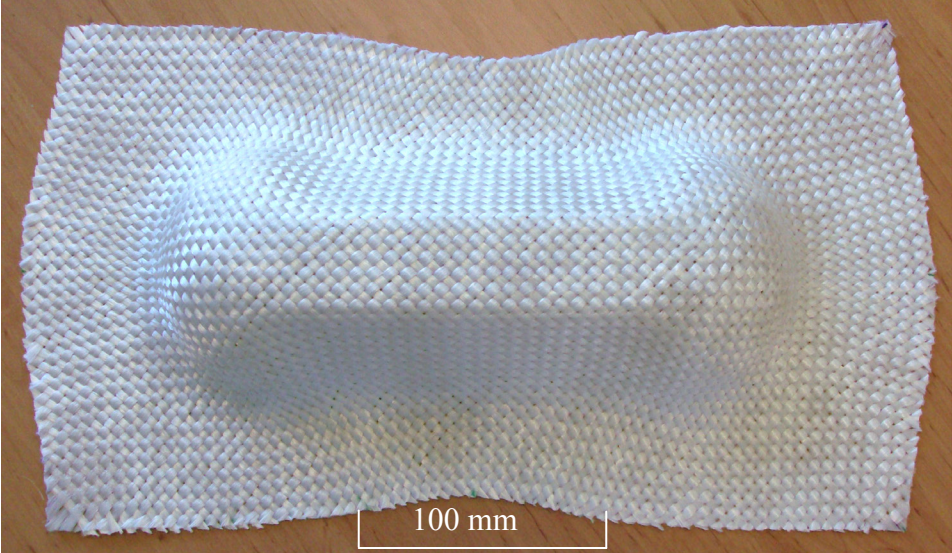


Fig. 4.12 Experimental test output of double dome benchmark tests with ±45° fibre orientations

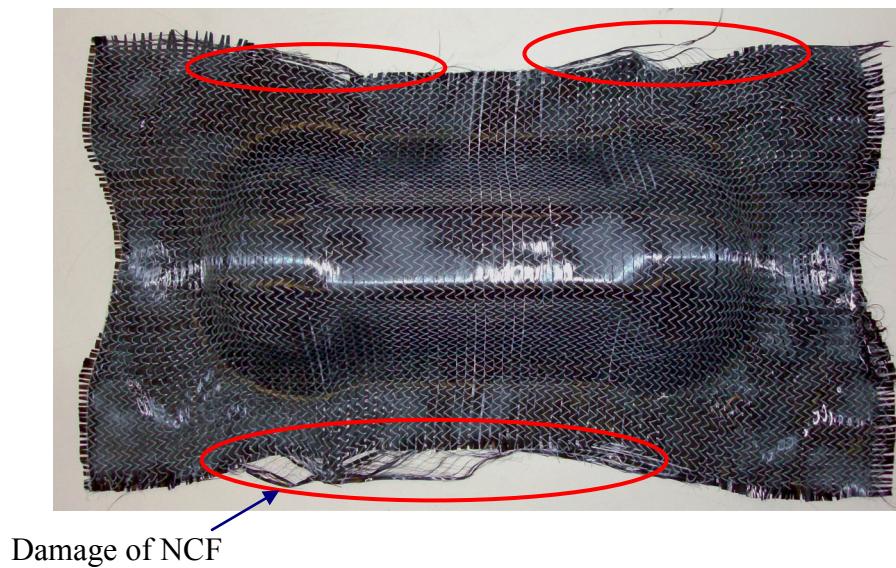


Fig. 4.13 Experimental test output with double dome benchmark forming device for 0°/90° fibre orientations using NCF

By using the same double dome forming tools, an experiment has been performed for NCF fabric with 0°/90° orientation of fibres and is shown in Fig. 4.13. It has been observed that the fabric is sufficiently damaged due to contact problem between the blank holder and the work piece. The holder is a six piece split entity and it also had some sharp edges which entangled with the stitching of NCF. Therefore, the damage of the fabric was occurred. In this context, it is recommended to use a plane (one piece) blank holder or either to increase the chamfering of the split binder.

4.4 3D Optical Strain Measurement (OSM)

The shear angle for the draped fabrics is considered an important parameter and determines the orientation of yarns in the final part. Therefore, there is a strong need for a reliable method so that correct measurement of shear angles can be made over the part after deformation. In order to achieve this objective, we have used 3D optical strain measurement (OSM) method

which is based on treating the final 3D digital image of the part after forming. These digital images are taken using a 3D digital image correlation (DIC) system of Vic-3D. Here, we discuss some important specificities of DIC system and then we shall converge towards our problem.

4.4.1 Digital Image Correlations (DIC)

The digital image correlation is an optical method to measure the contour, displacement and strains of an object surface. This technique consists on capturing consecutive images with a digital charge-coupled device (CCD) camera during the deformation period. DIC uses a mathematical correlation algorithm to analyse the digital image data. This permits to evaluate the change in surface characteristics and understand the behaviour of the specimen while subjected to incremental loads. To apply this method, the specimen needs to be prepared by the application of a random dot pattern called grey speckle pattern to its surface. For textile fabrics this can be the natural texture of the fabrics or additionally applied paint. A calibration of the camera set-up is essential before capturing the digital images. This technique starts with a picture before loading (reference image) and then a series of pictures are taken during the deformation process (deformed images). All the deformed images show a different random dot pattern relative to the initial undeformed reference image. The greyscale digital images are post processed by image correlation software that calculates first the displacement field over the selected region of interest (ROI) and then derives strains through differentiation of the displacement field. Strains of 0.02 % up to several hundred percents can be defined. For an optimal functioning of the displacement mapping a high-contrast random isotropic (natural or artificial) grey speckle pattern should be attached to the object surface: ‘randomness’ to unambiguously identify a particular point on the material, ‘isotropy’ and ‘high-contrast’ to have enough grey value gradients in all direction.

DIC has widely been used in textile composites recently [DUM03] [LOM08] [MOR08] [WIL08a] [DEL09]. The important terminology of DIC and concepts related to textile materials applications are defined as under:

A **subset window** is a square array of pixels defined in the reference image as a neighbourhood of a particular point as a grey scale template in the pattern matching process. Since the subset deforms over the subsequent images, therefore the speckle pattern of this neighbourhood should hold enough contrast and directional information to track the local

deformation. The deformed coordinates are calculated using a cross-correlation algorithm based on the first order transformation (deformation gradient).

A **step size** is the distance in pixels between the centres of neighbouring subset windows. The step size determines the spatial resolution and must be smaller than the subset size to enable overlapping of the subset windows in order to achieve the continuous displacement field.

A **strain window**, [LOM08], is an array of " $p \times p$ " neighbouring subset windows and where the strain is calculated. The differentiation algorithm uses a strain window to define strains derived through differentiation of the displacement field. The algorithm also involves a strain gauge length of " $m + n(p - 1)$ " for a subset of " $m \times m$ " pixels, a step size of " n " pixels and a strain window of " $p \times p$ " subsets.

Two-dimensional DIC requires one CCD camera to be positioned perpendicular to a flat surface. The displacement field obtained is only reliable under the assumption that out-of-plane deformation can be neglected. By definition, in-plane deformation of a textile is characterised by the strains of the fabric middle surface. The in-plane shear tests of picture frame and bias extension are normally studied using 2D DIC. In our laboratory: LaMCoS, INSA de Lyon, a locally developed 2D DIC software ICASOFT by Fabrice Morestin has been used for in-plane shear tests [DEL09].

Three-dimensional DIC needs two CCD cameras to be placed at different angles with respect to the object to be correlated. Primarily a calibration for the set-up of cameras is performed from which the relative camera position, focal length and lens distortions are identified. This information is required in the object tracking and enables to estimate the DIC accuracy. From the 3D displacement fields, strains are calculated in the tangential plane of the object. 3D DIC measurements give strains in the tangential plane to a local point on the fabric surface, which is defined by micro-relief of the fabric, and which deviates largely from the middle surface—hence the strains measured by 3D DIC cannot be used to characterise in-plane deformations of the fabric [LOM08]. In the present study of DIC measurements over double dome formed parts, stereo-correlation (3D DIC) has been employed. The in-plane shear has been measured using coordinates of the points over the deformed surface and following the yarn directions.

In **meso-scale DIC** measurement the strain gauge length is less than the repeat size of the fabric which allows studying meso-scale deformation mechanisms. Whereas, **macro-scale DIC** measurement the strain gauge length is larger than the repeat size of a fabric and enables

to verify boundary conditions and loading homogeneity. The area of interest (AOI) is spread over a large area of the test piece (more than one repeat size of the fabric).

4.4.2 DIC in The Dissertation

The case study of double dome draped parts has been used to measure shear angles using 3D DIC technique. Here it should be known that this is not the full-field strain measurement with DIC but it is the exploitation of the DIC system to perform 3D optical strain measurement. In case of textile composite forming processes, it is very difficult to gather full-field registration of strain measurement because of the nature of the forming process does not allow doing so. In fact, the contact of forming tools with the fabric deteriorates the speckle pattern and this problem is aggravated with the geometric nature of the fabric reinforcement. However, it is possible to adopt this technique in measuring the shear angle of the formed fabrics in the final state [LOM08] [WIL08]. This is achieved through extracting the 3D coordinates at a point of interest by treating the digital image in the correlation software. Fig. 4.14 shows an image with z-coordinates of the contour of double dome experimental model treated using a digital image correlation software Vic-3D. The surface contour is indeed the tangent plane of draped fabric. The area of interest in this picture is a quarter of the double dome model. This area was first applied with random grey dots at the crossovers of yarns to create differentiation in the neighbouring areas during analysis of the image by software. Following table shows the important parameter values adopted.

Table. 4.2 Some important data/parameters used in 3D OSM using DIC system

System	Vic-3D
Subset size (pixels)	41
Step (pixels)	3
AOI	Quarter of double dome

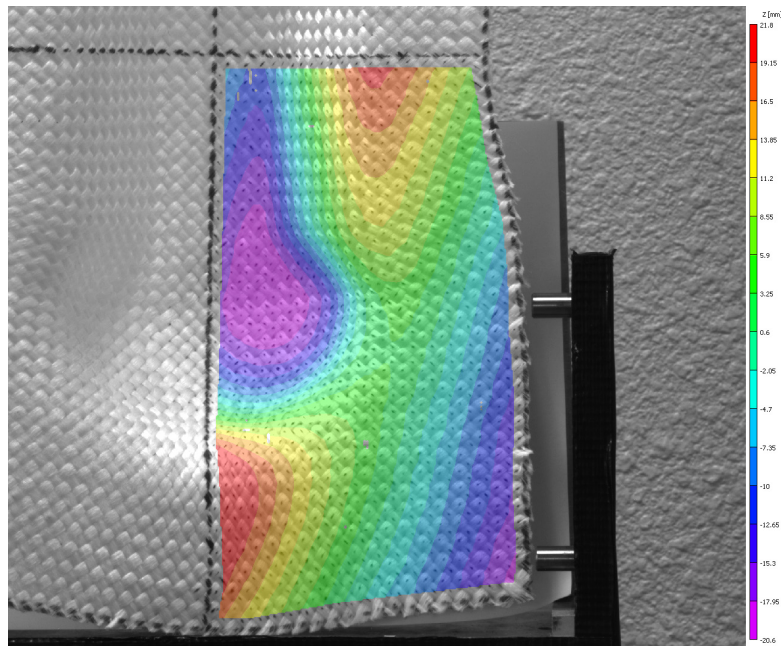


Fig. 4.14 A 2D contour profile of a double dome experiment ($\pm 45^\circ$ fibre orientations) with 3D DIC using Vic-3D

Two digital CCD cameras were installed at some angle with each other with reference to the part being inspected. However, the calibration of the cameras is made to focus properly the same object surface. The installation of cameras at certain angle was considered necessary to properly view the curved surfaces of the draped double dome model.

Fig. 4.15 is a zoom of the Fig. 4.14 and shows a clear visibility of the orientation of deformed fabric yarns. Here, it is possible to trace straight lines along the yarns up to a certain length. For example, the lines CA and CB are two straight lines drawn along the yarns with a common origin at C. The coordinates of the end points of these lines can be extracted while treating these images on software. Since ABC forms a triangle with known side lengths therefore, the angle θ at C (for instance) can be computed using the law of cosines. Initially this angle (undeformed) between the yarns is 90° . So the shear angle at C is " $90^\circ - \theta$ ".

$$\theta = \cos^{-1} \left(\frac{a^2 + b^2 - c^2}{2ab} \right) \quad (4.12)$$

$$\text{Shear angle, } \gamma = 90^\circ - \theta \quad (4.13)$$

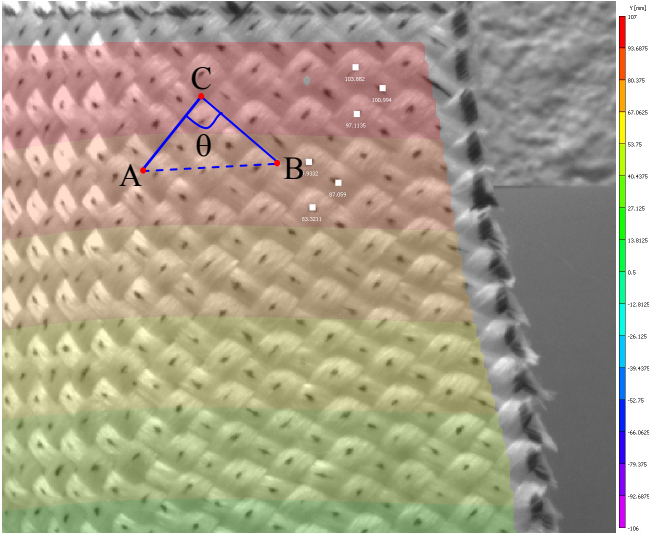


Fig. 4.15 A contour profile of surface coordinates of the double dome experiment ($\pm 45^\circ$ fibre orientations) showing the shear angle measurement

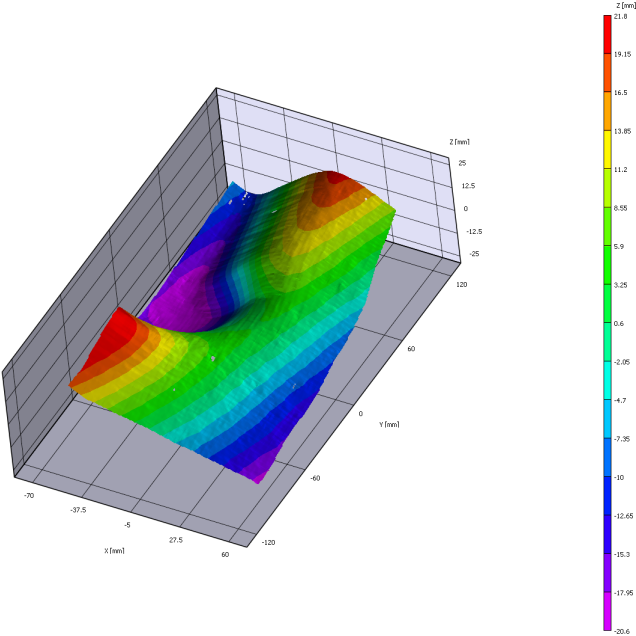


Fig. 4.16 A 3D contour profile of a double dome experiment ($\pm 45^\circ$ fibre orientations) with 3D DIC using Vic-3D

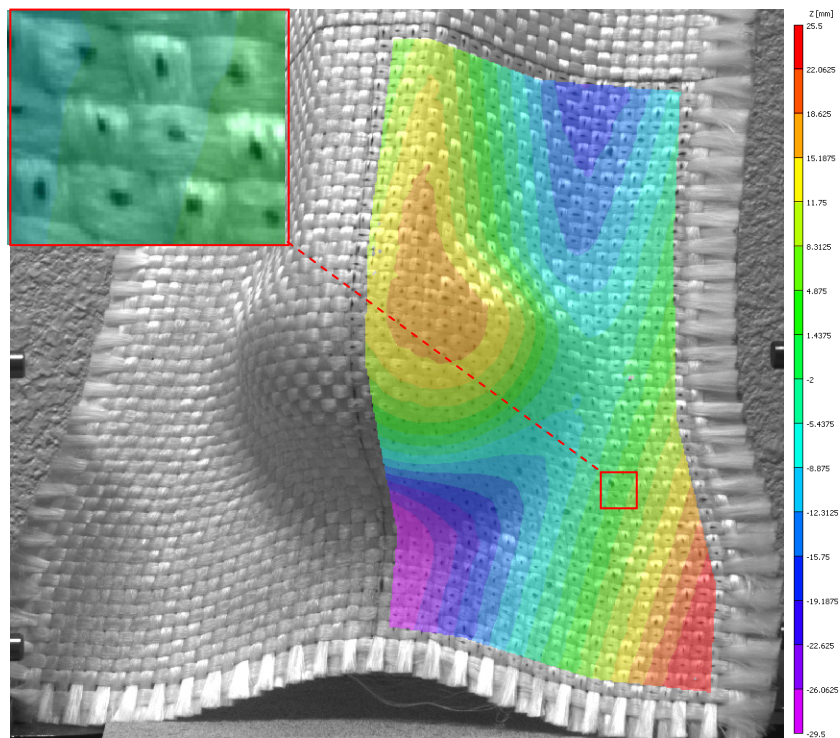


Fig. 4.17 A 2D contour profile of a double dome experiment $0^\circ/90^\circ$ fibre orientations with 3D digital image correlation using Vic-3D

The same procedure was adopted for shear angle measurements in case $0^\circ/90^\circ$ orientation of fibres. In the next chapter, the quantitative comparison of shear angles computed in the numerical results and the angle measured using 3D OSM will be presented. It is important to explain at this stage that this attempt of shear angle measurements using 3D OSM over 3D draped fabrics are carried out in case of balanced plain weave made of commingled glass/propylene. The nature of the weave and colour of the fabric has assisted sufficiently in exploitation of 3D coordinates at the desired positions for shear angle measurements. Therefore this procedure may not be adequate in other cases such as one adopted in [LOM08].

Conclusions of Chapter-4

In this chapter, the experimental work contributions have been presented which are mainly related to three important areas: the development of forming tools, fabric forming experiments and use of 3D OSM for shear angle measurements. This experimental study has been made for the dry fabric forming stage of the RTM process which is the area of interest in this study. The experimental work started from the development of forming tools and ended at optical analysis of the formed fabric. The experimental tests have conveyed many specificities of the fabric materials especially the deformation modes, the effects of forming process parameters (e.g. the binder force, forming speed...). One major objective of these tests is to validate the numerical model developed in chapter-3. 3D OSM analysis of the formed part has served to investigate the shear angle of the fabric after deformation. The determination of shear angle holds a great importance in the final part since it determines the orientation of the fibres. And, the known orientation of the fibres helps to determine the mechanical properties of the deformed fabric.

The fabric forming experiments are performed using BPW fabric only due to the constraint of the forming tools. The cavity gap between the punch and the die was kept 1mm which can only accommodate BPW fabrics. In order to perform forming tests for other two benchmark fabrics, there is a need to develop forming tools with a cavity gap which can accommodate the thicknesses of BTW and UBTW after forming. The development of new forming tools of double dome would have been a very hectic task which we could not afford in this research work.

5

Numerical Forming Simulations of Textile Woven Composites

5.1 Introduction

Numerical simulations of the composite forming processes have already an acknowledged worth and are essential in the design phase of the composite structures. The continuous approach based on a hypoelastic behaviour as described in chapter-3 has been used to perform the forming simulations of fibrous materials. The stress computation algorithm developed for fibrous materials and written in the user material subroutine VUMAT of ABAQUS/Explicit has been used here to predict the mechanical behaviour of woven composites. Moreover, the numerical forming tests are carried out with two methods presented in chapter 3 (1D2E and 2D1E). The fibrous materials selected for forming simulations are the benchmark fabrics described in chapter 4. The material characterisation and mechanical properties used in forming simulations for these fabrics are also the same as described in the preceding chapter. The numerical forming tests of fabrics have been performed using benchmark geometry of double dome as it has been used for experimental forming tests presented in chapter 4. The process parameters are selected with reference to those used in experiments and benchmark forum [WC08]. However, additional numerical tests based on varied process parameters will also be presented in this chapter. Another important aspect of the numerical tests is its extension to multilayer fabrics.

The numerical simulations will be performed using two different orientations (i.e. $\pm 45^\circ$, $0^\circ/90^\circ$) of yarns with respect to the rectangular edges of the die or punch. Then, the numerical results will be compared with the experimental test outputs quantitatively. In the end, it will also be presented that the same algorithm of fibrous materials based on hypoelastic behaviour can be used to perform forming tests for prepregs as already discussed in chapter 3. An

attempt to use the same algorithm to thermoforming simulations of the fabric forming will also be presented.

5.2 FEM Model of Double Dome

FEM model development of double dome and the forming tests have been carried out using a commercial finite element code of ABAQUS/Explicit using standard elements.

5.2.1 Model Setup

The double dome setup consists of die, punch and binder considered as the forming tools and forming test specimen of fabric reinforcement placed in between the die and the binder as shown in Fig. 5.1. All three forming tools are modelled as discrete rigid bodies and meshed with 3-D triangular rigid elements (R3D3) with a mesh size of 3mm. The fabric workpiece has been meshed using 3D quadrilateral membrane elements with reduced integration (M3D4R). The mesh size of 3 mm × 3 mm quadrilateral elements has been selected optimally after a series of different mesh size tests. Two different orientations of the fabric yarns (warp and weft) in the reference configuration (i.e. 0°/90° and ±45°) are displayed in Fig.5.1. The orientations of the fibres are taken along the edges of the quadrilateral elements. The same is true for the ±45° fibre orientations where the elements are meshed at 45° with respect to the blank sides so that fibres follow the edges of the elements. The aligning of mesh with fibre directions is one of the solutions to avoid intra-ply shear locking also proposed by Ten Thije [TEN08]. The use of reduced integration is also recommended as a solution to this problem. We shall demonstrate this problem through numerical examples in the sensitivity study of forming simulations for fibrous materials.

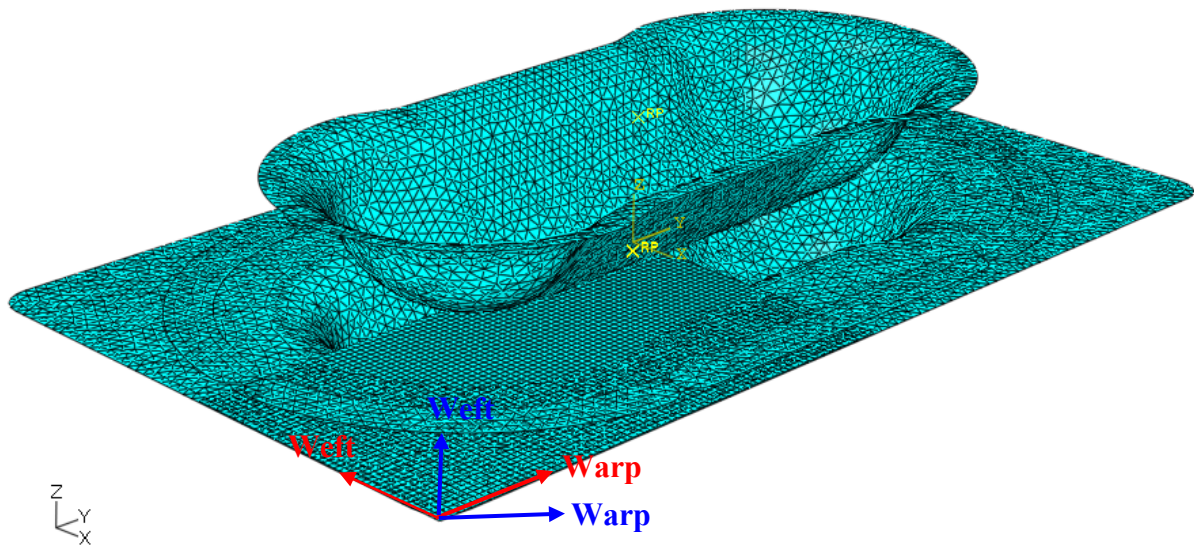
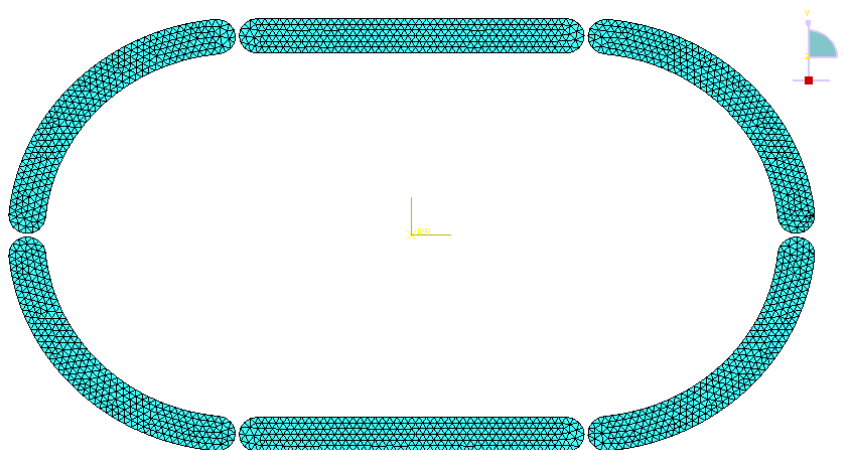
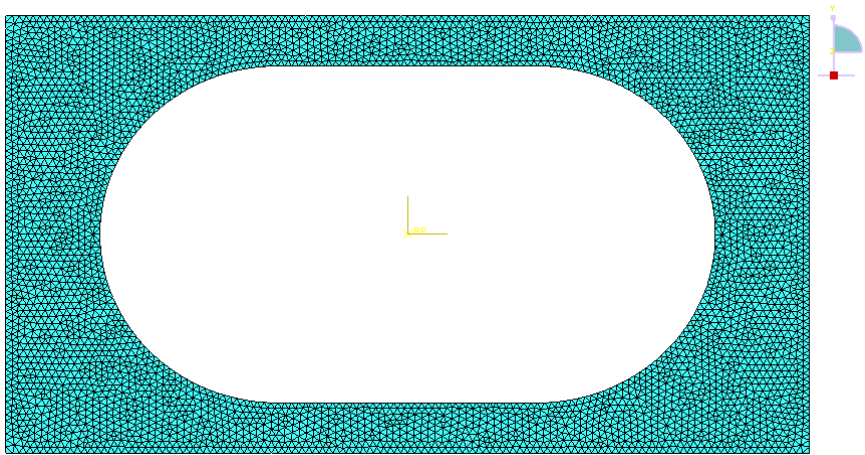


Fig. 5.1 Double dome model setup with meshing and two different orientations of yarns ($0^\circ/90^\circ$ and $\pm 45^\circ$) with respect to longitudinal symmetry of the model

Since the loading and material behaviour is symmetric in both of the orientations selected, hence only a quarter of the workpiece is modelled while symmetry boundary conditions are assigned along the symmetry planes. The fabric blank (quarter) sizes are 235 mm \times 135 mm. The numerical tests are performed using first two benchmark fabrics (BPW and BTW).



(a) Six-pieces binder



(b) Flat binder

Fig. 5.2 Blank holder models with meshing; (a) six piece serrated blankholder

(b) one piece with more flat contact area

Two different models of blankholder were selected for the numerical simulations of the fabric forming. The first one is segmented and six piece model as recommended by the benchmark forum [WC08] whereas the second one is a single piece and has more flat area which was selected on discretion to check the binder shape effects on the forming simulations of fabrics. The simulation results with two binder models will also be discussed in the subsequent sections. However, one apparent effect could be the smooth material draw-in during forming process when used one piece binder.

5.2.2 Material Characteristics and Process Parameters

The material characteristics and process parameters mostly used for numerical forming simulations carried out in this study are detailed as below:

- First elastic tensile modulus (warp direction), $E_1 = 35,400$ MPa
- Second elastic tensile modulus (weft directions), $E_2 = 35,400$ MPa
- Volumetric density, $\rho = 0.00253$ gm/mm³
- Poisson's ratio, $\nu_{12} = 0$

- In-plane shear rigidity, G_{12} , as BPW and BTW fabrics {Eq. (4.12) and (4.15)}
- Blank holder force=100 N
- Punch velocity= 6000 mm/sec
- Coefficient of friction= 0.2 (Fabric/ Fabric and Fabric/tools)

The elastic tensile rigidities of warp and weft are same in both of fabric tests using BPW and BTW. The difference between the two fabrics material behaviour is of shear behaviour which will differentiate between fabrics analysed numerically with continuous approach. The force applied on the blankholder is of same quantity as selected for experimental tests in order to compare the numerical results with experiments. However, the numerical tests will also be conducted with different blankholder forces as a part of parametric sensitivity study. The punch velocity selected for numerical tests is far more than used in experiments performed. The selection of this much velocity is also based on the study of optimal parameters over which the results converge quite satisfactory with an aim to reduce the simulation time. The coefficient of friction between fabric and tools is selected with an approximate value and it can also be found of the same range in literature related the study of textile fabric materials. The forum for benchmark study of double dome simulations also suggests an approximate value of 0.25. The sensitivity study related to the effects of process parameters selection will also be performed using different coefficient of friction. The algorithm of surface to surface contact (explicit) formulation is invoked using contact pair option. Also, the kinematic sliding constraint formulation is used in the definitions of contact interactions. Moreover, the penalty friction formulation using tangential behaviour as a contact property option has been adopted.

5.3 Numerical Forming Tests

As shown in Fig. 5.1, the numerical forming tests are carried out with two different initial orientations of the fabric yarns. Moreover, the tests are performed using two types of benchmark study fabrics i.e. balanced plain weave (BPW) which is mostly used and also

balanced twill weave (BTW). First the simulation results will be displayed and then the quantitative comparison of results will be presented.

5.3.1 Balanced Plain Weave (BPW)

Fig. 5.3 shows the full model simulation result of BPW fabric using geometry of double dome model with orientation of yarns ($0^\circ/90^\circ$) in the reference configuration. Whereas, Fig. 5.4 shows the draped model of BPW fabric having $\pm 45^\circ$ orientation of fibres with respect to the rectangular edges of the blank. The fabric sheet has been meshed with elements having its edges parallel to the fibre directions. It should be known that 3D triangular elements are placed along the contour to ensure the continuity of the rectangular blank.

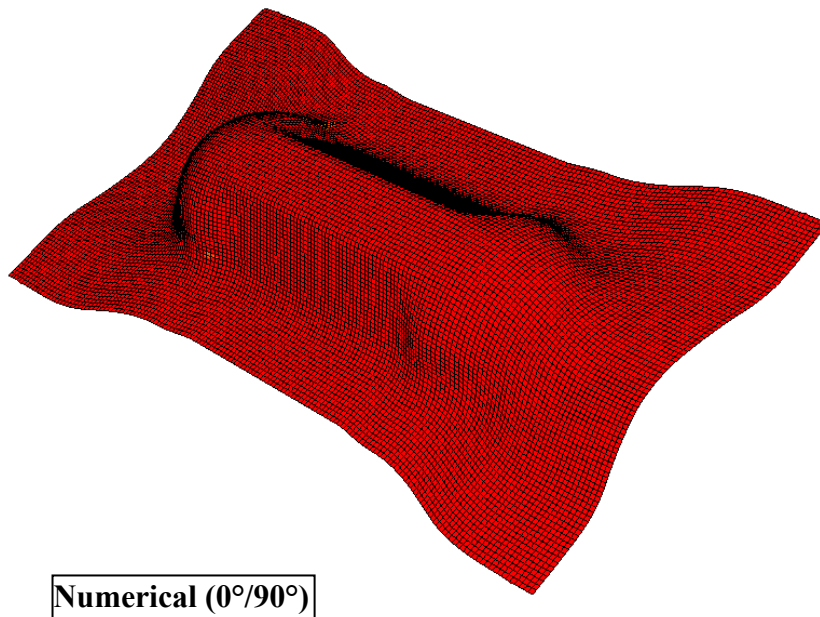


Fig. 5.3 Deformed shape through numerical simulations of a fabric with $0^\circ/90^\circ$ yarns in the reference configuration

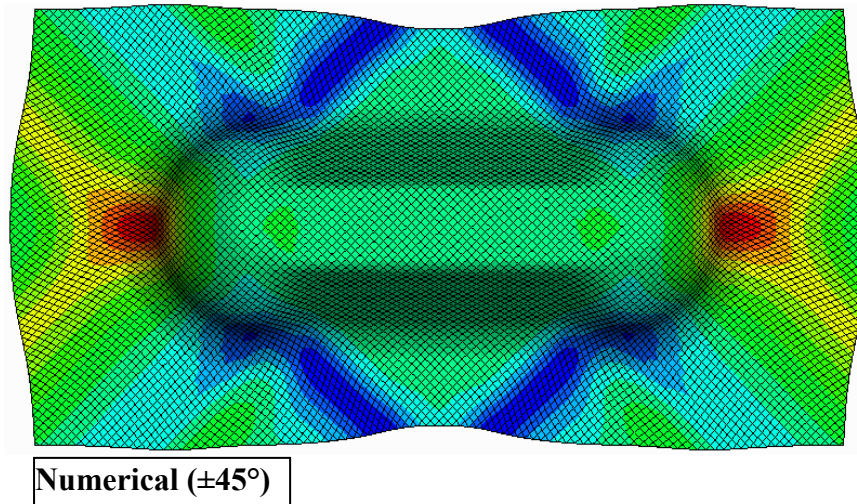


Fig. 5.4 Deformed shape through numerical simulations of a fabric with $\pm 45^\circ$ yarns in the reference configuration

5.3.2 Balanced Twill Weave (BTW)

Forming simulations of BTW fabrics have also been performed using their shear behaviour predicted in Eq. 4.11. Since their experimental tests have not been carried out therefore, only the numerical forming simulations will be presented here. This is due to the constraint of forming tools having cavity gap of 1 mm between the punch and die. Whereas, thickness of the original BTW fabric is 2mm. The full model simulations are exactly same in appearance as shown for BPW fabrics (Figs. 5.3 and 5.4) therefore, only the results of shear angle predicted will be shown in the subsequent sub-section 5.6.1.

5.4 Comparison between Experimental and Numerical Results

Two important and basic parameters, i.e. material draw-in and shear angle, at different regions of the deformed fabric have been selected for quantitative comparison of the tests. A quarter of the model has been selected for data comparison since this model is symmetric in x and y-axes with origin at the centre of the model. The symmetry of the models is also evident from numerical output of the full scale model shown in Figs. 5.3 and 5.4.

5.4.1 Material Draw-In

The material draw-in can be considered as one of the important parameters for comparison of the numerical results with the experimental output for composite reinforcement forming. This can be defined as the amount of material flow in the draping process along the contour from the undeformed position to the deformed one. Since, it has already been pointed out that continuous approach is capable of tracing the global behaviour for a fibrous media analysis, so the material draw-in parameter can be treated as a global characteristic exclusively for fabric reinforcement forming. It permits to validate the numerical model adopted for forming of fibrous materials. The material draw-in has been measured at the locations shown in Figs. 5.5 and 5.8 for $0^\circ/90^\circ$ and $\pm 45^\circ$ orientations of fibres. The points A and L/E are the end-points of the two symmetric models along width and longitudinal sides. While the points B to D and F to H are the evenly distributed points in the undeformed distance along width and lengths of the fabric blank respectively for the $0^\circ/90^\circ$ model. Similarly, the points B and D are the mid points along length and width over the quarter model with $\pm 45^\circ$ orientations of fibres. The comparative data shown in charts of Figs. 5.7 and 5.10 confirms that numerical and experimental outputs are quite equivalent.

5.4.2 Shear Angle Measurements

The change in the angle between warp and weft yarns during deformation commonly called the shear angle is of vital significance in the forming of woven fibrous reinforcements. Since, the tensile strength of fabric yarns is much greater as compared to their transverse strength, so it becomes imperative to know the position and orientation of fibres in the final shape after

fabric draping. The properties of final structure largely depend on the orientation of fibres. The density of fibrous reinforcement also changes with change in shear angle after deformation. Since the dry forming stage affects the subsequent stage of resin injection therefore, the determination of shear angle of the deformed reinforcement helps in successful execution of second stage of RTM process. Keeping in view of its significance, this necessitates adopting a correct and reliable method for measurement of the shear angle. For that, two methods are adopted and the shear angles obtained from these methods are equally precise and accurate. Considering, $\underline{\mathbf{f}}_1$, a normalized base vector along first fibre direction and $\underline{\mathbf{f}}_2$, a normalized base vector along second fibre direction. The shear angle (radians) is:

$$\gamma = \frac{\pi}{2} - \arccos \left(\frac{\underline{\mathbf{f}}_1 \cdot \underline{\mathbf{f}}_2}{\|\underline{\mathbf{f}}_1\| \|\underline{\mathbf{f}}_2\|} \right) \quad (5.1)$$

And, the second method is the use of Eq. (3.21) but in the accumulated state using mid-point integration rule of Hughes and Winget [HUG80] as under:

$$[\gamma^{n+1}]_{f^{n+1}} = [\gamma^n]_{f^n} + [d\gamma]_{f^{n+1/2}} \quad (5.2)$$

The Eq. (5.2) equally gives the correct measure of shear angle values in radians. The location of the shear angle measurements are shown in Figs. 5.5 and 5.8. The shear angle locations are selected at discretion keeping in view the different shear zones of the fabric after deformation. The graphical comparison of shear angle results can be seen in the Fig 5.6 and Fig. 5.9; the numerical output of the model along with the experimental measurements using 3D OSM discussed in chapter 4. Moreover, the coordinates of the points shown in Figs. 5.5 and 5.8 and the exact shear angles measured numerically and experimentally has also been shown in table-5.1 and table-5.2 along with numerical results.

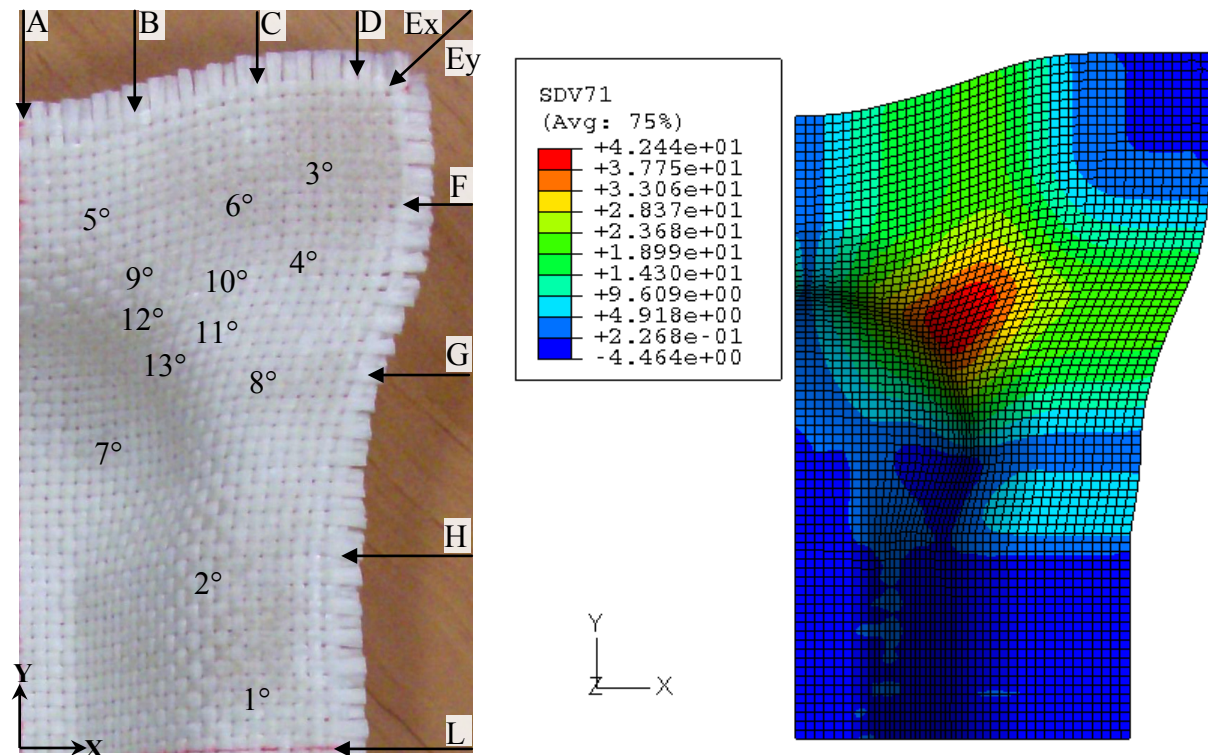


Fig. 5.5 The location of points for material draw-in and shear angle measurements for $0^\circ/90^\circ$ orientation. SDV71 is the shear angle result in degrees.

Table. 5.1 The coordinates of points as in Fig. 5.5 and their corresponding values of shear angle (degrees) for $0^\circ/90^\circ$ orientation

Points	X (mm)	Y (mm)	Shear angle (deg.)	
			Numerical	Experimental
1	88	33	0.256~0	0
2	64	88	2.13	1.34
3	116	219	4.4	2.8
4	91	180	8.84	10.5
5	23	181	13.09	15
6	72	192	16.88	15.5
7	38	123	17.8	16.5
8	82	132	19.57	22
9	40	157	26.88	23.45
10	60	168	28.34	29.4
11	67	148	36.29	33.43
12	52	136	42.16	39
13	45	145	43.18	39.5

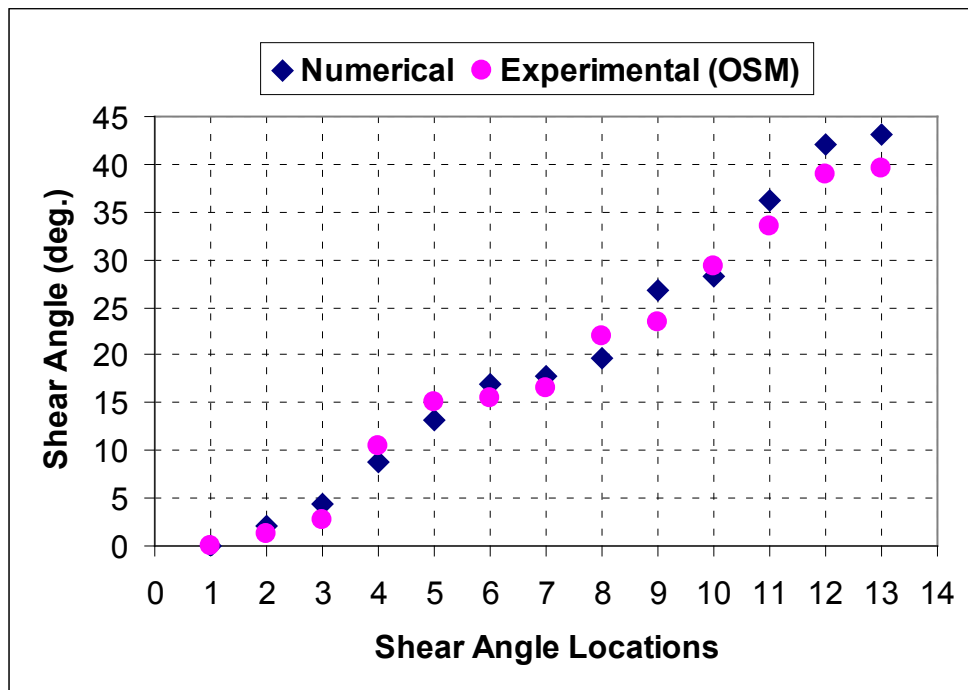


Fig. 5.6 The shear angle comparison of numerical and experimental outputs for $0^\circ/90^\circ$ orientations of fabric yarns

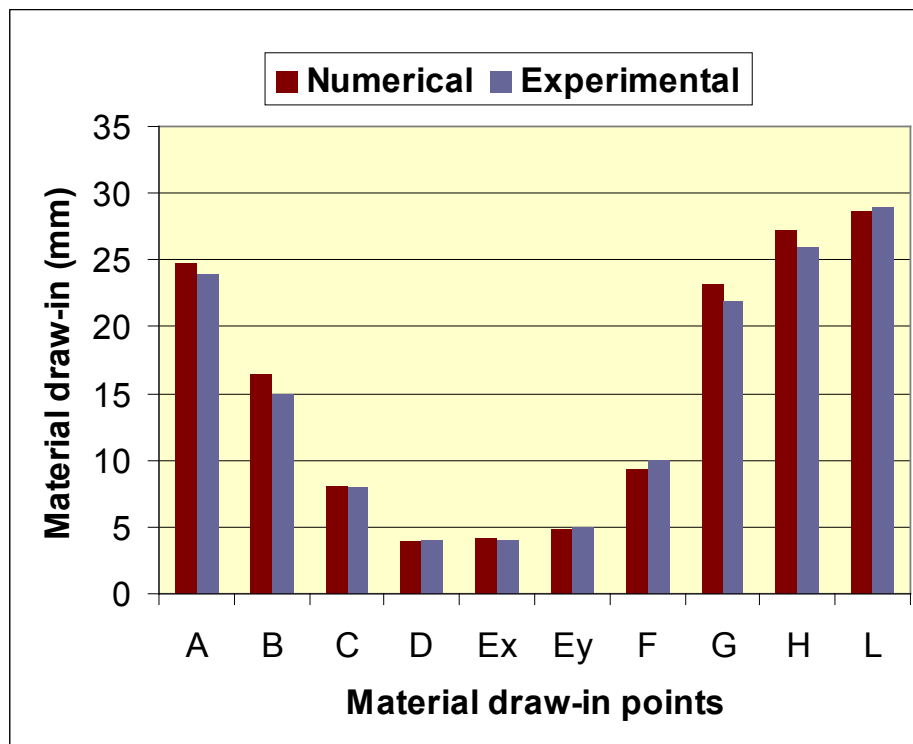


Fig. 5.7 The comparison of material draw-in for the draped double dome of $0^\circ/90^\circ$ orientation at locations shown in Fig.5.5

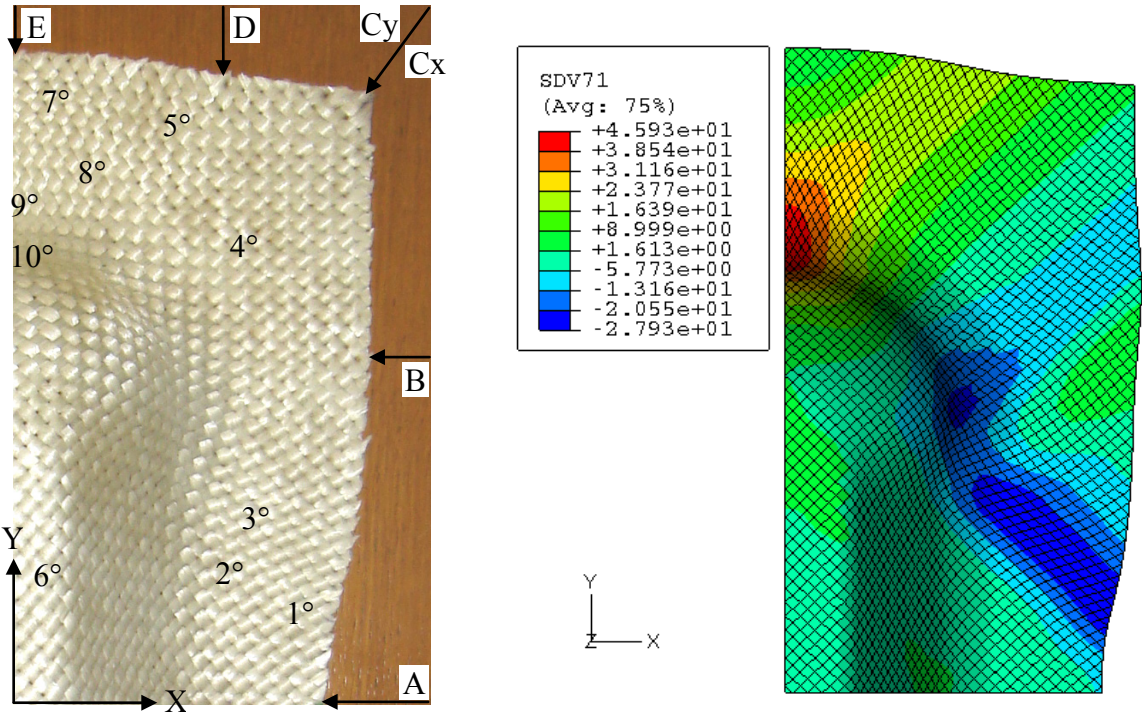


Fig.5.8 The location of points for material draw-in and shear angle measurements for $\pm 45^\circ$ orientation. SDV71 is the shear angle result in degrees

Table: 5.2 The coordinates of points as in Fig. 5.8 and their corresponding values of shear angle (degrees) for $\pm 45^\circ$ orientation.

Points	X (mm)	Y (mm)	Shear angle (deg.) Numerical	Shear Angle (deg.) Experimental
1	130	42	27.12	24.1
2	90	82	21.33	19.2
3	115	92	9.5	10.4
4	110	192	2.85	0
5	77	205	10.37	10
6	10	82	2.68	0
7	15	212	16.28	18.16
8	22	190	30.32	29
9	2	180	43.01	38.3
10	5	167	44.38	39.22

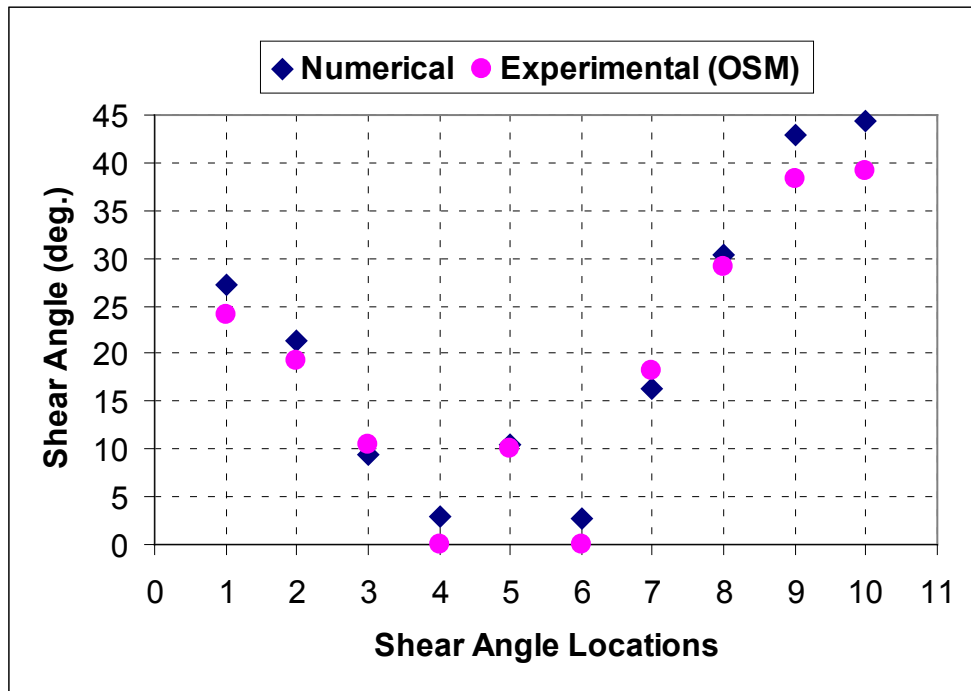


Fig. 5.9 The shear angle comparison of numerical and experimental outputs for $\pm 45^\circ$ orientations of fabric yarns.

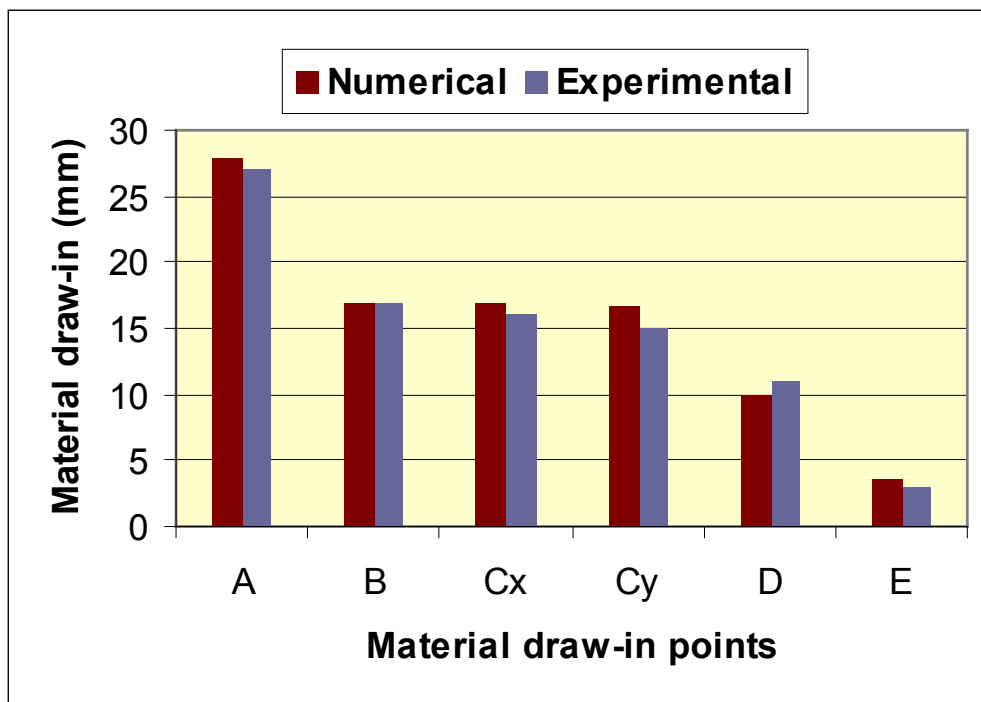


Fig.5.10 The comparison of material draw-in for the draped double dome of $\pm 45^\circ$ fibre orientations at locations shown in Fig.5.8

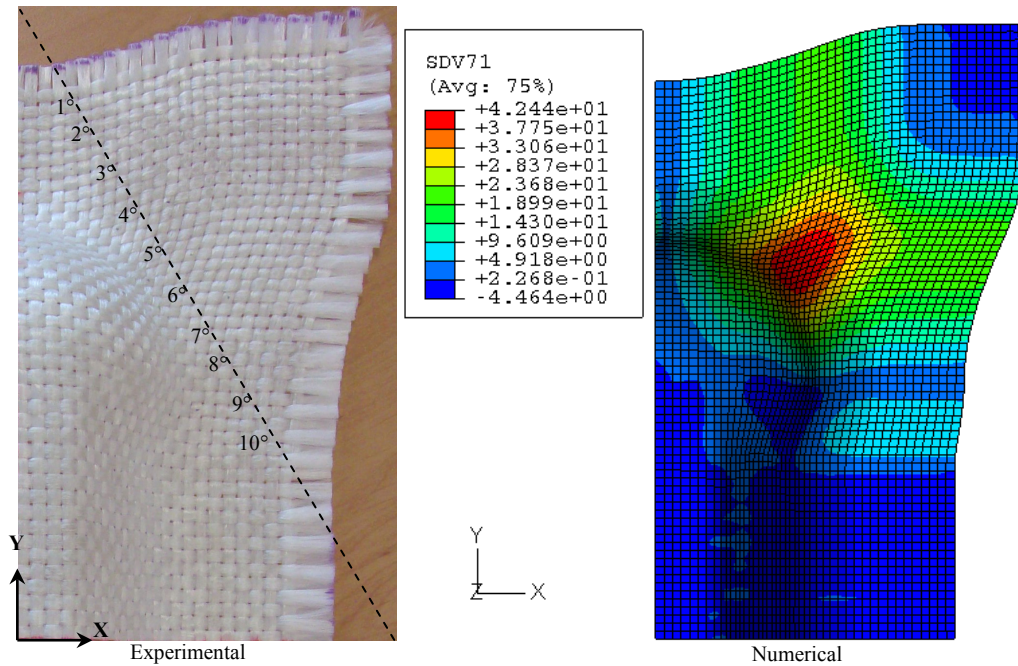


Fig. 5.11 The location of points for shear angle comparisons of the symmetric model of double dome benchmark with $0^\circ/90^\circ$ initial yarn orientations

SDV71 is shear angle (degrees)

The shear angle comparison of experimental and numerical results over the draped fabrics of $0^\circ/90^\circ$ orientations of fibres have also been carried out by selecting a path as shown in Fig. 5.11. Again this path has been selected at discretion along the diagonal in the undeformed state of the rectangular blank over quarter of the model. However, the selection of this path passes through different shear zones of the deformed fabric. The points selected from 1 to 10 are the equally spaced points along this path. The shear angles have equally been measured experimentally using 3D OSM method discussed in chapter 4. The comparison of shear angle results is shown in Fig. 5.12 in the form of a graph.

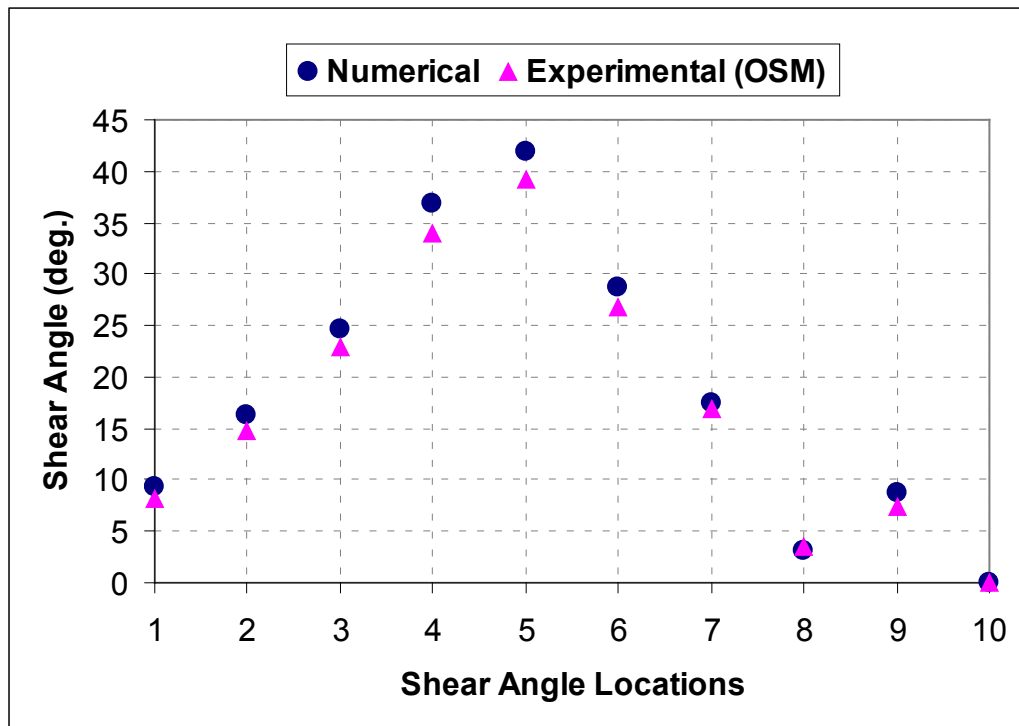


Fig. 5.12 The numerical and experimental (3D OSM) shear angle comparison for the points located in Fig. 5.11

The **comparisons of results** (numerical and experimental), in case of BPW fabrics, presented here for the forming of the double dome benchmark are within the limits of credible accuracy. The maximum shear angle recorded in simulation is almost 43° using $0^\circ/90^\circ$ orientation of yarns whereas it reaches up to 46° when $\pm 45^\circ$ fibres orientation is used. The use of 3D OSM method has enabled to measure the reorientation of yarns i.e. shear angle after forming. Although, DIC exploitation for forming processes of fibrous materials is in its preliminary stage of development yet the results produced are reliable. Indeed, to our knowledge it has only been applied by [LOM08] and [WIL08] for shear angle measurements in case of forming of textile composites. The maximum shear angle value evolved in double dome forming case can be considered a large shear strain which definitely affects the resin injection behaviour in the processes like LCM (Liquid Composite Moulding). The shear angle measurement points have been selected at random but care has been taken to choose different areas with different shear behaviour. The maximum error reflected in comparison of numerical and experimental results are up to 8%. The material flow (draw-in) during both of the dry forming processes of

double dome examples have been within maximum error of 5% when numerical and experimental results are compared.

The error contribution factors might have been due to the approximate input data used such as the coefficient of friction taken for numerical analysis. Also, the human error during sample cuttings and measurements of the experimental results for shear angles can not be ignored. The experimental values of shear angle are marked as less than numerical ones which can be attributed to the fact that fabric thickness is 1.2mm [WC08], whereas the cavity gap, used in the experiments, between the punch and die is 1mm.

5.5 Multilayer Simulations

The benchmark example of double dome has also been extended to the numerical analysis of multilayer fabric as shown in Fig. 5.13. Four different layers of BPW fabrics have been selected for fabric forming simulations. The fabric orientations of $0^\circ/90^\circ$ and $\pm 45^\circ$ have been placed from top to bottom alternatively. The coefficient of friction of 0.2 has been used either between fabric to fabric and fabric to tool. All other material characteristics and process parameters are exactly the same as described in section-5.2. This arrangement of fabrics has been a common practice in the domain of composite structures. The objective of this test here is to extend the validity of the developed numerical model for multilayer fibrous reinforcement forming. The numerical solutions converge satisfactorily and produce the desired results.

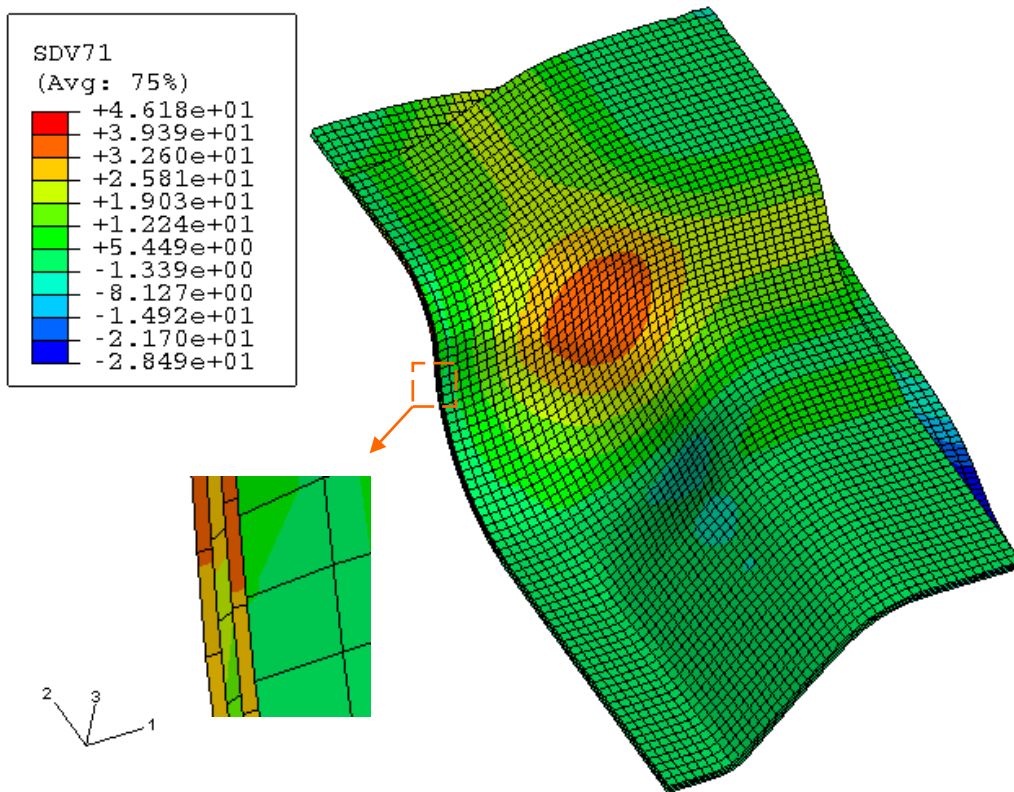


Fig. 5.13 Multilayer numerical simulation result of a fabric with alternate orientations of $0^\circ/90^\circ$ and $\pm 45^\circ$ yarns in the reference configuration.

SDV71 is the shear angle result in degrees

5.6 Parametric Sensitivity Study

This section investigates the sensitivity of the predicted local deformations to modifications in the material input (shear rigidity), process conditions (binder force and binder configuration, friction coefficient and punch velocity) and the choice of element type.

5.6.1 Shear Rigidity

The continuous approach used for macro-scale analysis of woven composites can only take into account the different shear behaviour by changing weave types with same fibre material. And it has already been presented in chapter-4 that by using the same fibre material (commingled glass/polypropylene) there is a change in shear behaviour of the fabric which is mainly attributed to the change in type of weave only. In the preceding section-5.4, the difference in shear angle predictions and material draw-in has already been shown. Here in Fig. 5.14, it is shown that shear angle evolution is different in case of BPW and BTW fabrics. However, it should be known that in the numerical simulations, the thickness of BTW fabric has also been 1mm due to the unavailability of the forming tools models with 2mm cavity gap between the punch and die.

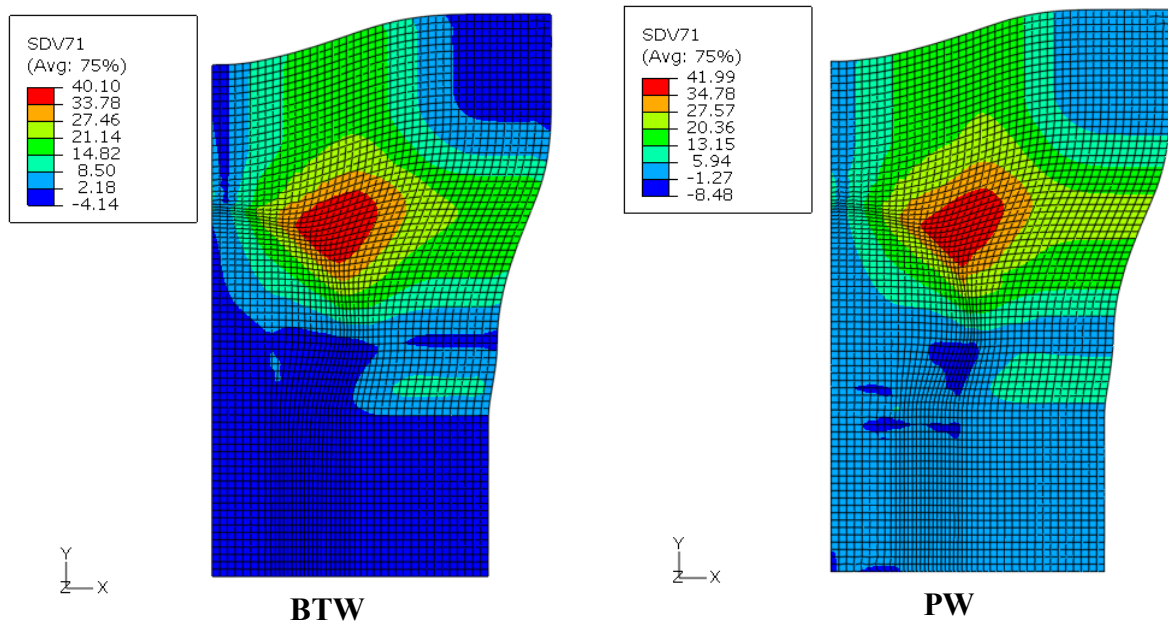


Fig. 5.14 Shear angle in degrees (SDV71) profile for BPW and BTW fabrics with orientations of $0^{\circ}/90^{\circ}$ yarns in the reference configuration

Mass proportional damping

In order to damp the high frequency oscillations of the forces generated during high speed dynamic event the material damping is introduced in the model. Usually, there are two important types of damping introduced: stiffness proportional damping and mass proportional damping. The stiffness proportional damping indeed affects the results of stress state evolution. Whereas, the mass proportional damping factor introduces damping forces caused

by the absolute velocities of the model and so simulates the idea of the model moving through a viscous “ether” (a permeating, still fluid, so that any motion of any point in the model causes damping). This damping factor defines mass proportional damping, in the sense that it gives a damping contribution proportional to the mass matrix for an element. If the element contains more than one material in ABAQUS/Explicit, the mass average value of damping factor is used to multiply the element's lumped mass matrix to define the damping contribution from this term. It has units of (1/time).

The observed results show that by using mass proportional damping significantly ameliorates the results but the calculation time of analysis is enhanced. Another, important aspect observed is the significant increase in the force required to deform the fabric. Although, we have used mass proportional damping in some rare cases yet it has proved helpful in converging the solutions for some case when process parameters used were of a bit odd limits.

5.6.2 Punch Velocity

The process parameter of punch velocity during simulation of fabric forming has an influence over forming results [DON00]. In the section-5.2.2 the optimised parameter of punch velocity (6mm/msec) has been selected when results are compared with experiments. Although, the forming simulations have been performed with a variety of punch speeds e.g. 0.6/6/60/600/6,000/60,000 mm/sec. However, in this section the results of shear angle evolution have been compared between two punch velocities i.e. 6000 mm/sec and 60 mm/sec. The low velocity selected underestimates the shear angle in the final state by 2.5° whereas the calculation time is also hundred time larger (≈ 60 hours) than the optimised punch velocity. The high speed of punch has its own implications and has been addressed to counter the problems engendered.

The accelerated numerical computations have for sure the reduced CPU time where the forming process is simulated at artificially higher draping rates (increased punch speed). However, this increases artificially the inertia effects in Eq. (3.4) and generates high frequency numerical oscillations. To control these oscillations, a small amount of artificial damping is introduced in the dynamic analysis in the ABAQUS/Explicit code in the form of an artificial bulk viscosity. Its purpose is as a numerical effect only to improve the modelling of high speed dynamic events, therefore the bulk viscosity pressure is not included in the

material point stresses, in another words, it is not considered as a part of the material's constitutive response.

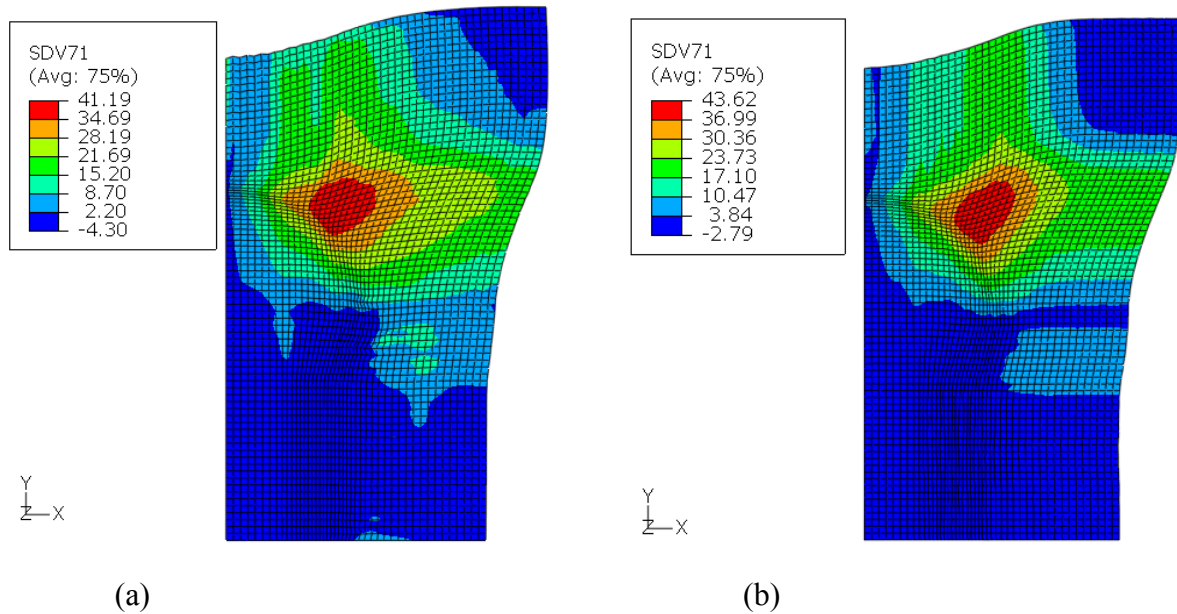


Fig. 5.15 Forming results of shear angle in degrees (SDV71) with punch velocities of (a) 60 mm/sec and (b) 6000 mm/sec

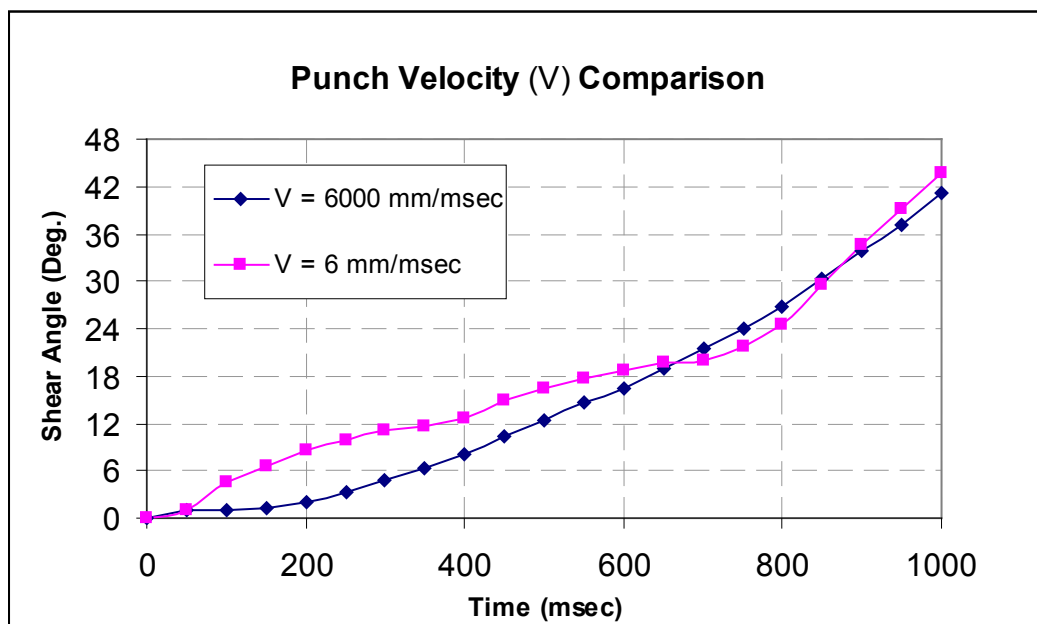


Fig. 5.16 Maximum shear angle (Degrees) evolution with process time in the whole model for two forming cases with punch velocities of (a) 60 mm/sec and (b) 6000 mm/sec

5.6.3 Mesh Orientation

The effect of orientation of fibres with respect to mesh has been explored with an aim to determine the shear locking phenomenon. Indeed, there is a great influence of fibre orientation with respect to mesh. For example when mesh is not aligned with the fibres initially and when used the same process parameters as of section-5.2.2, the mesh distorts excessively and solution does not converge and therefore, results are no more presentable. However, by manipulating over coefficient of friction, i.e. reducing it to 0.1 and by introducing artificial damping coefficient as discussed above, the solution is somewhat reliable as it has been shown in Fig.5.17. The max shear angle value is overestimated by 2.64° when fibres are not aligned with mesh. The mass proportional damping of 100 has been used in this analysis.

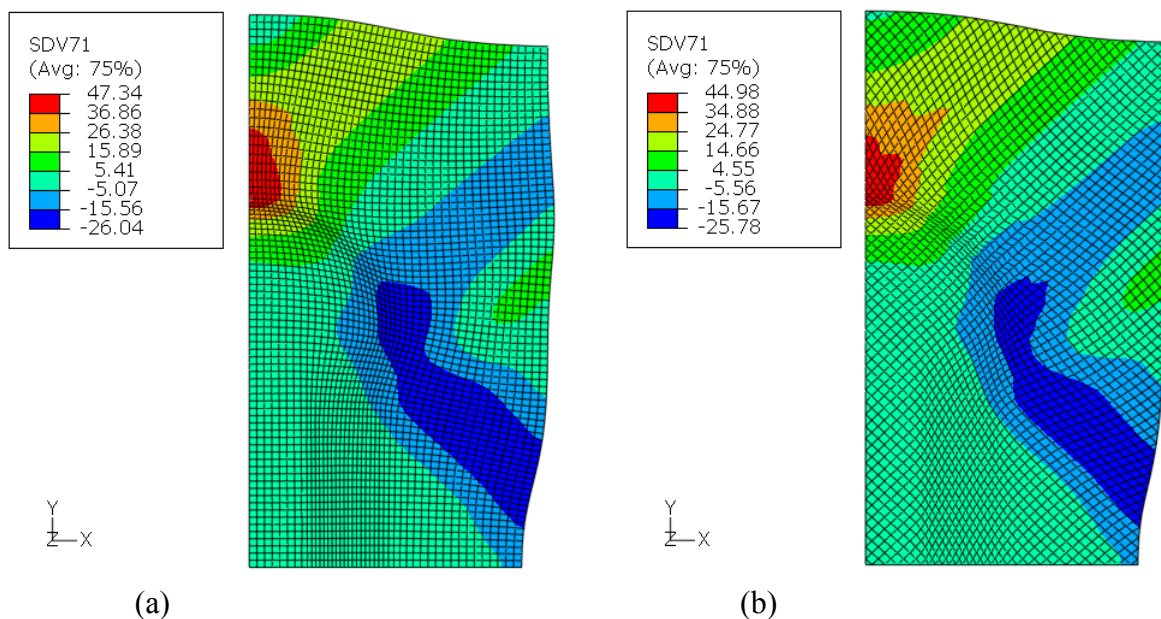


Fig. 5.17 The shear angle (degrees) evolution in the two models having different mesh orientations with respect to fibre directions (a) mesh not aligned with fibre directions (b) mesh aligned with fibres

5.6.4 Element Type

The numerical results of double dome forming are also verified with different type of element selection. Normally, the elements used in this project study are of 3D quadrilateral membrane elements with reduced integration M3D4R; where R stands for elements with reduced

integration (A small amount of artificial stiffness is assigned to these elements to avoid hourglass mode: a zero-energy deformation mode). However, the forming test is extended to use 3D triangular membrane elements M3D3. As shown in 5.18 there is a difference of almost 1.5° in the maximum shear angle output.

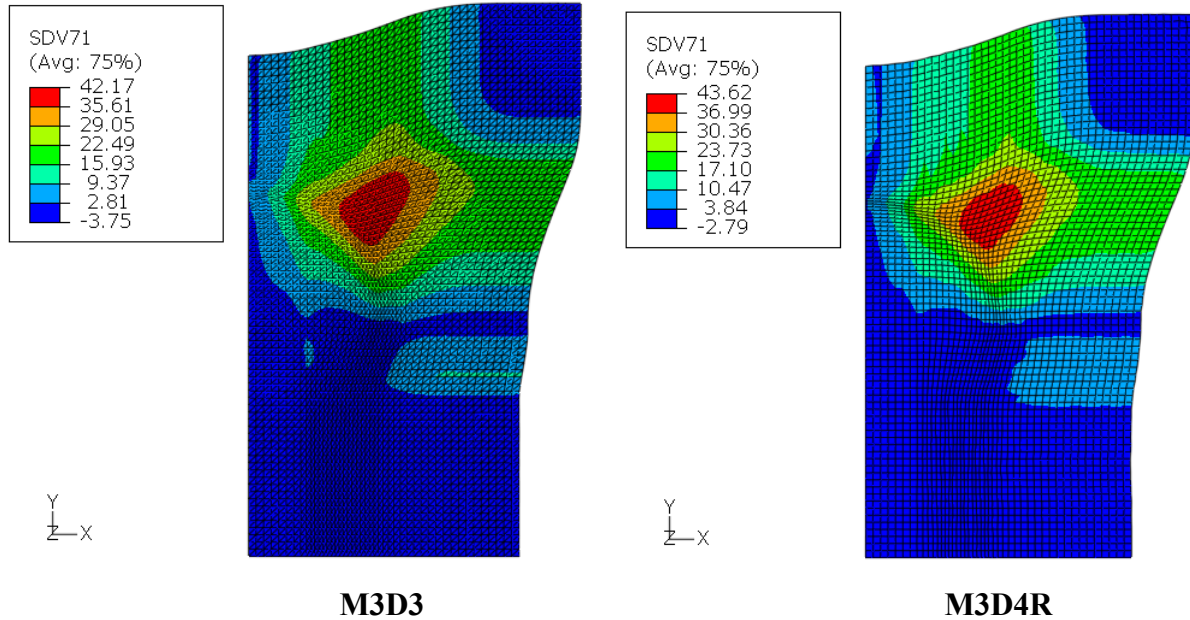


Fig. 5.18 The maximum shear angle (degrees) evolution in the two models with different types of element meshes

5.6.5 Coefficient of Friction

The coefficient of friction used in almost all simulations is 0.2, however to check its sensitivity different values were used. Here, for example, in Fig.5.19 the simulation results with two coefficients of friction i.e. 0.15 and 0.25 are presented. The evolution of maximum shear angle is affected to the least but its minimum value differs by almost 4° which is enormous. Moreover, the distribution of shear angle contour shows a large variance when the coefficient of friction of 0.3 is used, the results deteriorate largely and are no more presentable. So, this is a serious draw-back so far in the simulations. As shown in Fig. 5.20, the shear angle shoots to a high value of more than 48° which is probably due to the vertical movement of an element out of the plane and which is ultimately controlled when that portion comes in contact with the binder under pressure.

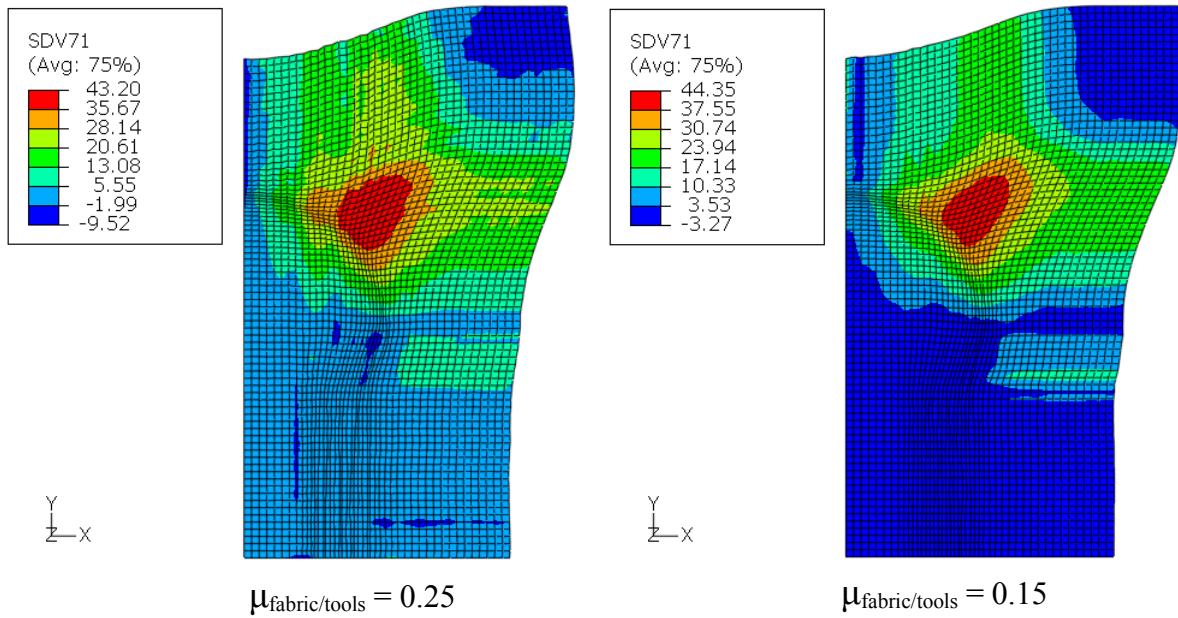


Fig. 5.19 The maximum shear angle (degrees) evolution in the two models with two different coefficients of friction

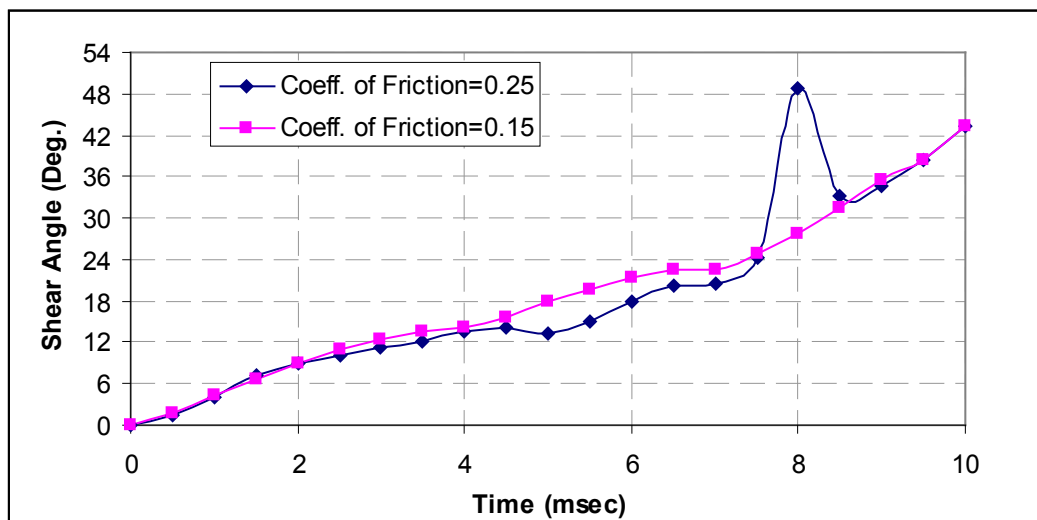


Fig. 5.20 The maximum shear angle (degrees) evolution in the two models with two different coefficients of friction

5.6.6 Blank Holder Shape

Two kinds of blank holder shapes (as shown in Fig.5.2) have been selected as one of the criteria for carrying out the sensitivity study. These results are extracted with coefficient of friction as 0.15 for both types of blank holders. The blank holder shapes are shown in Fig. 5.2 and simulation results show that the model with larger contact area of binder induces some problems. The shear angle distribution over the model with flat binder has large variations in the negative shear angle zone when compared with segmented binder model outcome.

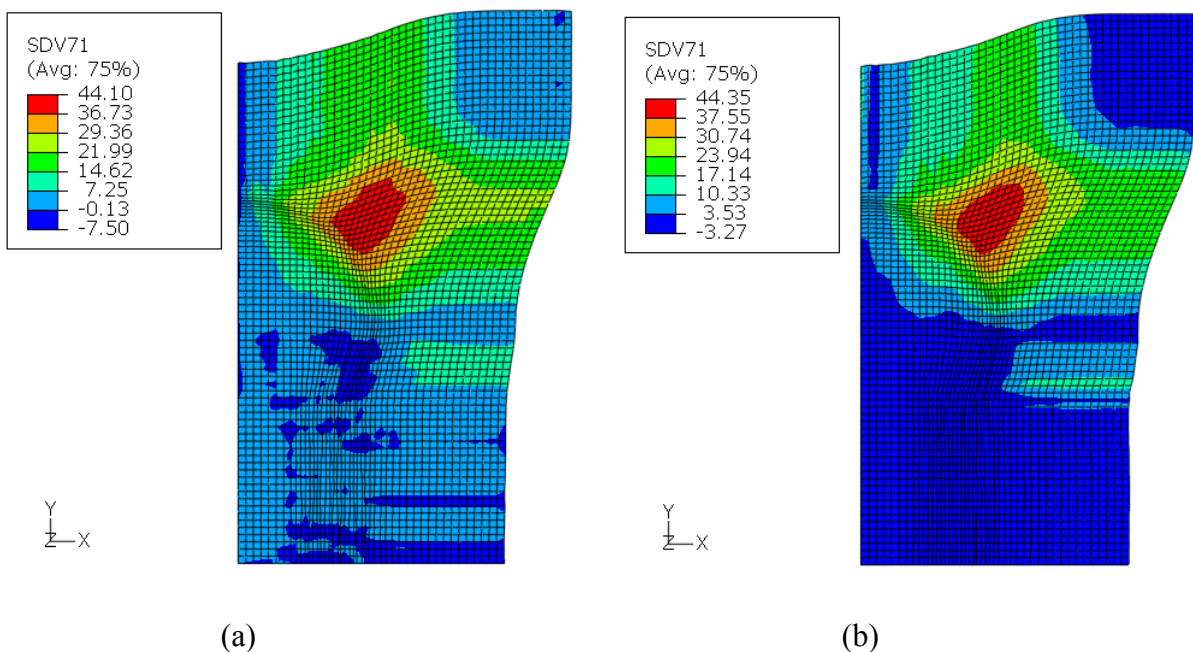


Fig. 5.21 The shear angle (degrees) evolution in the two models with different types of blankholder used (a) flat one (b) segmented binder

5.6.7 Binder Force

The role of binder or blank holder in forming processes of composite materials is very important and has been a recognized fact [SKO07]. Normally it is used to eliminate or avoid the wrinkling of the fabric in forming. Similarly, the binder force plays a crucial role and should be optimized in conjunction with other forming process parameters. It also affects the evolution of shear angle over formed part.

The effect of blankholder (binder) force, indeed the unbalanced pressure over binder, can be seen not only with the evolution of non-symmetric contour profile along the edges but also the shear angle output has showed a great variation (Fig. 5.22). The two opposite diagonal corners have emerged with the same shape and almost the same shear angle contour. This is due to the fact that they have experienced the same binder force during the test. Two binder pressures i.e. of 0.3 MPa and 0.03 MPa have been applied over the segmented blankholder.

The blank holder force plays a crucial role in the forming simulations of fabrics and here in Fig. 5.25 the results of shear angle output are shown with two different forces i.e. of 300N and 500N. These are concentrated forces applied to the binder and therefore distributed equally. The blank holder in this case is six pieces serrated holder.

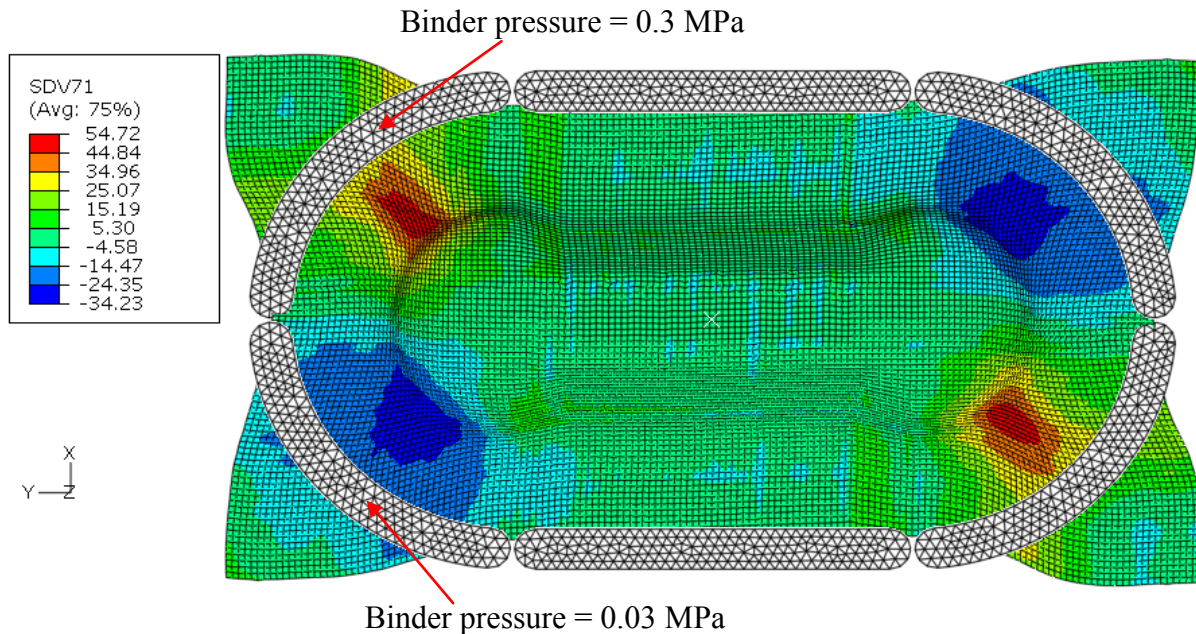


Fig. 5.22 The shear angle (degrees) evolution in the full double dome model with unbalanced binder pressure

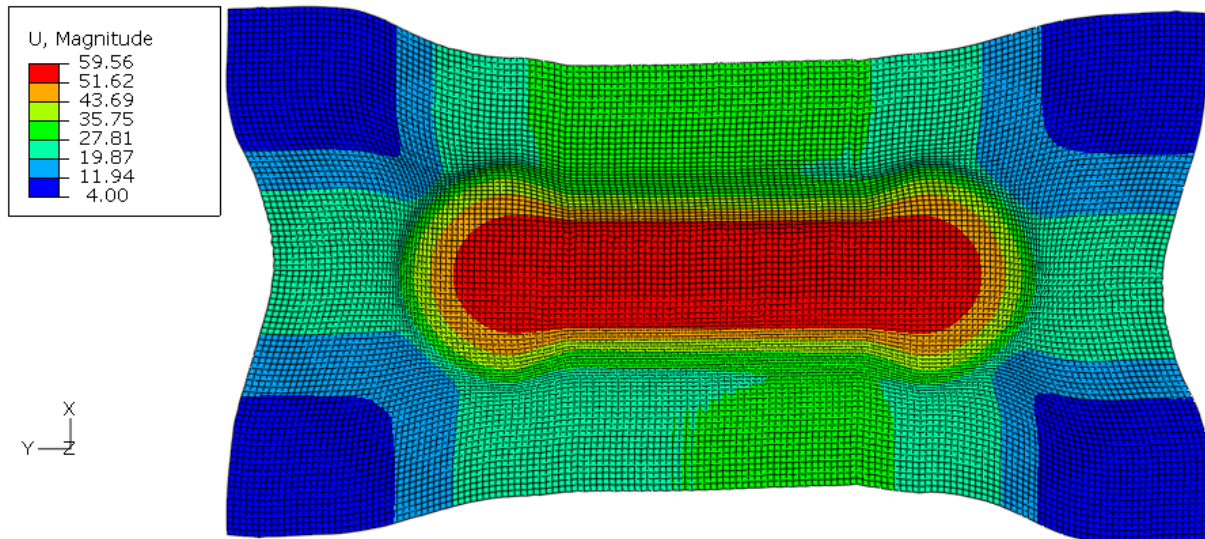


Fig. 5.23 The contours of nodal displacements (material draw-in) in the full double dome model with unbalanced binder pressure

Fig. 5.23 shows that material draw-in has been affected largely with the application of unbalanced pressure. The opposite diagonal corners have the same binder pressure and therefore present the same amount of material flow during forming. In other words, it can be said that binder force has serious implications during fabric forming and needs to be optimised for a certain application.

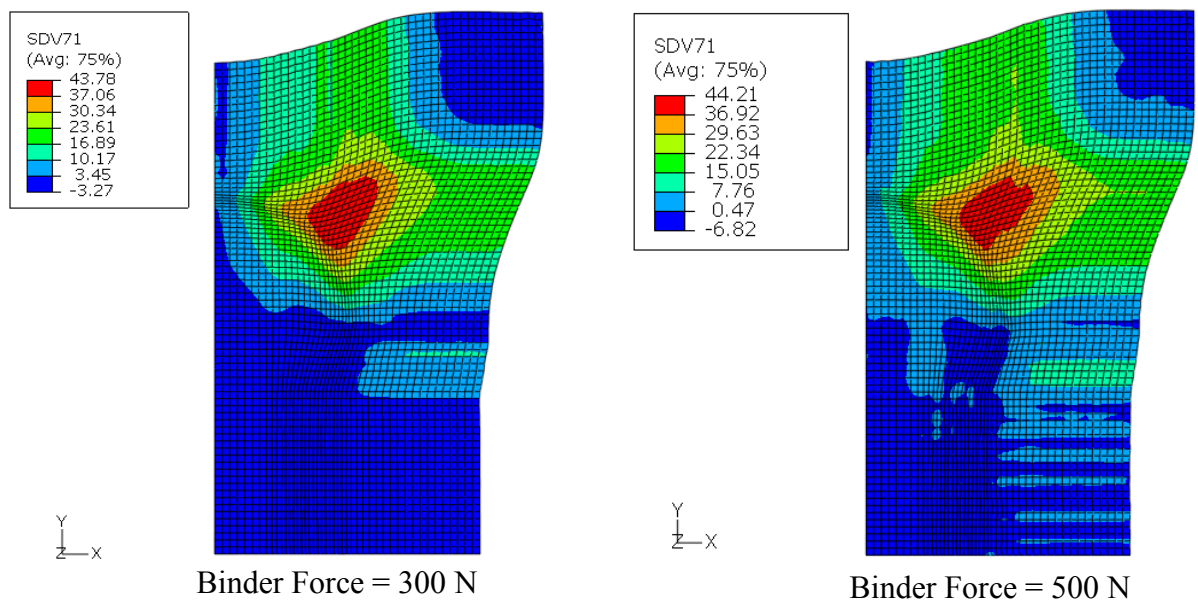


Fig. 5.24 The shear angle (degrees) evolution in the full double dome model with unbalanced binder pressure

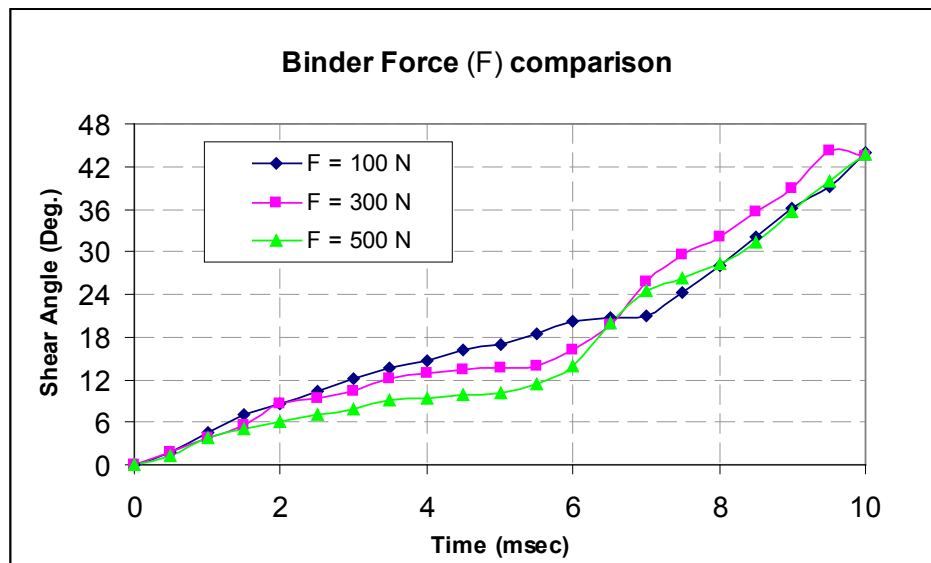


Fig. 5.25 Maximum shear angle (degrees) evolution with process time in the whole model for three different binder loads, i.e. 500 N, 300 N and 100 N, in case of orientations of $0^\circ/90^\circ$ yarns in the reference configuration with unbalanced binder pressure

5.7 Thermo-forming Case Study

Thermo-forming simulations of the BPW fabrics have been performed in order to check the effects of preheating over glass fibres. This is, indeed, the requirement of benchmark study of double dome forming simulations where the fabrics are made of commingled glass/polypropylene fibres. In this particular study, thermo-forming simulations have been attempted with the same numerical model of stress computation algorithm developed. The aim was also to verify the working of this algorithm with preheating. The simulations of thermo-forming are two steps analysis: the preheating of the fabric sheet to 300°C and then perform the forming operation at the same temperature. The forming tools have also been used with pre-defined temperature of 300°C .

Table 5.3 shows the thermal properties of glass fibres used in the thermo-forming simulations. These properties are available on the benchmark website [WC08].

Table: 5.3 Thermal properties of Glass fibres [WC08]

Property	Glass type E
Coefficient of thermal Expansion ($\times 10^{-6} / ^\circ\text{C}$)	5.0
Thermal conductivity (W/ m/ $^\circ\text{C}$)	1.3
Specific heat (J/ kg/ $^\circ\text{K}$)	840

Fig. 5.26 shows the preheating of the fabric sheet in the first step of the analysis up to 300 °C and it is maintained in the second step. The fabric specimen is of 135 mm \times 235 mm in size which is a quarter model of double dome. In Fig. 5.27, it is shown that there is increase in stress in the first direction of fibres due to heating of the fabric.

The mechanical material input data and the process parameters are selected exactly the same as for forming simulations without preheating of fabrics. The contact definitions are also same which were explained in section-5.2. However, the elements used are 4-node thermally coupled doubly curved thin or thick shell, reduced integration, hourglass control, finite membrane strains (S4RT) and also a mass proportional damping factor of 100 was during simulations. The thermo-forming simulations attempted without damping always resulted in severe deformation of elements during forming operation and solutions stopped without completion.

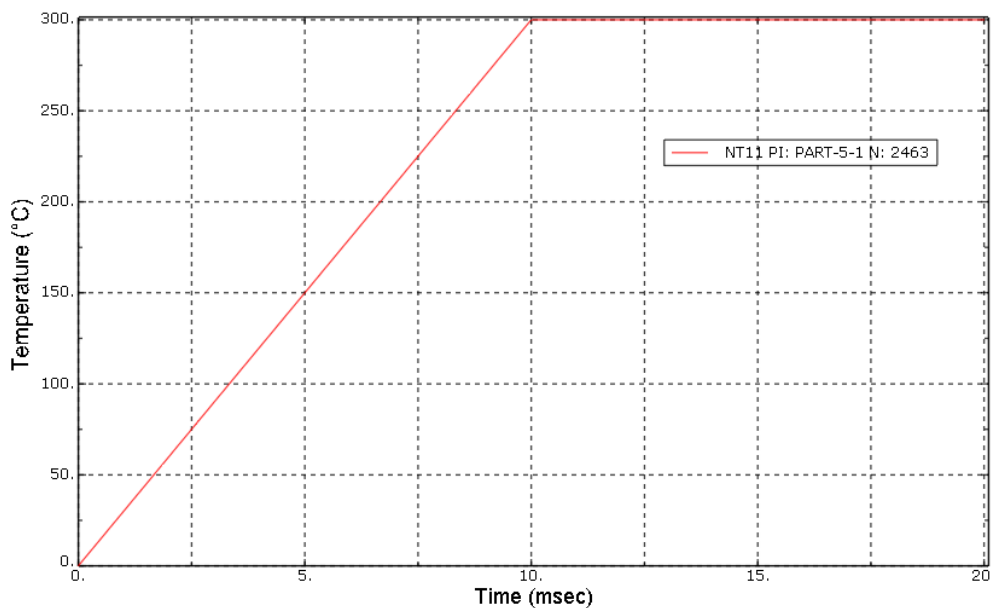


Fig. 5.26 Preheating of the glass fabric sheet during simulations and maintained during forming stage.

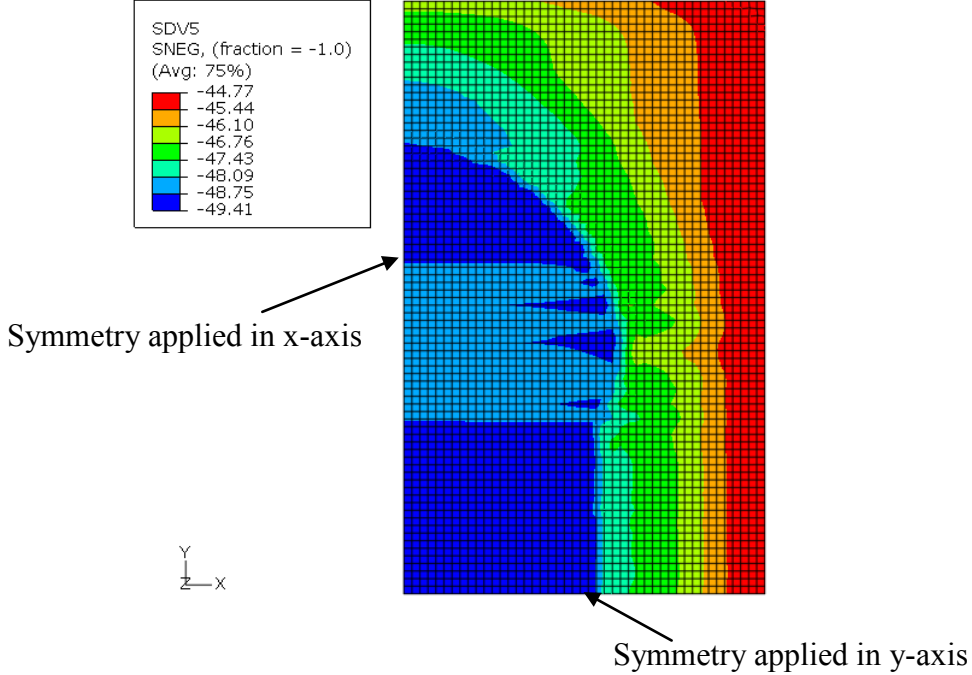


Fig. 5.27 Stresses in MPa (SDV5) along first fibre directions resulted due to preheating of the fabric

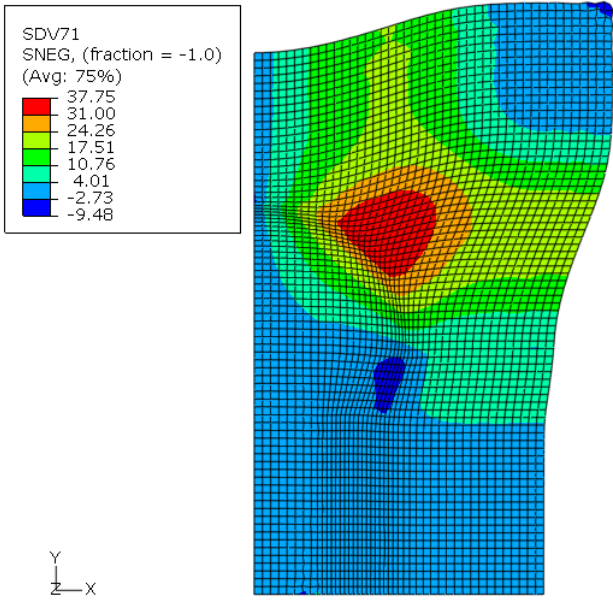


Fig. 5.28 Shear angles in degrees (SDV71) resulted in the glass fabric sheet after thermo-forming operation with preheat of 300 °C.

Conclusions of Chapter-5

In this chapter, we dealt with the FE simulations for forming analysis of woven composite reinforcements. This analysis is based on the use of a hypoelastic approach using a commercial FE code ABAQUS/Explicit with standard elements. The stress computation algorithm developed and presented in chapter 3 has been used via a user material subroutine VUMAT. The forming simulations are performed with the process parameters similar to those used in the experiments presented in chapter 4. Two different orientations of fabric yarns i.e. $0^\circ/90^\circ$ and $\pm 45^\circ$ have been used to compare the numerical results with the experimental measurements. The quantitative comparisons of results show that the developed numerical model has the capability to correctly trace the fibrous material behaviour during a forming process.

The second stage of numerical forming simulations is to check the sensitivity of the forming process parameters in case of fibrous materials. A large number of process parameters and a wide range of parametric study data have been used to analyse the woven reinforcement behaviour. The study has explored many critical specificities of the fabric materials such as sensitivity to the frictional effects, punch velocities and the blankholder forces. The analysis has also discovered the limitations of the numerical model especially the use of coefficient of friction beyond 0.25.

To the end of this, we have attempted to perform thermo-forming case study of double dome. This forming case study has been carried out in order to verify the working of developed stress computation algorithm with preheating of the fabric. Yet, it has not been explored to the extent which could produce some remarkable results and therefore, it is still in progress to be studied thoroughly.

6

Summary and Conclusions

The ever-growing use of composite materials in the high performance domains assigns them a huge significance. In this context, the numerical tools have always been trusted and are considered powerful instruments to analyze the distortions and complexities in the design phase and can ideally lead to a first-time-right design. In this project of PhD study, we have focused over analyzing the forming processes of composite materials. The textile composites having continuous fibrous reinforcements were chosen to explore their specific behavior during deformation. The first forming stage of RTM process which consists of forming the dry fabric reinforcement has specifically been the objective of this study.

The benchmark geometry of double dome was used to perform the fabric forming tests. This is an international forming model and has been originally designed to carry out draping operations with benchmark fabrics. The latter have already been studied in detail and shear behavior was characterized experimentally by six different universities of the world. The second stage of the benchmark study, which is also pertinent to the present study, is the FE simulations using double dome forming model.

This particular study has been accomplished with three main stages: the development of a stress computation algorithm for analysis of fibrous materials; the experimental forming analysis of woven fabrics with a local development of double dome forming device and the FE forming simulations using the same benchmark geometry with the help of developed algorithm for numerical analysis.

The numerical analysis of textile composite reinforcement was performed at macro-scale using continuous approach. The reinforcement is actually discontinuous at lower length

scales; however, the former can be treated as continuous at macro-level and continuous approach has been proven to be successful in case of fabric forming simulations. The stiffness of fibres is dominant along length and therefore, it should be followed accurately to predict the true behavior of a fabric during forming. Moreover, the proper use of rate constitutive equations is very important to achieve the real output of fibrous materials.

In this particular study, the hypoelastic law has been used as a rate constitutive equation which is considered suitable at finite strains. An algorithm based on a hypoelastic behavior has been proposed for composite reinforcement forming simulations. It was shown that using hypoelastic law with an objective derivative based on the warp and weft fibre rotation tensors can successfully trace the correct behavior of fibrous materials.

Since, the two fibre directions usually do not remain orthogonal to each other after deformation; therefore, two orthogonal fibre frames have been defined where each one is based on one of the two fibre directions. The constitutive tensor was divided to operate in the two orthogonal fibre frames and the stresses were accumulated using mid-point integration rule of Hughes et Winget. The stresses computed in the two fibre frames are then transformed to the default work basis of FE code (GN basis in case of ABAQUS/Explicit).

The very first implementation of the developed stress computation algorithm was the validation of numerical output in case of elementary tests with the theoretical results. A number of elementary tests have been performed especially the case of simple shear test when GN axes do not follow the fibre axes after deformation. In both of the cases; when juxtaposed single fibre axis is used and when bi-axially reinforced fibres in an element are assumed, the stress output is numerically zero (of the order of $\times 10^{-6}$ MPa) for horizontally oriented fibres. This confirms the real output in case of fibrous material analysis. The second important elementary test was to verify the objectivity of the numerical model used where the rigid body rotation under traction validate the test results.

The de-facto standard tests of picture frame and bias extension, used to characterize the in-plane shear behavior of thin textile fabrics, were also validated numerically. The experimental results of BPW and BTW fabrics characterized by benchmark study [CAO08] were used to validate the in-plane shear tests. The aim was to corroborate the developed stress computation algorithm for fibrous materials over these tests.

The in-house development of benchmark forming device has been one of the major contributions in this study. This is an international forming benchmark dedicated for analysis

woven composites. The experimental tests have been duly performed using one of the benchmark fabrics (i.e. BPW fabric). Two different initial orientations ($0^\circ/90^\circ$ and $\pm 45^\circ$) of fabric yarns were selected which produced very interesting results when observed from the point of views of shearing of the fabric yarns and of the material draw-in along the contours of woven fabrics. These experimental results were measured quantitatively in order to compare the numerical simulation outputs.

The exploitation of 3D optical strain measurements (OSM) has remained very useful in measuring the shear angles of the deformed fabrics. 3D digital images were obtained by using DIC (digital image correlation) system of Vic-3D. These images were treated to extract 3D coordinates at the desired positions and then by manipulating the data with some post-processing produced the shear angle at the points of interests. Although, this procedure (implementation of 3D OSM) took a lot of time yet the results obtained were valuable when compared with the numerically measured shear angles during simulations.

The ultimate goal of this study was to perform the FE simulations of double dome model using the stress computation algorithm developed for forming analysis of fibrous materials. The objective has been achieved using the BPW fabric shear behavior characteristics [CAO08] with exactly same two initial orientations of fabric yarns. The quantitative comparisons of results were made (chapter-5) with the forming tests performed experimentally. This comparison has contributed to prove the successful development of stress computation algorithm, using a continuous approach and based on hypoelastic behavior, in case of analyzing numerically the textile composite reinforcements.

An important aspect of the numerical tests is to use two superimposed elements having common nodes. The elementary tests, in-plane shear tests and a double dome forming tests have revealed that this idea works well in analyzing the bi-axially reinforced materials with single fibre axes oriented differently in the two superposed elements. This method becomes very interesting when two different materials were tested and the results are shown in case of bias extension test for a prepreg analysis. With this scheme, it is also possible to do 3D forming tests for prepregs. As a supplementary work to this thesis is the execution of thermoforming tests which have produced a few interesting results presented to the end of this thesis dissertation (chapter-5).

The future task would be to analyse different weaving patterns that would mainly change the in-plane shear behaviour and also to consider the bending behaviour of the fabrics within the numerical model. Another point will be the comparison of the proposed continuous approach

with alternative methods in particular with discrete approaches as of [DUR05] and [DUH06] or semi-discrete approaches as of [HAM09]. Moreover, the forming tests of double dome benchmark can be conducted using process conditions under heating of the blanks prior to draping operation so that the thermal effects on the commingled glass/polypropylene fabric could be observed experimentally as well as numerically.

The introduction of bending behaviour of textile fabrics to the developed algorithm would be very useful work. This may help to simulate the wrinkling of the woven reinforcements which is very important and crucial in order to design a defect free (without wrinkles) composite part. There may be another improvement in the stress computation algorithm which may apply a constitutive matrix which can couple the tensile and in-plane shear behaviours of the fabrics. On the basis of such requirements, there exists a potential improvement in the numerical algorithm adopted.

BIBLIOGRAPHY

- [ABA68] **ABAQUS** user manual documentation V-6.8
- [ABA68a] **ABAQUS** analysis user manual V-6.8, conventions 1.2.2
- [AIM07] **AIMENE Y.** Approche hyper-élastique pour la simulation des renforts fibreux en grandes transformations. Thèse de doctorat LaMCoS. Lyon : INSA de Lyon, 2007, 133 p.
- [AIM08] **AIMENE Y, HAGEGE B, SIDOROFF F, VIDAL-SALLE E, BOISSE P, DRIDI S.** Hyperelastic approach for composite reinforcement forming simulations. In : Proceedings of the 11th International ESAFORM conference on material forming, Lyon, France, 2008.
- [BAD07] **BADEL P, VIDAL-SALLE E, BOISSE P.** Computational determination of in-plane shear mechanical behaviour of textile composite reinforcements Computational Materials Science 40 (2007) 439–448
- [BAS00] **BASAR Y, WEICHERT D.** Non linear continuum mechanics of solids. Berlin, Germany: Springer-Verlag, 2000, 193 p. ISBN 3-540-66601-x
- [BEL00] **BELYTSCHKO T, WING KL, MORAN B.** Nonlinear finite elements for Continua and structures. Chichester: Jhon Wiley Edt., 2000
- [BOU97] **BOUBAKAR ML, BOISSE P, GELIN JC.** Numerical implementation of orthotropic plasticity for sheet metal forming analysis. J. Mater. Process. Technol. (1997) 65:143–52.
- [BEN07] **BEN BOUBAKER B, HAUSSY B, GANGHOFFER JF.** Discrete models of woven structures. Macroscopic approach Composites: Part B 38 (2007) 498–505
- [BOI01] **BOISSE P, BUET K, GASSER A, LAUNAY J.** Meso/macro-mechanical behaviour of textile reinforcements for thin composites. Composites Science and Technology 61 (2001) 395±401
- [BOI05] **BOISSE P, GASSER A, HAGEGE B, BILLOET JL.** Analysis of the mechanical behaviour of woven fibrous material using virtual tests at the unit

- cell level. *International Journal of Material Science*, 2005, vol. 40, pp 5955-5962.
- [BOI06] **BOISSE P.** Meso-macro approach for composite forming simulation. *J Mater Sci* (2006) 41:6591–6598
- [BOI07] **BOISSE P.** Finite element analysis of composite forming. In: Long AC, editor. *Composite forming technologies*. Woodhead Publishing; 2007. p. 46–79 [chapter 3].
- [BOI08] **BOISSE P, HAMILA N, HELENON F, HAGEGE B, CAO J.** Different approaches for woven composite reinforcement forming simulation. *Int J Mater Form* (2008) 1:21–29
- [BOI09] **BOISSE P, Y. AIMENE, A. DOGUI , S. DRIDI, S. GATOULLAT, N. HAMILA, A. KHAN, T. MABROUKI, F. MORESTIN, E. VIDAL-SALLEE.** Hypoelastic, hyperelastic, discrete and semidiscrete approaches for textile composite reinforcement forming. Submitted in *Int J Mat Form*, 2009.
- [BUE01] **BUET K, BOISSE P.** Experimental analysis and modeling of biaxial mechanical behavior of woven composite reinforcements. *Experimental Mechanics*, 2001, vol. 41, n°3, pp. 260-269.
- [CAO08] **CAO J, AKKERMAN R, BOISSE P, CHEN J et al.** Characterization of Mechanical Behavior of Woven Fabrics : Experimental Methods and Benchmark Results. *Composites. Composites: Part A* 39 (2008) 1037–1053
- [COX97] **COX BN, FLANAGAN G.** Handbook of analytical methods for textile composites. Hampton, VA: Langley Research Center, NASA; 1997.
- [CRI97] **CRISFIELD MA.** Nonlinear finite element analysis of solids and structure: advanced topics, vol. 2. Chichester: John Wiley Edt.; 1997.
- [DEB08] **DE BILBAO E, SOULAT D, HIVET G, LAUNAY J, GASSER A.** Bending Test of Composite Reinforcements. *Int J Mater Form* DOI 10.1007/s12289-008-0265-z Springer/ESAFORM 2008
- [DEL08] **DE LUYCKER E, MORESTIN F, BOISSE P, MARSAL D.** Simulation of 3D interlock composite performing Composite Structures xxx (2008) xxx–xxx
- [DEL09] **DE LUYCKER E.** PhD thesis: Simulation et expérimentation en mise en

- forme de renforts composites 3D interlocks. Feb. 2009, INSA de Lyon, France
- [DON01] **DONG L, LEKAKOU C.** Processings of composites: Simulations of the draping of fabrics with updated material behaviour law. *Journal of Composite Materials*, 2001, vol. 35, pp. 138-163.
- [DON00] **DONG L, LEKAKOU C, BADER MG.** Solid-mechanics finite element simulations of the draping of fabrics: a sensitivity analysis *Composites: Part A* 31 (2000) 639–652
- [DUH06] **DUHOVIC M, BHATTACHARYYA D.** Simulating the deformation mechanisms of knitted fabric composites. *Composites: Part A* 37 (2006) 1897–1915
- [DUM03] **DUMONT F, HIVET G, ROTINAT R, LAUNAY J, BOISSE P, VACHER P.** Mésures de champs pour des essais de cisaillement sur des renforts tissés. field measurements for shear tests on woven reinforcements. *Mécanique and Industries*, 4(6):627–635, 2003.
- [DUR05] **DURVILLE D.** Numerical simulation of entangled materials mechanical properties *Journal of materials science*. 40 (2005): 5941–5948.
- [DUR08] **DURVILLE D** A finite element approach of the behaviour of woven materials at microscopic scale. 11th Euromech-Mecamat conference - Mechanics of microstructured solids : cellular materials, fiber reinforced solids and soft tissues, Torino : Italie (2008)
- [GAT09] **GATOUILLAT S, VIDAL-SALLE E, BOISSE P.** Différentes approches pour la simulation de la mise en forme des renforts fibreux de composites. Les intérêts de l'approche mésoscopique. *Congrès Français de Mécanique*, 2009.
- [GIL09] **GILL AF, ROBINSON P, PINHO S.** Effect of variation in fibre volume fraction on modes I and II delamination behaviour of 5HS woven composites manufactured by RTM. *Composites Science and Technology*. doi:10.1016/j.compscitech.2009.02.008
- [HAG04] **HAGEGE B.** Simulation du comportement mécanique des milieux fibreux en grandes transformations. Thèse de doctorat. Paris : ENSAM, 2004, 263 p

- [HAG05] **HAGEGE B, BOISSE P, BILLOET JL.** Finite element analyses of knitted composite reinforcement at large strain. *Revue européenne des éléments finis*, 2005, vol. 14, n° 6-7, pp. 767-776.
- [HEA01] **HEARDMAN E, LEKAKOU C, BADER MG.** In-plane permeability of sheared fabrics. *Composite: Part A* 32 (2001) 933-940
- [HAM96] **HAMMAMI A, TROCHU F, GAUVIN R, WIRTH S.** Directional permeability measurement of deformed reinforcement. *J. Reinf. Plas. Compos.* 15 (1996): 552–562
- [HAM07] **HAMILA N,** Simulation de la mise en forme des renforts composites mono et multiplis. Thèse de doctorat. Lyon : INSA de Lyon, 2007.
- [HAM09] **HAMILA, N, BOISSE, P, SABOURIN F, BRUNET M.** A semi-discrete shell finite element for textile composite reinforcement forming simulation. *Int. J. Numer. Meth. Engng.* (2009) DOI: 10.1002/nme.2625
- [HAR04] **HARRISON P, CLIFFORD MJ, LONG AC.** Shear characterization of viscous woven textile composites: a comparison between picture frame and bias extension experiments. *Composites Science and Technology* 2004;64:1453–65.
- [HEA01] **HEADERMAN E, LEKAKOU C, BADER, MG.** In-plane permeability of sheared fabrics. *Composite: Part A.* 32 (2001): 933-940
- [HIV08] **HIVET G, BOISSE P.** Consistent mesoscopic mechanical behaviour model for woven composite reinforcements in biaxial tension *Composites: Part B* 39 (2008) 345–361
- [HUG80] **HUGHES TJR, WINGET J.** Finite rotation effects in numerical integration of rate constitutive equations arising in large deformation analysis. *Int. J. of num methods in engg.* 1980; 15:1862-1867
- [HUE06] **HUETINK J.** On anisotropy, objectivity and invariancy in finite thermomechanical deformations. In: *Proceedings on the 9th International ESAFORM Conference on Material Forming*, Glasgow, United Kingdom, 2006, pp. 355–358.

- [KEL06] **KELKAR AD, TATE JS, BOLICK R.** Structural integrity of aerospace textile composites under fatigue loading *Materials Science and Engineering B* 132 (2006) 79–84
- [KHA08] **KHAN MA, MABROUKI T, GAUTHIER S, VIDAL-SALEE E, BOISSE P.** Preforming simulation of the reinforcements of woven composites: continuous approach within a commercial code. 11th ESAFORM conference 2008, Lyon, France.
- [KHA09] **KHAN MA, MABROUKI T, BOISSE P.** Numerical and experimental forming analysis of woven composites using double dome benchmark. 12th ESAFORM conference 2009, Enschede, The Netherlands.
- [KHO97] **KHONDKER OA, LEONG KH, HERSZBERG I, HAMADA H.** Impact and compression-after-impact performance of weft-knitted glass textile composites. *Composites: Part A* 36 (2005) 638–648
- [LOA08] **LOANE B.** Compression transverse de renforts tissés. Application au taffetas. Master rapport MEGA (2008), INSA de Lyon
- [LOM08a] **LOMOV SV, IVANOV DS, VERPOEST I, ZAKO M, KURASHIKI T, NAKAI H, MOLIMARD J, VAUTRIN A.** Full-field strain measurements for validation of meso-FE analysis of textile composites *Composites: Part A* 39 (2008) 1218–1231
- [LOM08b] **LOMOV SV, BOISSE P, DELUYCKER E, MORESTIN F, VANCLOOSTER K, VANDEPITTE D, VERPOEST I, WILLEMS A.** Full-field strain measurements in textile deformability studies *Composites: Part A* 39 (2008) 1232–1244
- [LAU08] **LAUNAY J, HIVET G, DUONG AV, BOISSE P.** Experimental analysis of the influence of tensions on in plane shear behaviour of woven composite reinforcements *Composites Science and Technology* 68 (2008) 506–515
- [LEG09] **LEGRAND X, BOUSSU F, BLOT P, UITARD D.** A new technique of weaving 3D surface application to Carbon/Epoxy corner fitting plies. 12th ESAFORM Conference 2009.
- [LIU06] **Liu L, Zhang BM, Wang DF, Wu ZJ.** Effects of cure cycles on void content and mechanical properties of composite laminates. *Composite Structures* 73 (2006) 303–309

- [LOM07] **LOMOV SV, IVANOV DS, VERPOEST I, ZAKO M, KURSHAKI T, NAKAI H, HIROSAWA S.** Meso-FE modelling of textile composites: Road map, data flow and algorithms *Composites Science and Technology* 67 (2007) 1870–1891
- [LOM08] **LOMOV SV, BOISSE P, DELUYCKER E, MORESTIN F, VANCLOOSTER K, VANDEPITTE D, VERPOEST I, WILLEMS A.** Full-field strain measurements in textile deformability studies *Composites: Part A* 39 (2008) 1232–1244
- [LON07] **LONG AC.** Composites forming mechanisms and materials characterisation. In *Composites forming technologies*. Woodhead publishing Limited and CRC Press LLC, 2007.
- [MAT08] **MATTSSON D, JOFFE R, VARNA J.** Damage in NCF composites under tension: Effect of layer stacking sequence. *Engineering Fracture Mechanics* 75 (2008) 2666–2682
- [MOR08] **LEE W, PADOVOISKIS J, CAO J, DE LUYCKER E, BOISSE P, MORESTIN F, CHEN J, SHERWOOD J.** Bias-extension of woven composite fabrics *Int J Mater Form* (2008) Suppl 1:895–898 DOI: 10.1007/s12289-008-0240-8 Springer/ESAFORM 2008
- [MOU99] **MOURITZ AP, BANNISTER MK, FALZON PJ, LEONG KH.** Review of applications for advanced three-dimensional fibre textile composites, *Composites Part A* 1999; 30: 1445–1461.
- [NGU99] **NGUYEN M, HERSZBERG I, PATON R.** The shear properties of woven carbon fabric *Composite Structures* 47 (1999) 767±779
- [PEN04] **PENG XQ, CAO J, CHEN J, XUE P, LUSSIER DS, LIU L.** Experimental and numerical analysis on normalization of picture frame tests for composite materials. *Composites Science and Technology* 64 (2004) 11–21
- [PEN05] **PENG XQ, CAO J.** A continuum mechanics-based non-orthogonal constitutive model for woven composite fabrics. *Composites Part A* 2005;36:859–74

- [PIC05] **PICKAETT AK, CREECH G, DE LUCA P.** Simplified and Advanced Simulation Methods for Prediction of Fabric Draping. *European J. of Comput. Mechanics*, 14-6-7 (2005) 677-691
- [POT99] **POTTER KD.** The early history of the resin transfer moulding process for aerospace applications *Composites: Part A* 30 (1999) 619–621
- [POT01] **POTLURI P, SHARMA S, RAMGULAM R.** Comprehensive drape modelling for moulding 3D textile performs. *Composites: Part A.* 32 (2001): 1415-1424
- [ROB81] **ROBERTSON RE, HSIUE ES, SICKAFUS EN, YEH GSY.** Fibre rearrangements during the molding of continuous fibre composites. Part I. Flat Cloth to a Hemisphere. *Polym. Compos.* 2(3) (1981): 126–131
- [ROB84] **ROBERTSON RE, HSIUE ES, SICKAFUS EN, YEH GSY.** Fibre rearrangements during the modelling of continuous fibre composites. Part II: flat cloth to a rounded cone. *Polym. Compos.* 5(3) (1984):191–197
- [SAG03] **SAGAR TV, PORLURIP, HEARLE JWS, Textile Composites Group.** Mesoscale modelling of interlaced fibre assemblies using energy method. *Computational Materials Science* 28 (2003) 49–62
- [SHA03] **SHARMA SB, SUTCLIFFE MPF, CHANG SH.** Characterisation of material properties for draping of dry woven composite material. *Composites Part A* 2003;34:1167–75.
- [SHA04] **SHARMA SB, SUTCLIFFE MPF.** A simplified finite element model for draping of woven material *Composites: Part A* 35 (2004) 637–643
- [SON06] **SONG YS.** Mathematical analysis of resin flow through fibrous porous media. *Appl. Compos. Mater.* 13 (2006): 335–343
- [SKO07] **SKORDOS AA, MONROY AC, SUTCLIFFE MPF.** A simplified rate dependent model of forming and wrinkling of pre-impregnated woven composites *Composites: Part A* 38 (2007) 1318–1330
- [TEN07] **TEN THIJE RHW.** Finite element simulations of laminated composite processes. PhD thesis, University of Twente, 2007.

- [TEN07a] **TEN THIJE RHW, AKKERMANN R, HUETINK J.** Large deformation simulation of anisotropic material using an updated Lagrangian finite element method *Comput. Methods Appl. Mech. Engrg.* 196 (2007) 3141–3150
- [TEN08] **TEN THIJE RHW, AKKERMAN R.** Solutions to intra-ply shear locking in finite element analyses of fibre reinforced materials. *Composites Part A: Applied Science and Manufacturing*, 39(7):1167–1176, 2008.
- [VAN91] **VAN DER WEEN F.** Algorithms for draping fabrics on doubly curved surfaces. *Int. J. Numer. Meth. Eng.* 31 (1991): 1414–1426
- [VAN96] **VANDEURZEN P., IVENS J., VERPOEST IA.** Three dimensional micromechanical analysis of woven-fabric composites: II. Elastic analysis. *Composites Science and Technology* 56 (1996) 1317-1327
- [WAN98] **WANG J, PAGE JR, PATON R.** Experimental investigation of the draping properties of reinforcement fabrics. *Compos Sci Technol* 1998;58:229–37.
- [WIL08] **WILLEMS A.** PhD thesis: Forming simulation of textile reinforced composite shell structures. December 2008, KATHOLIEKE UNIVERSITEIT LEUVEN, Belgium.
- [WIL08a] **WILLEMS A, LOMOV SV, VERPOEST I, VANDEPITTE D.** Optical strain fields in shear and tensile testing of textile reinforcements *Composites Science and Technology* 68 (2008) 807–819.
- [WC08] **“WOVEN COMPOSITES BENCHMARK FORUM”**
<http://www.wovencomposites.org/index.php> (accessed September 2008)
- [XIA97] **XIA H, BRUHNS OT, MEYERS A.** Hypo-elasticity model based upon the logarithmic stress rate. *Journal of Elasticity.* 1997; 47(1): 51-68
- [YU02] **YU WR, POURBOGHRATA F, CHUNG K, ZAMPALONI M, KANG TJ.** Non-orthogonal constitutive equation for woven fabric reinforced thermoplastic composites. *Composites: Part A*, 2002, vol. 33, pp. 1095–1105.
- [YU05] **YU WR, HARRISON P, LONG A.** Finite element forming simulation for non-crimp fabrics using a non-orthogonal constitutive equation. *Composites: Part A*, 2005, vol. 36, pp. 1079–1093.

- [YU06] **YU X., CARTWRIGHT B., MCGUCKIN D, YE L, MAI YW.** Intraply shear locking in finite element analyses of woven fabric forming processes. *Composites Part A: Applied Science and Manufacturing*, 37(5):790–803, 2006.
- [YUY08] **YUYANG MIAO, ERIC ZHOU, YOUQI WANG, BRYAN A. Cheeseman.** Mechanics of textile composites: Micro-geometry. *Composites Science and Technology* 68 (2008) 1671–1678
- [ZHO04] **ZHOU G, SUN X, WANG Y.** Multi-chain digital element analysis in textile mechanics *Composites Science and Technology* 64 (2004) 239–244
- [ZHU07] **ZHU B, YU TX, TAO XM.** An experimental study of in-plane large shear deformation of woven fabric composite. *Composites Science and Technology* 67 (2007) 252–261

FOLIO ADMINISTRATIF

THESE SOUTENUE DEVANT L'INSTITUT NATIONAL DES SCIENCES APPLIQUEES DE LYON

NOM : KHAN
(avec précision du nom de jeune fille, le cas échéant)

DATE de SOUTENANCE : 09 octobre 2009

Prénoms : Muhammad Aurangzeb

TITRE :
NUMERICAL AND EXPERIMENTAL FORMING ANALYSES OF TEXTILE COMPOSITE REINFORCEMENTS BASED ON A HYPOELASTIC APPROACH

NATURE : Doctorat

Numéro d'ordre : 09 ISAL 0071

Ecole doctorale : MEGA

Spécialité : GENIE MECANIQUE

Cote B.I.U. - Lyon : T 50/210/19 / et bis CLASSE :

RESUME :

Numerical simulations of the composite forming processes are essential in the design phase of composite structures. Fabric Forming simulations have many objectives: these determine the feasibility of forming or conditions of this feasibility and help determine the position of fibres after forming. This is important for the identification of mechanical characteristics of composites in service and to calculate the permeability after dry reinforcement draping for correct analysis of injection moulding process. This particular study has been accomplished with three main stages: the development of a stress computation algorithm for numerical analysis of fibrous materials; the experimental forming analysis of textile fabrics with an in-house development of double dome benchmark forming device; and finite element forming simulations using the benchmark model.

Continuous approach has been used to predict the mechanical characteristics of woven composite fabrics during forming which considers the fibrous materials as a continuum on average at macroscopic scale. An algorithm based on a hypoelastic behaviour has been proposed for composite reinforcement forming simulations. It has been shown that using hypoelastic law with an objective derivative based on warp and weft fibre rotation tensors can successfully trace the correct behaviour of fibrous materials in deformation. The algorithm has been validated through a number of elementary tests with theoretical results. The de-facto standard in-plane shear tests of picture-frame and bias-extension have also been validated numerically. Double dome fabric forming tests have been carried out experimentally. 3D optical strain measurements were performed exploiting digital image correlation system of Vic-3D in order to measure the shear angles of the deformed fabrics. The forming simulations performed with the proposed numerical approach show a good agreement with the experimental results obtained with double dome device.

MOTS-CLES :

Textile Reinforcement, Composite Processing, Forming Simulation, Hypoelasticity, Continuous Approach, International Forming Benchmark

Laboratoire (s) de recherche : LaMCoS

Directeur de thèse: Philippe BOISSE, Tarek MABROUKI

Président de jury : Philippe OLIVIER

Composition du jury : Olivier POLIT, Laurent GUILLAUMAT, Philippe OLIVIER, Tarek MABROUKI, Philippe BOISSE